ADDIS ABABA INSTITUTE OF TECHNOLOGY
(AAiT)
School of Civil and Environmental Engineering

Fatigue Life Analysis of Rail-Welds Based on Linear Fracture Mechanics

By

Yalelet Endalemaw

A thesis submitted to the school of Graduate Studies of Addis Ababa University in Partial fulfillment of the degree of Master of Science in Civil Engineering

(Railway Engineering)

Advisor

Mequanent Mulugeta (MSc.)

February, 2016

Fatigue Life Analysis of Rail-Welds Based on Linear Fracture Mechanics

By

Yalelet Endalemaw

Approved by board of Examiners:

Mequanent Mulugeta (MSc.) ***Thesis Advisor***	***Signature***	***Date***
Internal Examiner	***Signature***	***Date***
External Examiner	***Signature***	***Date***
Chair man	***Signature***	***Date***

Fatigue Life Analysis of Rail-Welds based on Linear Fracture Mechanics

Masters of Science thesis in Civil Engineering

School of Civil and Environment Engineering

AAiT

ABSTRACT

Engineered structures can fail in various ways including yielding, buckling and brittle fracture. While all materials suffer fatigue, the effect is particularly pronounced for ductile materials, such as metals and glassy polymers. For such a ductile material, fracture may occur after a small number of cycles, when cyclic loads repeatedly cause large-scale plastic deformation. In most engineering structures, however, loads are kept small so that the structures deform elastically. Even so, a crack may initiate somewhere in such a structure, and extend by a small amount during each cycle of the load.

Rail welds are the weak link in continuously welded rails i.e. Small imperfection in welds can cause cracks to initiate. Detection and rectification of rail-weld defects are major issues for all rail players around the world. If undetected and/or untreated these defects can lead to rail breaks and derailments. These are challenges to perform effective inspection and cost effective maintenance decisions. If these issues are addressed properly, inspection and maintenance decisions can reduce potential risk of rail breaks and derailments.

This thesis work was majorly aimed at determining probability of failure as a result of cyclic fatigue loading of the wheel on the Weldments so as to arrive at an inspection frequency.

Primarily, a finite element model (Abaqus model) was used to estimate the contact stress between the wheel section and the rail section at the weld and at the base rail, as well. Second, flaw (i. e the presence and size of cracks) was determined using an Ultrasonic flaw detector at different locations. Third, the model was updated to fracture mechanics-based fatigue models (FRANC3D model), based on Paris law with a flaw inserted inside. There by, the critical crack size and the number of cycles to failure was determined as 0.146955mm and 20,957,747 cycles of wheel passage, respectively.

Then, probabilistic reliability model was developed with uncertainties in the detected crack size and final crack size. Thus, using the LEFM approach the reliability to failure was determined using Advanced First Order Reliability Method, Hasofer-Lind Reliability Index, as 96.69%.

Finally, addressing some of the issues associated with probability of failure, an inspection frequency was suggested to be in five months interval based on reducing the long term life cycle cost.

Last, a recommendation is set to future researchers for a development of a detailed maintenance strategy.

Key Words: Rail-Weld, Ultrasonic Test, Paris Law, Linear Fracture Mechanics, Reliability Analysis, Inspection Interval.

ACKNOWLEDGEMENTS

"Above all, Glory and fame shall be to the Almighty GOD for all His provisions."

I am grateful to express my gratitude and deep appreciations to my advisor, Mequanent Mulugeta, for all his valuable comments, countless suggestions and remarkable advices throughout preparation of this thesis. I am very fortunate to have him as my advisor.

Next, I want to acknowledge Addis Ababa Institute of Technology (AAiT) for all technical and financial assistances and also to Ethiopian Railway Corporation (ERC) for the full scholarship I am granted to study Railway Engineering in MSc Program.

I want to acknowledge staffs of Metal Development Industry Institute particularly, Dereje Asfaw, Technology Director and Ermias M, Engineering Hade. And staffs of AAiT Mechanical Engineering workshop especially, Tolesa, Workshop hade and Dereje S, Laboratory test coordinator for all their assistance in undertaking the ultrasonic flaw detecting test.

I am also thankful to Omar D, Communication facilitator, who helped me get a one month free license for fracture Analysis Software, FRANC3D. I also need to thank Neway Genene, from AALRT, and Pujari, from Sweroad, who provided me all the suitable data while undertaking a data collection.

I am greatly indebted to my wife Bethelhem Tadesse, her care helps me stand alone with no support and to withstand the ups and downs in life that contributes a lot to my success. The contributions my mother Tsehaynesh Iyasu and my uncle Yemataw Kibret with his beloved family since my childhood is great and without their input my today`s success would have been unrealized.

Last, Heartfelt gratitude and blessings are extended to a great group of friends and colleagues, especially to Zewdu Mekonnen and Petros Fekadu for all their unyielding encouragement and friendship.

Addis Ababa, 2015

Yalelet Endalemaw

LIST OF CONTENTS

LIST OF TABLES

LIST OF FIGURES

ACCROYMS AND SYMBOLS

ACCRONYMS:

ERC:	*…Ethiopian Railway Corporation.*
AT:	*…Alumino-Thermic Welding.*
FB:	*…Flash Butt Welding.*
UT:	*…Ultrasonic Test.*
NDT:	*…Nondestructive Test.*
HAZ:	*…Heat Affected Zone.*
LEFM:	*…Linear Elastic Fracture Mechanics.*
EPFM:	*…Elastic-Plastic Fracture Mechanics*
MGT:	*…Million Gross Ton.*
SIF:	*…Stress Intensity Factor.*
MPP:	*…Most Probable Point.*
UIC	*…International Union of Railway.*
FRANC3D:	*…Fracture Analysis (For 3D).*
BHN:	*…Brinell Hardness Number.*
AAR:	*…Association of American Railroad.*

SYMBOLS:

R_1, R_2:	*…Nominal Rolling Radius of the Wheel and the Rail, respectively.*
R_1', R_2':	*…Nominal Transversal Radius of curvature of the Wheel and the Rail, respectively.*
E_1, E_2:	*…Modules of Elasticity of the Wheel and the Rail.*
ν_1, ν_2:	*…Poisson's Ratio of the Wheel and the Rail, Respectively.*
ψ:	*…Angle between the radius of the wheel and the Rail.*
θ:	*…Angle between the principal Axes.*
a,b	*…Principal axes of the Hertzian Elliptic contact area*
m, n:	*…Hertz's coefficients.*
F_V	*…Vertical Wheel Load*
K^{DYN}:	*…Dynamic Amplification Factor.*
P_o:	*…Maximum Hertzian Contact Pressure.*
V	*…Velocity of Sound in different media*
f	*…Sound frequency.*
λ	*…Wave length.*
σ:	*…Remote Stress.*
a:	*…Crack length.*
a_i:	*…Initial Crack size.*

a_c: **…***Critical Crack Size.*

P_f: **…***Probability of Failure.*

P_r: **…***Reliability of Structure.*

Φ(.): *…Cumulative function of Standard normal Variance.*

K_I, K_{II}, K_{III}: *…Stress Intensity Factor in Mode I, II and III, respectively.*

S^m: *…Mean-Stress range effect.*

β: *…Reliability Index.*

T: *…Annual Gross Tonnage.*

C_{insp}: *…Rail Defect Inspection Cost.*

C_F: *…Failure Cost.*

C_P: *…Rail Replacement Cost.*

K: *…Defect Inspection Frequency.*

1. INTRODUCTION

1.1 BACKGROUND OF THE RESEARCH

Railways are large infrastructures and are the prime mode of transportation in many countries. As it is closely associated with passenger and cargo transportation, it owns high risk in terms of human lives and cost of assets. There will always be some risk associated with track irregularities and rail break but it can be reduced by detailed researches of the root causes. Some of the causes which require improvement in skill and efficiency, for example human error and some may be improved by optimization of inspection frequency. Thus, a proper maintenance strategy is required to govern optimization of inspection frequency and/or improvement in skill and efficiency of quality control personnel. A detailed study of the defects which emerge both on the rolling stock and rail infrastructure is essential to frame out the correct maintenance strategy. Among the aforementioned causes, rail-welds and associated defects are the main ones and the focus of this thesis work.

The service performance of such welds is affected by their ability to support the service load without fatigue damage. Fatigue and fracture behavior are important considerations in determining the condition of metal structures subjected to cyclic loads. Specifically, the expected life of a rail subjected to random, variable-amplitude traffic cycles are highly dependent upon damage accumulation caused by various fatigue mechanisms. Structural failure is seldom attributed to load considerations; the occurrence of stresses exceeding those predicted by the designer is rare [34].

Probabilistic fracture mechanics is a field in modern engineering that is rapidly developing. For the specimen to be analyzed, fracture mechanics requires knowledge of the crack. By considering the randomness of crack size and location, material properties, external loads and geometry, deterministic analysis provides an incomplete evaluation of the safety of a specimen. To address these problem probabilistic fracture mechanics is a useful tool, since it combines fracture mechanics with stochastic methods. The basic of probabilistic fracture mechanics and its application to the analysis of uncertainties in structural systems can be founded in Liu and Belytschko (1989). By considering the complexity of the failure mechanism this thesis is aimed at determining the reliability of failure, a combination of Paris's equation (Paris and Erdogan, 1963) with the theory of statistics and structural reliability is employed [10].

Preventing broken-rail-caused derailments is a high priority for the rail industry and government. The current practice is to periodically inspect rails using non-destructive technologies such as ultrasonic rail inspection. Determining the inspection frequency is a critical decision in railway infrastructure management [10]. In this thesis different cost models are employed to address the trade-offs among various factors related to rail defect inspection frequency. There by the inspection frequency which balances failure cost from a wide inspection interval and repeated detection costs from a close inspection interval is determined to be 2.35 times a year which is nearly in a five month interval. This economic detection interval is to maximize rail transportation safety and efficiency of the National Railway Network of Ethiopia.

1.2 STATEMENT OF THE PROBLEM

In railway tracks, rail welds are the main sources of irregularities and discontinuities, usually pores and inclusions, these initial cracks are subjected to increment with cyclic wheel loading which potentially cause derailment and devastating accidents.

Thus, the area requires intact observation and researches from a point of improving increasing service life of the rails and on-time inspection and replacement of the rails.

1.3 OBJECTIVES OF THE RESEARCH

The objectives of this research, through probabilistic approach are:

1.3.1 General Objective:

The main objective of the thesis is to determine the reliability to service life-induced fatigue crack growth rate of the rails on the weldment and estimation of inspection Interval.

1.3.2 Specific Objectives:

1. To analyze contact stress on the weld due to a vertical wheel load at different train speed.

2. To determine flaw (i.e. presence and size of crack) using an Ultrasonic flaw detector.

3. To determine the critical crack size (i.e. Size of a crack beyond which results fracture to the rail)

4. To predict Fatigue life of the rail-weld.

5. To determine probability of failure of the welded joint due to the vertical wheel load.

6. To determine the inspection interval of weld detection and rail replacement from a point of minimizing overall long term cost.

1.4 RESEARCH DELIMITATIONS

The scope of this thesis is to address the reliability to failure determination of the rail-welds unto computation of an economic interval of inspection for defects. Applicability of the result is to the National Railway Network of Ethiopia.

The research work has some limitations. These are:

1. Analysis is done with mechanical loads, only one load case, vertical wheel load, and only mode I failure is considered since these are critical to the damage tolerance of the weld at the bottom in its fatigue life.

2. Fatigue test is not conducted on the weld; rather, material parameters as K_{th}, K_{IC}, m and c are simply taken from literatures.

3. Weld irregularity based on either geometry or response to load is not considered,
4. Finite Element modeling is done using Abaqus. Even though Abaqus/CAE is a good modeling tool for various engineering applications, modeling welds is a complicated task; the simulation uses a sequentially coupled approach in which a thermal analysis is followed by a stress analysis. The temperature results from the thermal analysis are read into the stress analysis as loading to calculate the thermal stress effects. The thermal analysis makes use of Abaqus user subroutines [1]DFLUX, [2]GAPCON, and [3]FILM. The objective of these [4]AWI simulations is to predict post-weld deformation and residual stress distribution. However, this thesis is limited to use Abaqus/CAE since all these plug-ins are commercial. Thus, the thermal analysis is substituted by surface interaction, normal and tangential, between the base rail and the weld.

[1] To define the welding torch heat input as a concentrated flux [26]
[2] To activate the conduction of heat between the deposited weld material and the parent material [26]
[3] To activate film coefficient to simulate convective ambient cooing [26]
[4] Abaqus Weld Interface

1.5 RESEARCH METHODOLOGY

To address the general and specific objectives set in this thesis, a research methodology is developed which is summarized in figure 1.1.

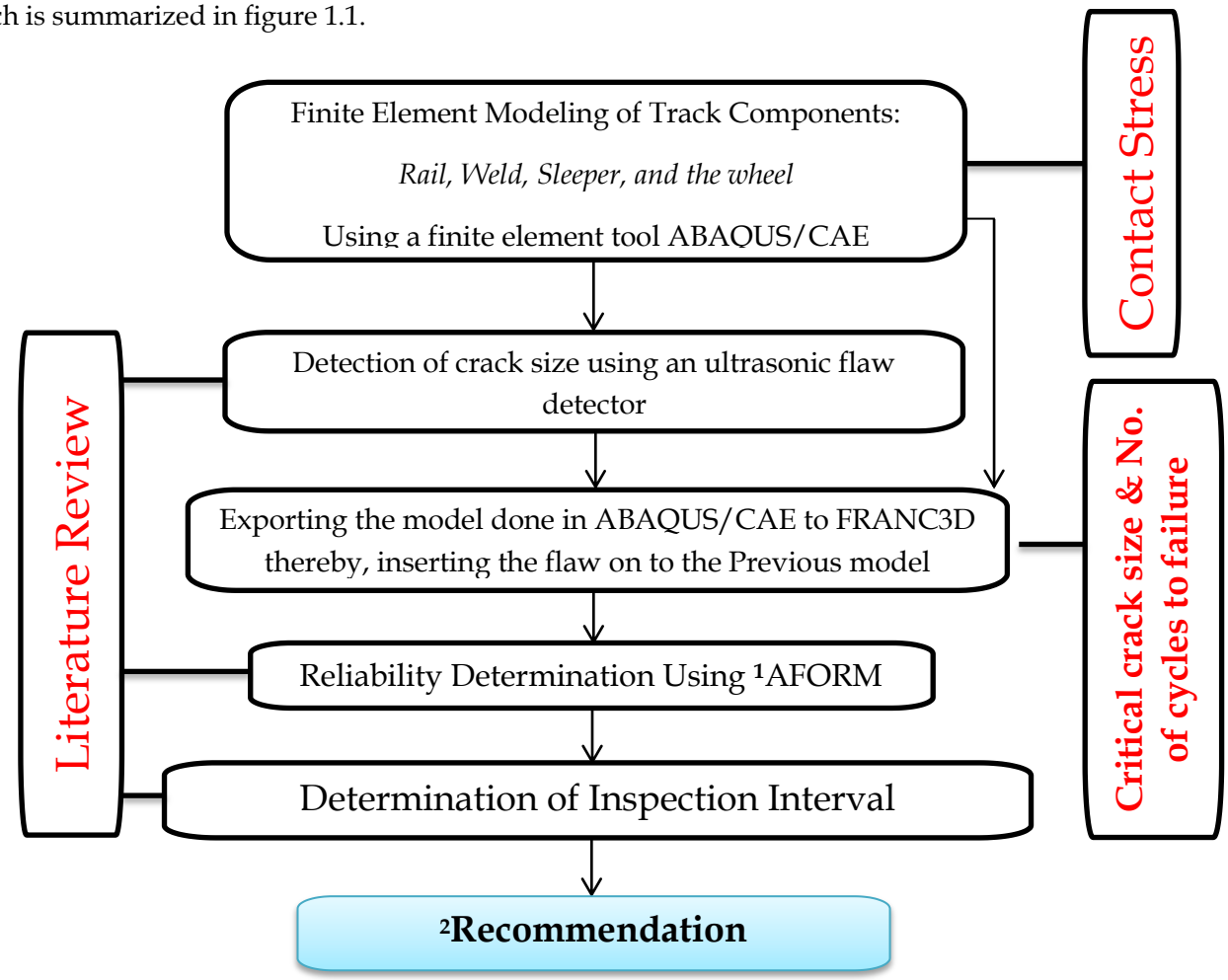

Figure 1.1: Research Methodology Flow Chart

[1]*Advanced First Order Reliability Method*
[2]*A Proper Maintenance Strategy*

1.6 SITE CHARACTERIZATION

Even though this paper work is not a case study, the data used for analysis are from the national railway and the applicability of the result shall also be to the national Railway.

***Table 1.1 Summary of Values of some parameters in the National Railway Network* [11]**

Parameter	**Values in National Railway Network**
Running Speed	80-120Km/hr.
Rail Section	50Kg/m
Rail Material	U75V rail
Tensile strength of the Rail	≥980Mpa.
Yield Strength of the Rail	≥880Mpa.
Specific length of the Rails	50m and 100m long
Method of joining the rails	most of the section is CW

***Figure 1.2: Rail joining with a screw (Left): Continuously Welded Rail (Right)* [4].**

2. LITERATURE REVIEW

2.1 OVERVIEW OF RAIL STRUCTURE

2.1.1 Introduction

Rails are longitudinal steel members that accommodate wheel loads and distribute these loads over the sleepers or supports, guiding the train wheels evenly and continuously. The rails must possess sufficient stiffness so that they can act as beams and transfer the concentrated wheel loads to the spaced sleeper supports without excessive deflection between supports. Rails are made from up to 0.82 % of carbon), which provides high fatigue toughness. Higher quality steels are now being produced, which has led to a significant improvement in rail fatigue performance and a considerable reduction in residual stress development [8].

Railway rails are manufactured in sections of 25 - 120 m length which are joined in track by either bolting or welding. Two advantages with welded rail sections in contrast to bolted ones are the lower maintenance cost and the improved dynamic behavior of the train-track-rail system [7]. Nowadays whenever possible, rails are joined by welding [3]. There are primarily two welding processes used today, flash-butt welding and Alumino-thermic (thermite) welding, but other methods are also employed such as gas pressure welding and enclosed arc welding.

Rail is one of the most important components of the track structure. Usually a flat bottom rail is used in conventional railway track, which could be divided into 3 parts: rail head, rail web and rail foot. Figure 2.1 shows the rail section. Many standards are used for classifying rail profiles, which are UIC, ASCE, AREMA and BS [8].

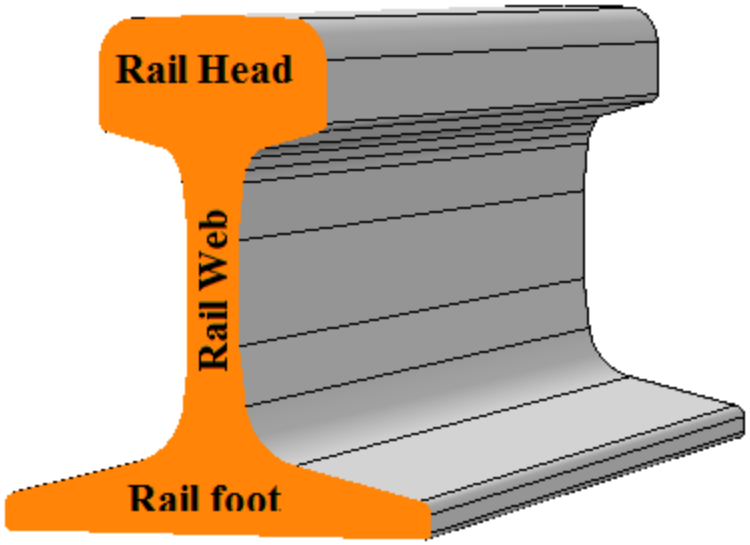

Fig 2.1 Cross section of a flat bottom rail

Rail steel is commonly carbon- manganese steel with mostly pearlitic microstructure. The methods used to make the steel for rails vary between the oxygen furnaces and more moderns electric-arc furnaces with vacuum degassing to remove hydrogen and oxygen and other gases from the molten steel from. The hydrogen is most likely to cause cracks in the rail head [8].

2.1.2 Rail defects

Rail failures can be divided into three main groups:

→ The rail manufacturing defects e.g. hydrogen cracks;
→ Defects due to the inappropriate handling, installation and use;
→ Defects caused by the exhaustion of the rail steels inherit to resistance to fatigue damage.

Due to the harsh working environment rails are susceptible to failure. In addition to bending and shear stresses, rails have to withstand dynamic loads, contact, thermal and residual stresses. The contact stresses between the wheel and rail are high with a very small contact area less than $1cm^2$. Residual stresses are also introduced into the rail during the straightening process during manufacturing.

Majority of rail failures are due to the transverse defects caused by the rail inner defects such as inclusions or fatigue cracks. The main reason for forming inner defects is hydrogen and oxygen. The hydrogen cracks within the steel that can lead to formation of kidney shape transverse defects upon traffic. Vacuum degassing and control cooling is used to extract gases [29].

2.1.3 Suitability of rails for welding

To ensure longevity of thermite weld, it is essential that only good quality rails are used for thermite welding. Good quality rails means fulfillment of the following requirements [3]:

→ Rail should be ultrasonically tested.
→ Rail should not be twisted or warped.
→ Rail ends should not be hogged or battered.
→ Rail should not be corroded.
→ Rail ends should not have bolt holes within 40mm from the rail ends. If bolt holes are existing within this limit, then micro cracks on periphery of the hole will propagate in the weld metal and cause weld fracture.
→ Rails should be free from excessive corrosion, reams, laps in flange, excessive wear at rail seat, scabs or wheel burns and corrugations.
→ For both new as well as second hand rails, before welding, it should be ensured that the end bends of the rails are within +0.5mm, -0.5mm in vertical and +0.5mm in lateral direction, when checked with one meter straight edge.
→ No Alumino-thermic welded joint shall be located closer than 4m from any other welded or fish-plated joint.

2.2 WELDING

2.2.1 Introduction

According to American Society of Welding, welding is a localized coalescence of metal where coalescence is produced by heating to suitable temperature, with or without the use of filler metal. The filler metal either has a melting point approximately the same as the base metal or below that of the metal. Heating to suitable temperature is compulsory; in addition either pressure or filler metal is required for welding to take place [15]. To heat metal during the (Alumino) thermic welding process, a powdery mixture of metallic aluminum (Al~22%) and iron scale (Fe3O4~78%) are used as a thermite [32].

There are 35 different methods of welding. However, all these methods are not suitable for rail welding. Out of which are only four suitable methods of welding for rails [15]:

1) Flash butt welding;
2) Alumino thermic welding;
3) Gas pressure welding, and
4) Metal arc welding.

Out of these four methods mentioned, the National Railway Network of Ethiopia uses the second one, Alumino thermite welding. Thus, this thesis work is focused on this welding type.

2.2.2 Alumino-Thermic Welding

2.2.2.1 Introduction

Alumino thermic welding is a process that produces coalescence of metals by heating them with superheated molten metal from an Alumino thermic reaction between a metal oxide and Aluminum. The Alumino thermic process is extensively being used world-wide for joining the ends of the rail. Alumino thermic process, known as Gold Schmidt process was developed in 1896 by a German chemist, Professor Hans Gold Schmidt. Alumino thermic process is based on the chemical reaction of iron oxide with Aluminum. The reaction, being 'exothermic' is associated with heat generation. Depending upon the particular oxide of iron used as shown below, the reaction can liberate heat energy sufficiently high to even vaporize the resultant iron. However, heat losses, which invariably occur, ensure that iron in molten state is available. The reaction process can be described by the following equations [15]:

$$3Fe_3O_4 + 8Al = 4Al_2O_3 + 9Fe \ (3088℃, 719.3 \text{ kcal}) \quad [2.1]$$

$$3FeO + 2Al = Al_2O_3 + 3Fe \ (2500℃, 187.1 \text{ kcal}) \quad [2.2]$$

$$Fe_2O_3 + 2Al = Al_2O_3 + 2Fe \ (2960℃, 181.5 \text{ kcal}) \quad [2.3]$$

2.2.2.2 Process and Method Improvement in Alumino-Thermic Welding

Even though process and method improvement of the AT welding is not in the scope of this thesis, It's worth listing some improvements in the technology. The proper utilizations of these technological advancements and other further researches have a lot do with minimizing the initial crack size on the weldment. This is summarized in Table 2.1. For further reading on these improvements [29] can be referred.

***Table 2.1: Process and Method Improvement in AT* [29].**

Process Improvement	Method Improvement
Weld hardness and grain size Improvement	Squeeze Welding Practice
Crucible Improvement	Vibration in Liquid Weld steel
Mold Improvement	Filtration of Liquid Weld Steel
Manufacturing practice Improvement	Electro-Magnetic Stirring of liquid Weld steel
	Post-Weld Normalizing

2.2.3 Rail weld tests

The first test after the welding is visual examination of the weld for visible defects such as geometry, and is usually carried out by the welding personnel on site. The tests carried out in the laboratory are: Ultrasonic test, hardness test, slow bends test, fracture surface examination, and micro- and macro structure examination.

Test methods for both TW and FBW welds are similar.

2.2.3.1 Ultrasonic Test

2.2.3.1.1 Introduction

Ultrasonic Testing (UT) uses high frequency sound waves (typically in the range between 0.5 and 15 MHz) to conduct examinations and make measurements. It has wide use in engineering applications (such as flaw detection/evaluation, dimensional measurements, material characterization, etc.)

In general, ultrasonic testing is based on the capture and quantification of either the reflected waves (pulse-echo) or the transmitted waves (through-transmission). Each of the two types is used in certain applications, but generally, pulse echo systems are more useful since they require one-sided access to the object being inspected [28].

2.2.3.1.2 Basic Principles

A typical pulse-echo UT inspection system consists of several functional units, such as the pulser/receiver, transducer, and a display device. A pulser/receiver is an electronic device that can

produce high voltage electrical pulses. Driven by the pulser, the transducer generates high frequency ultrasonic energy. The sound energy is introduced and propagated through the materials in the form of waves. When there is a discontinuity (such as a crack) in the wave path, part of the energy will be reflected back from the flaw surface. The reflected wave signal is transformed into an electrical signal by the transducer and is displayed on a screen. Knowing the velocity of the waves, travel time can be directly related to the distance that the signal traveled. From the signal, information about the reflector location, size, orientation and other features can sometimes be gained [28].

2.2.3.1.3 Advantages and Disadvantages:

The primary advantages and disadvantages when compared to other NDT methods are:

Advantages

→ It is sensitive to both surface and subsurface discontinuities.
→ The depth of penetration for flaw detection or measurement is superior to other NDT methods.
→ It provides instantaneous results.
→ Detailed images can be produced with automated systems.
→ It is nonhazardous to operators or nearby personnel and does not affect the material being tested.
→ It has other uses, such as thickness measurement, in addition to flaw detection.
→ Its equipment can be highly portable or highly automated.

Disadvantages

→ Surface must be accessible to transmit ultrasound.
→ Skill and training is more extensive than with some other methods.
→ It normally requires a coupling medium to promote the transfer of sound energy into the test specimen.
→ Materials that are rough, irregular in shape, very small, exceptionally thin or not homogeneous are difficult to inspect.
→ Linear defects oriented parallel to the sound beam may go undetected.
→ Requires accurate measurement of microseconds, which is sometimes difficult.
→ Reference standards are required for both equipment calibration and the characterization of flaws.

2.2.3.1.4 Physics of Ultrasonic

Sound is produced when a body vibrates and is propagated only within a medium. Sound waves are classified in terms of frequency, which is the number of vibrations per second or Hertz; the frequency scale relating the sonic and ultrasonic ranges is shown in Fig. 2.2.

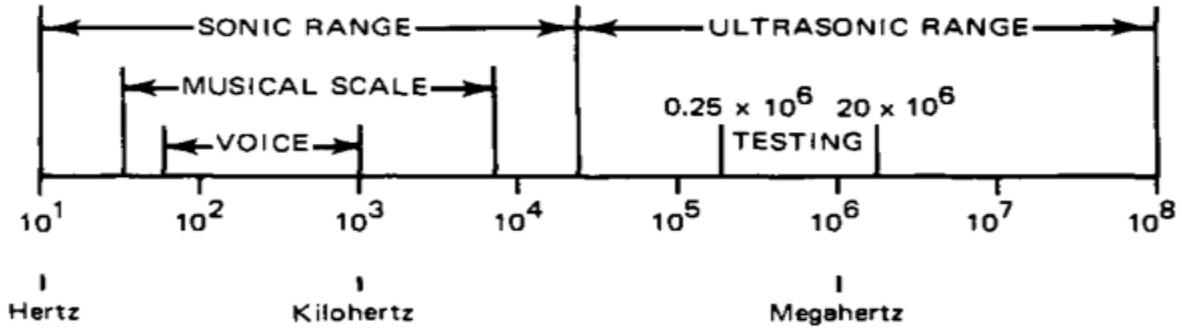

Figure 2.2: Frequency scale relating to the sonic ad ultrasonic ranges [2].

The basic formula, to which reference is made throughout the whole study of ultrasonic examination, is:

$$V=f*\lambda \qquad [2.4]$$

…Where: V-Velocity [mm/s]

f- Frequency [Hz]

λ- Wave length [mm]

Table 2.2 Value of sound velocity for a number of different media **[28]:**

Material	**Sound Velocity [mm/s*10^6]**	**Density [gm./mm^3*10^{-9}]**
Steel	5.85	7.8
Oil	1.38	0.92
Water	1.49	1
Air	0.38	0.0013
Glycerine	1.9	1.23
Plexiglas	2.7	1.2

2.2.3.1.5 Measurement and Calibration Techniques

A. Normal Beam Inspection

Pulse-echo ultrasonic measurements can determine the location of a discontinuity in a part or structure by accurately measuring the time required for a short ultrasonic pulse generated by a transducer to travel through a thickness of material, reflect from the back or the surface of a discontinuity, and be returned to the

transducer. In most applications, this time interval is a few microseconds or less. The two-way transit time measured is divided by two to account for the down-and-back travel path and multiplied by the velocity of sound in the test material. The result is expressed in the well-known relationship:

$$d=Vt/2 \quad [2.5]$$

d- Distance from the surface to the discontinuity

t- Round trip travel time

V-Velocity of sound in the specimen

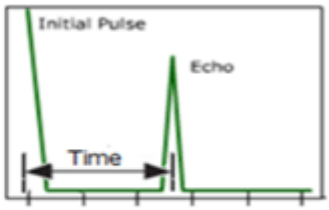

Fig 2.3 Pulse Echo Ultrasonic Measurement [28]

B. Angle Beam Inspection

Angle beam transducers and wedges are typically used to introduce a refracted shear wave into the test material. An angled sound path allows the sound beam to come in from the side, thereby improving detectability of flaws in and around welded areas.

Angle beam inspection is somehow different than normal beam inspection. In normal beam inspection, the back wall echo is always present on the scope display and when the transducer passes over a discontinuity a new echo will appear between the initial pulse and the backwall echo. However, when scanning a surface using an angle beam transducer there will be no reflected echo on the scope display unless a properly oriented discontinuity or reflector comes into the beam path.

If a reflection occurs before the sound waves reach the back wall, the reflection is usually referred to as first leg reflection. The angular distance (Sound Path) to the reflector can be calculated using the same formula used for normal beam transducers (but of course using the shear velocity instead of the longitudinal velocity). Knowing the angle of refraction for the transducer, the surface distance to the reflector and its depth can be calculated as:

$$\textbf{Surface Distance} = \textbf{Sound Path} * \sin\theta_R \quad [2.6]$$

If a reflector came across the sound beam after it has reached and reflected off the backwall the reflection is usually referred to as second leg reflection. In this case the Sound Path (the total sound path for the two legs) and the surface Distance can be calculated using the same equations given above.

The most commonly occurring defects in welded joints are porosity, slag inclusions, lack of side-wall fusion, and lack of intermediate-pass fusion, lack of root penetration, undercutting, and longitudinal or transverse cracks. With the exception of single gas pores all the listed defects are usually well detectable using ultrasonics. [30]

2.3 FRACTURE MECHANICS

Fracture mechanics is broadly classified into two types: Linear Elastic Fracture Mechanic (LEFM) and elastic plastic fracture mechanic (EPFM). LEFM assumes small deformation and minimal yielding at the crack tip, while EPFM can account large deformation and plastic effects.

2.3.1 Linear Elastic Fracture Mechanics

In Linear elastic fracture mechanics stress intensity factors (SIF), K is a measure of the stress field at the crack tip.

The stress intensity factors are used for the expression of the stress field at a crack tip and serve as a measure of the severity of the crack tip for different crack configurations. They have a central role in crack assessment, where they can be related to critical levels of stresses resulting in crack growth and eventually fracture.

There are three independent loading modes used in fracture mechanics; Mode I, II and III. They can be seen in Figure 2.4 a-c. Mode I is the crack opening mode where the crack surfaces move apart and is the most common load type. The Mode II is an in- plane shear mode where the crack surfaces slide apart perpendicular to the crack. Mode III is an out-of-plane shear mode where the crack surfaces slide apart in a tearing manner.

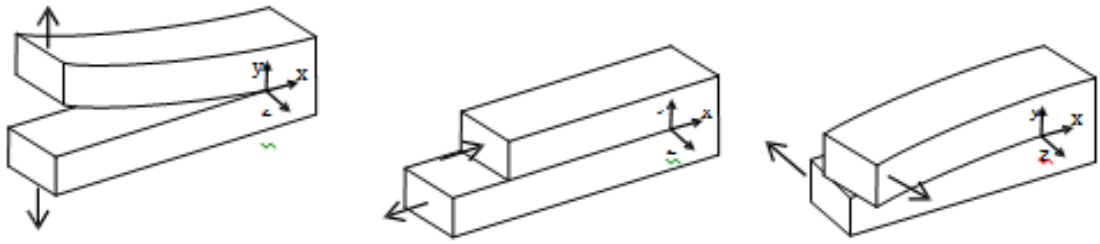

. a) Mode Ⅰ, b) Mode Ⅱ, c) Mode Ⅲ

Figure 2.4: The three loading modes [23].

The elastic stress field near the crack tip is defined using K_I, K_{II}, and K_{III}. Where K_I, K_{II}, and K_{III} are the stress intensity factors for the respective mode. A schematic definition of the stress field, radial distance and angle can be seen in Figure 2.5.

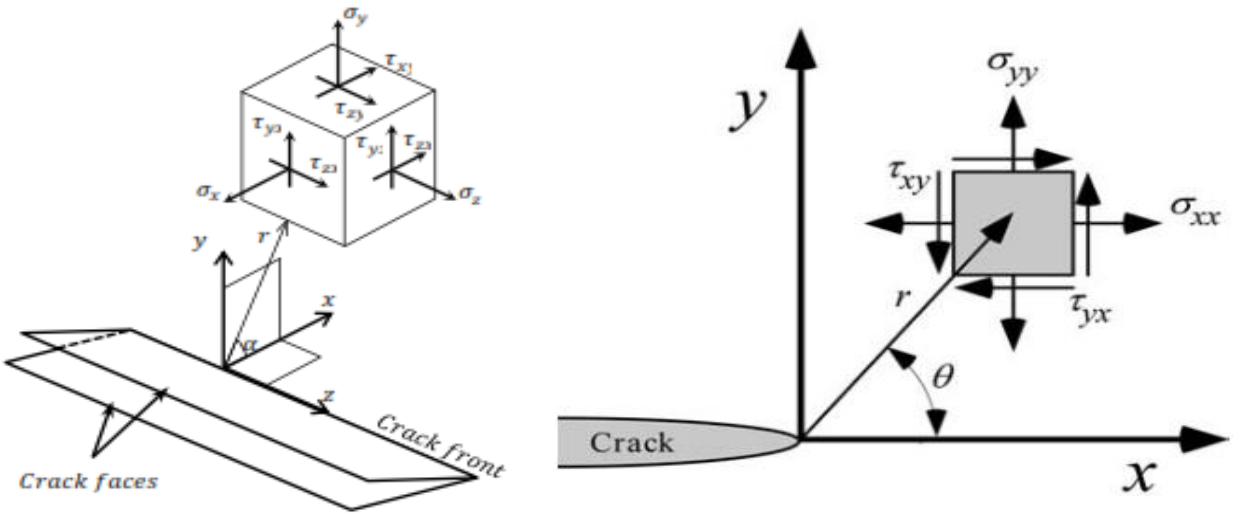

Figure 2.5: A three-dimensional coordinate system describing the stresses near the crack front [21, 42].

In general, the stress intensity factors K are proportional to the remote stress σ, crack size a and the geometry of the mechanical component with crack:

$$\mathbf{K} = \mathbf{f}(\boldsymbol{\sigma}, \mathbf{a}, \mathbf{geometry}) . \qquad \mathbf{[2.7]}$$

For common test specimens equations for (mainly mode I) stress intensity factors K can be found in professional literature [1].

2.3.2 Fracture Testing of Weldments

Welded joints have decidedly heterogeneous microstructures and, in many cases, irregular shapes. Weldments also contain complex residual stress distributions. Most existing fracture toughness testing standards do not address the special problems associated with weldment testing. The factors that make weldment testing difficult (i.e., heterogeneous microstructures, irregular shapes, and residual stresses) also tend to increase the risk of brittle fracture in welded structures. Thus, one cannot simply evaluate the regions of a structure where ASTM testing standards apply, and ignore the fracture properties of Weldments. A weldment may be sectioned and examined metallographicaly to determine whether or not the fatigue crack sampled the intended microstructure.

For weld metal testing, the through-thickness orientation is usually preferable because a variety of regions in the weld are sampled. However, there may be cases where the surface-notched specimen is the most suitable for testing the weld metal. For example, a surface notch can sample a particular region of the weld metal, such as the root or cap, or the notch can be located in a particular microstructure, such as unrefined weld metal.

It is to present the effect of temperature on the mechanical properties of high-strength alloy structural Q460 steel. The strength and stiffness properties of steel degrade with temperature and this deterioration has to be properly accounted for in the fire resistant design of steel structures. The

strength and stiffness degradation is also influenced by the composition of steel. Because of a lack of data specific to high-strength steel, design standards assume the high temperature strength variation of steel to be same as that of conventional mild steel. To overcome this drawback, strength and stiffness properties of steel were measured at various temperatures in the range of 20-800°C. A relative comparison of measured data indicates that high-strength steel experiences a slower loss of strength and stiffness with temperature than conventional steel. Data generated from the experiments, namely, load- displacement relationships and vibration frequency, were utilized to develop relations for yield strength, tensile strength, and elastic modulus of steel as a function of temperature.

It showed that there is a loss of '-2% Elastic Modules with an increment of every 167.481℃ for high strength alloys and for lower strength alloys there is a large variation in effect of temperature.

The proposed relations developed specifically for high-strength steel can lead to better fire resistance prediction of steel structure systems. For thermite welds after crystalline rearrangement poison's ratio and modules of Elasticity are in the range of -17% to +13% and∓5%, respectively [43]. Since the material at the running surface, and some millimeters beneath, is strongly deformed and compressional residual stresses are generated in that region, and since the global bending stresses are highest in the foot, fatigue cracks in the welded rails tend to grow from underneath rather than from the rail head. [17]

Figure 2.6: Fracture of a Thermic weld in the foot [17]

2.3.3 Fatigue Crack Growth and Laws

Based on fracture mechanic theory, fatigue crack growth models have been developed to evaluate damage tolerance in structures.

A better understanding of the fatigue life under cyclic loading can be obtained from the block diagram suggested by Beden et al, 2009 is shown in Figure 2.7. It shows that the process consists of two phases, the crack initiation life (nucleation and micro crack growth) followed by a crack growth period (macro crack growth) until failure.

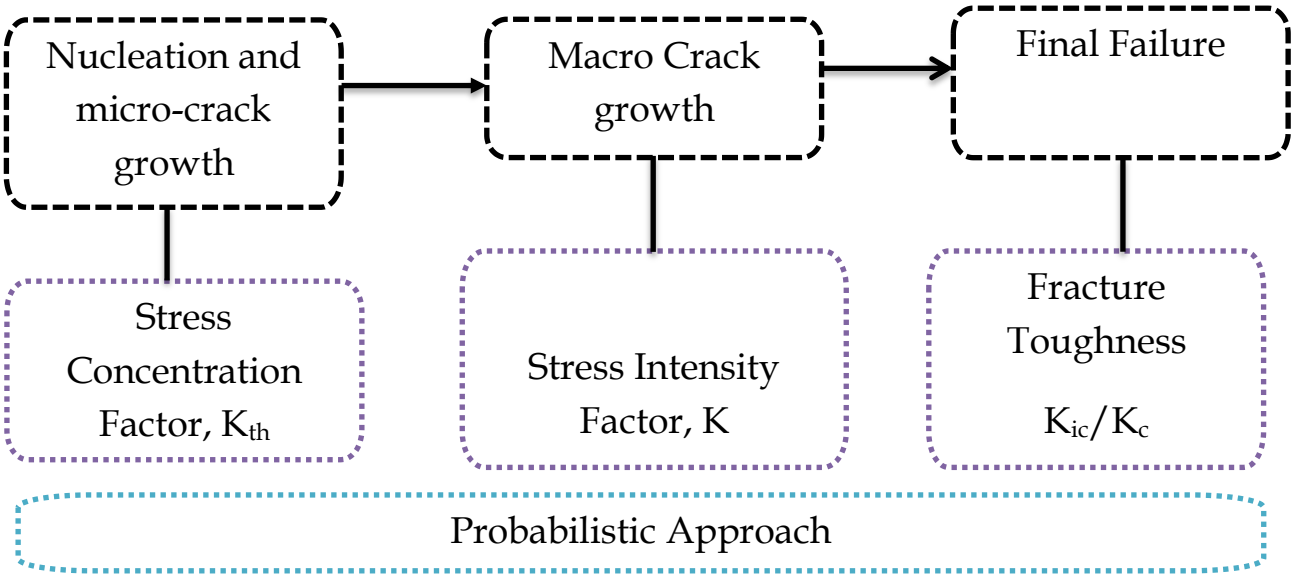

***Figure 2.7: Block Diagram of a crack growth* [35].**

2.4 STRUCTURAL RELIABILITY

2.4.1 Introduction

For many years it has been assumed in design of structural systems that all loads and strengths are deterministic. The strength of an element was determined in such a way that it exceeded the load with a certain margin. The ratio between the strength and the load was denoted the safety factor (SF). This number was considered as a measure of the reliability of the structure. In codes of practice for structural systems values for loads, strengths and SF are prescribed [19].

These values are traditionally determined on the basis of experience and engineering judgment. However, in new codes partial safety factors are used. Characteristic values of the uncertain loads and resistances are specified and partial safety factors are applied to the loads and strengths in order to ensure that the structure is safe enough. The partial safety factors are usually based on experience or calibrated to existing codes or to measures of the reliability obtained by probabilistic techniques. This shows structural analysis and design have traditionally been based on deterministic methods. However, uncertainties in the loads, strengths and in the modeling of the systems require that methods based on probabilistic techniques in a number of situations have to be used. This drawback of the deterministic method generates a structural Reliability Approach [20].

Structural reliability theory is essentially the application of probability theory to the modeling of structural failures and the prediction of success probability. Reliability of structural systems can be defined as the probability that the structure under consideration has a proper performance throughout its lifetime. Reliability methods are used to estimate the probability of failure. The information of the models, which the reliability analyses are based on, is generally not complete. Therefore the estimated reliability should be considered as a nominal measure of the reliability and not as an absolute number.

However, if the reliability is estimated for a number of structures using the same level of information and the same mathematical models, then useful comparisons can be made on the reliability level of these structures. Further design of new structures can be performed by probabilistic methods if similar models and information are used as for existing structures which are known to perform satisfactory. If probabilistic methods are used to design structures where no similar existing structures are known then the designer has to be very careful and verify the models used as much as possible [44].

In order to be able to estimate the reliability using probabilistic concepts it is necessary to introduce stochastic variables and/or stochastic processes/fields and to introduce failure and non-failure behavior of the structure under consideration.

The main steps followed are [35]:

1. Select a target reliability level.
2. Identify the significant failure modes of the structure.

Typical failure modes to be considered in a reliability analysis of a structural system are yielding, buckling (local and global), fatigue and excessive deformations.

3. Decompose the failure modes in series systems or parallel systems of single components (only needed if the failure modes consist of more than one component).
4. Formulate failure functions (limit state functions) corresponding to each component in the failure modes.
5. Identify the stochastic variables and the deterministic parameters in the failure functions. Further specify the distribution types and statistical parameters for the stochastic variables and the dependencies between them.

The uncertainty modeled by stochastic variables can be divided in the following groups:

   a. Physical uncertainty: or inherent uncertainty is related to the natural randomness of a quantity, for example the uncertainty in the yield stress due to production variability.
   b. Measurement uncertainty: is the uncertainty caused by imperfect measurements of for example a geometrical quantity.
   c. Statistical uncertainty: is due to limited sample sizes of observed quantities.
   d. Model uncertainty: is the uncertainty related to imperfect knowledge or idealizations of the mathematical models used or uncertainty related to the choice of probability distribution types for the stochastic variables.

6. Estimate the reliability of each failure mode.
7. In a design process change the design if the reliabilities do not meet the target reliabilities. In a reliability analysis the reliability is compared with the target reliability.

2.4.2 First Order Reliability Method (FORM)

First-order reliability method, (FORM), is a semi-probabilistic reliability method devised to evaluate the reliability of a system. These methods are characterized by the iterative, linear approximation to the performance function

The simplest way of explaining this approach is to examine the simplest case of two independent random variables. Let R represent a random variable describing the strength of a system and let S represent a random variable describing the stress or load placed on the system. System failure occurs when the stress on the system exceeds the strength of a system: $\Omega = \{(r, s): S > R\}$. Figure 2.8 depicts the concepts of a limit state function and the associated failure/success regions.

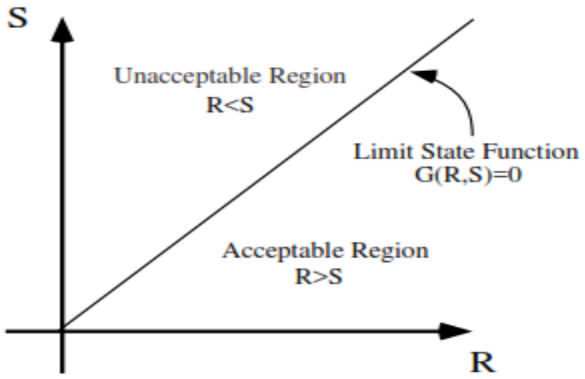

Figure 2.8: Limit State Function

Not only fatigue but also strength of materials is so sensitive that they are statistical by nature. In addition, it is intricate to evaluate meticulous probability of failure in materials applied to cycle loads in variable times. Even if estimated, the results can be much widely varied.

In general, solving the integrals from the above equation is a complicated process and can be done in closed form only for a simple case. Moreover, the calculation of multi-dimensional integral requires the information of the joint probabilistic density function or each probabilistic density functions of variables. For practical reasons, the information is often unavailable or too difficult to obtain sufficient data. Therefore, some alternative methods are needed in order to evaluate the probability of failure; these methods can be either analytical or numerical. Analytical methods represent the reliability as a reliability index: beta. One of them is the first order reliability method based on determining mean and variance of variables. Numerical methods evaluate directly through simulations, such as the Monte Carlo simulation, or by using reliability software's such as STRUREL, COMREL and VAP.

The concept by Cornell has an invariance problem that the results change by the way to define limit state function. Hence, Hasofer - Lind (1974) improves the concept to first order reliability method. The reliability index: beta is defined as the minimum distance from the origin to a failure surface of a space defined with the random vectors in this approach. The most probable point (MPP) of failure, the design point, or the point on the limit state that lies closest to the origin, is found in a standard normal space U for a single failure driven limit state equation. The components of U are normally distributed with zero mean and unit variance and are statically independent.

Any set of continuous random vectors can be transformed in to U using the Rosenblatt transformation.

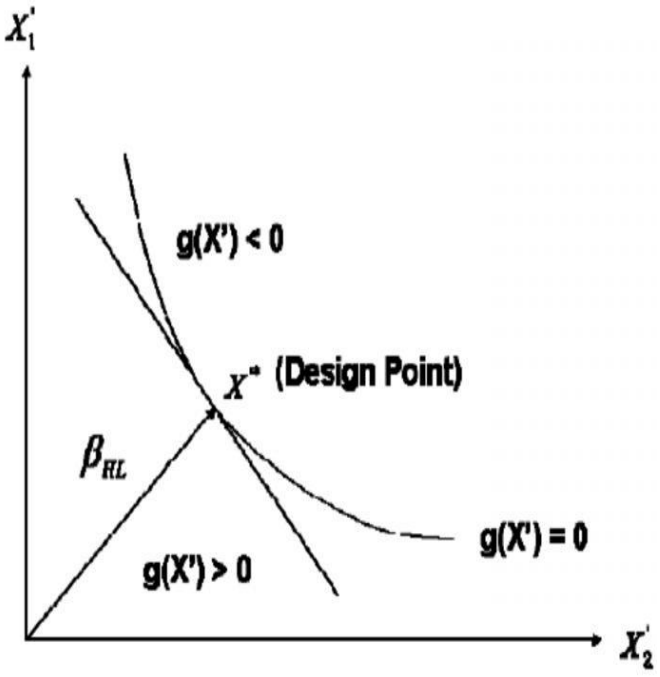

The most probable point u* also lives in the hyper surface and the location is the closest point on the limit state function to the origin in U space. The most probable point can be found by figuring out the following constrained optimization problem.

$$\mathbf{MinD}=\sqrt{U^T U} \qquad \textbf{[2.8]}$$

Where D is the distance from the origin to the most probable point, and T is the transpose notation.

Although various algorithms exist to perform the most probable point search, one of them is Rackwitz-Fieesler (1978) algorithm, which is based on Newton-Raphson root solving recursive approach

***Figure 2.9: Hasofer-Lind Reliability Index: Non Linear Performance Function* [20].**

When the limit state equation is nonlinear, the gradient is not constant and varies from one point to another point. Hence, the most probable point has to be searched through the recursive formula. If the limit state equation is linear, first order reliability method gives the correct value regarding probability of failure.

The algorithm convergence satisfying the following criteria:

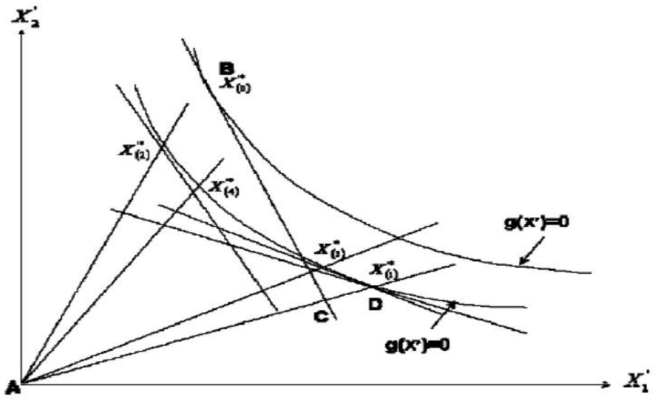

***Figure 2.10: Algorithm for finding D* [20].**

$$\textbf{If } g(U_k) \leq \in, \boldsymbol{Stop} \qquad \textbf{[2.9]}$$

Where ε is a small quantity ($=10^{-3}$)

2.5 INSPECTION INTERVAL

A larger proportion of rail breaks are caused by rail fatigue due to cyclic loading of the rail by the passage of trains [10]. As rail fatigue fracture surfaces grow in size, they may be identified by non-destructive inspection methods, such as ultrasonic testing.

Preventive replacement and periodical inspections are two major approaches used for improving system availability and reducing maintenance cost. Preventive replacement approach replaces a system/component/unit at a certain time interval or at a failure, depending on which one is earlier. A great deal of work has been done on inspection and preventive maintenance strategies. Most of the published papers on inspection strategies focus on finding hidden failures [25]. Hidden failure refers to the case where a failure remains undiscovered unless an inspection or a test is performed. The interval between two successive inspections is therefore called the failure finding interval. There are two types of hidden failures in general.

Type I: Protective devices or standby unit. The function of these devices is to protect the main system in case of failures. Safety devices, emergency devices, standby units are this type of hidden failure devices their failure will not cause direct loss if they are not detected.

Type II: Operating devices, railway rails are this type of devices. They are operating systems, and their failure will cause direct loss. Different from the above mentioned hidden failures, some failures can be detected even before they happen. For example, a growing crack length on a joint or a thinning connector line is an early sign of an imminent failure. This type of failures is called revealed failures, which is the focus of this thesis. This inspection strategy is especially useful for failures caused by degradation. Units that are going to fail soon will be replaced or repaired at inspection if there is evidence of an oncoming failure. For example, if a failure is going to happen at time 100, an inspection at time 20 may not be able to detect it since the signs of the coming failure may not be strong enough. However, if an inspection is conducted at time 95, then strong evidences can be seen that the component is going to fail soon.

3. WHEEL-RAIL CONTACT STRESS COMPUTATION

3.1 INTRODUCTION

The general conditions considered during the wheel rail contact simulation are the assumption of the Hertz contact theory. The common Hertz assumptions are:

→ Isotropic and homogenous material;
→ No friction (completely smooth body interaction);
→ Elastic Contact, and
→ Both bodies were considered as half-spaces.

When two bodies (wheel and rail) are in contact, stresses and strains appear. A large force from the first body (wheel) is transferred to the second body (rail) through a small contact patch of about lcm^2.

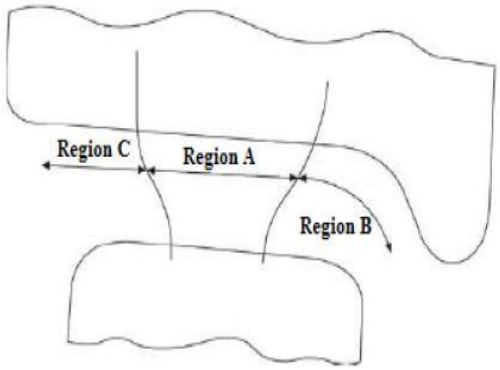

Figure 3.1: Wheel- Rail Contact Zones/Regions

Wheel rail contact regions can be classified as shown in the above figure:

a) Region A - wheel tread -rail head contact: this contact zone is most common contact region with lower contact stress.

b) Region B - wheel flange- rail gauge corner: this contact zone is much smaller contact area and more severe; higher contact stresses and wear rates occurs.

c) Region C - wheel and rail outer sides contact: this contact zone is least likely contact region with high contact stress, and undesirable wear lead to incorrect steering of wheelset.

3.2 RAIL-WHEEL CONTACT STRESS

The forces arising between wheel and rail contact generate contact stresses in a local volume of the two bodies. Hertzian-Contact-Model is most well-known calculation model for this local stresses. Hertzian model describes the local stresses with good accuracy for the most common wheel-rail contact problems. This model also provides a good understanding of general contact phenomena. Although

Hertzian theory is valid only for elastic contacts it can be useful far beyond that. Limited plasticity will not affect the contact stresses very much. In wheel-rail contact the two bodies generally have a non-conformal contact.

3.2.1 Hertzian Contact

The contact forces (stresses) from the wheel load are transferred at a small contact patch, in one or several contact locations. According to Hertz theory, the normal pressure is distributed as an ellipsoid over the elliptic contact area.

When a wheel and a rail are brought into contact under the action of the static wheel load, the contact area and the pressure distribution are usually determined using the Hertz theory. In Hertz contact theory, no plastic deformation in the contact patch is assumed, and the radii of the curvature of wheel and rail profiles in the contact patch are assumed to be constant.

The distribution of the contact pressure in this elliptical area represents a semi-ellipsoid, which can be expressed as:

$$\mathbf{P(x,\ y)} = \sqrt{\mathbf{1} - \frac{x^2}{a^2} - \frac{y^2}{b^2}} \left[\frac{3N}{2\pi ab}\right] \qquad [\mathbf{3.1}]$$

The wheel-rail contact problem has two parts

→ Contact geometry (i.e. contact location and contact angle)
→ Contact forces (normal and tangential contact force)

The wheel-rail contact solution, both determining the contact geometry (contact location, contact angle, etc) and calculation of contact forces, is important and are interrelated.

The location of the contact point depend on the relative position of the wheelset with respect to the rail and the two bodies profile

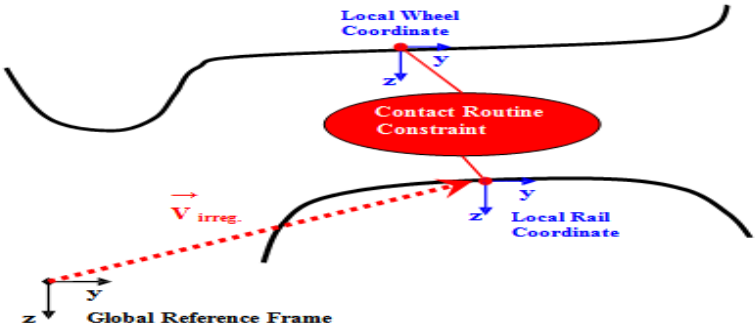

Figure 3.2: Contact location (i.e. relative position of the rail to the wheel)

Based on the Hertz contact theory, the contact point is very small relative to the overall dimension of railway wheel and rail surfaces. This very small contact point has elliptical shape. From

the above formula a and b are semi axes of the contact ellipse whereas X and Y are the required coordinates to specify the point of contacts on the rail surface based on the lateral rail surface parameter.

If x=0 and y=0 that is if the point of contact is on the centerline of the rail head the stress is maximum, which is equal to:

$$\mathbf{P_0}=\frac{3N}{2\pi ab} \qquad [3.2]$$

Where, a and b are the half width of the contact area in the longitudinal x and lateral y directions, respectively, and N is the total normal contact force.

Important assumptions that are made here are linear elastic material, small contact area compared to the radii at the contact of the bodies and to other dimensions (semi-infinite bodies are assumed), and smooth surfaces at both macro and micro scale.

The contact ellipse semi-axes a and b are determined as follows:

$$a=m\sqrt[3]{\frac{3\pi}{4}\frac{(K1+K2)N}{A+B}} \qquad [3.3]$$

$$b=n\sqrt[3]{\frac{3\pi}{4}\frac{(K1+K2)N}{A+B}} \qquad [3.4]$$

Where the modulus K_1 and K_2 are material properties of wheel and rail (the relative change in the volume of a body produced by unit compressive or tensile stress acting uniformly over its surface) and are given by:

$$\mathbf{K_i}=\frac{1-vi^2}{\pi Ei} \qquad [3.5]$$

$$\mathbf{A+B}=\frac{1}{2}\left(\frac{1}{R1}+\frac{1}{R1'}+\frac{1}{R2}+\frac{1}{R2'}\right) \qquad [3.6]$$

$$\mathbf{A-B}=\sqrt{\left(\frac{1}{R1}-\frac{1}{R1'}\right)^2+\left(\frac{1}{R2}-\frac{1}{R2'}\right)^2+2\left(\frac{1}{R1}-\frac{1}{R1'}\right)\left(\frac{1}{R2}-\frac{1}{R2'}\right)cos2\varphi} \qquad [3.7]$$

$$\mathbf{Cos}\theta=\frac{B-A}{B+A} \qquad [3.8]$$

…where in equation 3.3-3.8

R_1-Is the nominal rolling radius of the wheel

R_2-is the nominal rolling radius if the rail.

R_1'- is the nominal transverse radii of curvature of the wheel

R_2'-is the nominal transverse radii of curvature of the rail.

E_1 and E_2-are the Modules of Elasticity of the Wheel and the rail, respectively

v_1 and v_2 –are the Poisson's ratio of the wheel and the rail, respectively.

m, n- are geometric properties of the wheel and the rail.

φ-is the angle between the radius of the wheel and the rail, called yaw rotation

θ-is the angle between the principal axes.

***Table 3.1: Hertz Coefficients n, m for different angle θ* [40]**

$\theta(deg)$	m	n	$\theta(deg)$	m	n	$\theta(deg)$	m	n
0.5	61.4	0.1018	10	6.604	0.3112	60	1.486	0.717
1	36.89	0.1314	20	3.813	0.4125	65	1.378	0.759
1.5	27.48	0.1522	30	2.731	0.493	70	1.284	0.802
2	22.26	0.1691	35	2.397	0.53	75	1.202	0.846
3	16.5	0.1964	40	2.136	0.567	80	1.061	0.893
4	13.31	0.2188	45	1.926	0.604	85	1	0.944
6	9.79	0.2552	50	1.754	0.641	90	1	1
8	7.86	0.285	55	1.611	0.678			

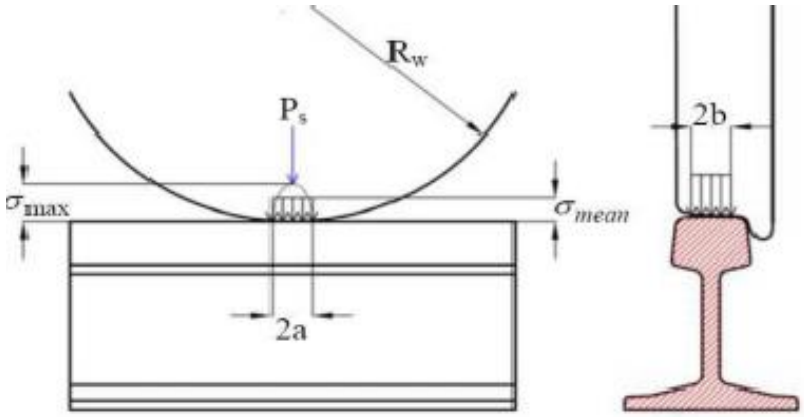

Figure 3.3: Wheel-Rail Contact Stress

3.2.2 Dynamic Effect

Stresses in the wheel and rail contact area at dynamic load modes usually occur in the elastic- plastic areas and loading this area usually leads to a breakage which is a result of low cyclic fatigue.

For a static axle or wheel load, the dynamic load F_V^{dyn} can be modeled as a statistical distribution, the upper bound of which can be used as worst condition for design purpose.

This is realized by multiplying the static load with a magnification factor K_{dyn} as:

$$\mathbf{F_v^{dyn}=K_{dyn}*F_v} \qquad [3.9]$$

$$\mathbf{F_v=1+3*n*\varphi} \qquad [3.10]$$

According to Deutsche Bahn [40], the magnification factor depends on the properties and quality of the train and the track, and on the train speed.

Where … n= 0.15 to 0.25 for different types of tracks, 0.2 for normal wheel-rail contact

φ is coefficient due to speed

$$\varphi = \begin{cases} 1 & for\ V \le \frac{60Km}{hr} \\ 1+\frac{0.5(V-60)}{190} & for\ 6o \le V \le \frac{300Km}{h}\ Passenger\ Train \\ 1+\frac{0.5(V-60)}{80} & for\ 60 \le V \le \frac{140Km}{h}\ freight\ Train \end{cases} \qquad [3.11]$$

For the National railway network design the design axe load is 25Ton, thereby a 460mm radius standard wheel impose a 12.5Tone load on a 300mm radius wheel head. So the maximum contact pressure will be calculated from the Hertzian contact stress.

Table 3.2: Material Constants used in the model

Materials	Steel	Weld	Wheel
$E(N/mm^2)*10^3$	210 Gpa	190GPa	210GPa
V	0.3	0.34	0.3
R(mm)	∞	∞	460
R'(mm)	300	300	∞

$F_V = mg = 12.5ton * \frac{1000Kg}{Ton} * 9.81m/s^2$ = 122.625KN

For a static axle or wheel load, the dynamic load F_V^{dyn} can be modeled as a statistical distribution, the upper bound of which can be used as worst condition for design purpose. Thus for the design maximum speed on the line the dynamic load is obtained by multiplying with respective amplification factor.

$$\varphi = 1 + \frac{0.5(120-60)}{80} = 1.375 \ \ and\ taking\ n = 0.2$$

K_v=1+3*0.2*1.375=1.825

F_v^{Dyn}=1.825*122.625=223.79KN

$A+B=\frac{1}{2}(\frac{1}{R1}+\frac{1}{R1'}+\frac{1}{R2}+\frac{1}{R2'})$ =0.002754/mm

$$\mathbf{A-B=}\sqrt{(\frac{1}{R1}-\frac{1}{R1'})^2+\frac{1}{R2}-\frac{1}{R2'})^2+2\left(\frac{1}{R1}-\frac{1}{R1'}\right)\left(\frac{1}{R2}-\frac{1}{R2'}\right)cos2\varphi}=\mathbf{0.0005872/mm}$$

$Cos\boldsymbol{\theta} = \frac{B-A}{B+A}$=77.757°

Then, the Hertzian coefficients can be obtained from Table 3.1 interpolation between 75° and 8o°

m=1.161; *n*=**0.872**

$K_1 = \frac{1-0.3^2}{3.14*2.1*10^{11}Pa} = 1.38e^{12}$

$K_2 = \frac{1-0.34^2}{3.14*1.9*10^{11}Pa} = 1.48e^{12}$

At this point it's possible to determine the contact patch elliptical geometric dimensions a and b

$a = 1.161 * \sqrt[3]{\frac{3\pi}{4}\frac{(1.38e^{12}+1.48e^{12})N}{\frac{0.002754}{mm}}} = \mathbf{9.499mm}$

$b = 0.872 * \sqrt[3]{\frac{3\pi}{4}\frac{(1.38e^{12}+1.48e^{12})N}{0.002754/mm}} = \mathbf{7.135mm}$

Thus, the maximum contact pressure for this particular case is

$P_o = \frac{3*223.79e^3N}{2\pi 1.565*1.175} = \mathbf{1577.31MPa}$

Table 3.3: Contact Pressure comparison of the base Rail to the weld with lesser toughness at different speed

Case 1: Under toughness							For Weld			For base rail		
Case	Speed (Km/hr.)	F_{ver} (N)	R_1 (mm)	R_1' (mm)	R_2 (mm)	R_2' (mm)	a (mm)	b (mm)	P_o (N/mm2)	a (mm)	b (mm)	P_o (N/mm2)
1	60	196200	460	∞	∞	300	8.92	6.7	1566.73	8.983	6.747	1546.58
2	70	200798	460	∞	∞	300	8.99	8.99	1185.86	9.052	6.799	1558.57
3	80	205397	460	∞	∞	300	9.06	6.8	1590.84	9.121	6.85	1570.38
4	90	209995	460	∞	∞	300	9.12	6.85	1602.63	9.188	6.901	1582.01
5	100	214594	460	∞	∞	300	9.19	6.9	1614.24	9.255	6.951	1593.48
6	110	219192	460	∞	∞	300	9.26	6.95	1625.69	9.321	7	1604.78
7	120	223791	460	∞	∞	300	9.32	7	1636.98	9.385	7.049	1615.92

Table 3.4: Contact Pressure comparison of the base metal to the weld with higher toughness at different speed

Case 2: Over toughness							For Weld			For base rail		
Case	Speed (Km/hr)	F_{ver} (N)	R_1 (mm)	R_1' (mm)	R_2 (mm)	R_2' (mm)	a (mm)	B (mm)	P_o (N/mm2)	a (mm)	b (mm)	P_o (N/mm2)
1	60	196200	460	∞	∞	300	9.0923	6.829	1509.49	8.983	6.747	1546.58
2	70	200798	460	∞	∞	300	9.1628	6.8819	1521.19	9.052	6.799	1558.57
3	80	205397	460	∞	∞	300	9.2322	6.9341	1532.72	9.121	6.85	1570.38
4	90	209995	460	∞	∞	300	9.2322	6.9341	1567.03	9.188	6.901	1582.01
5	100	214594	460	∞	∞	300	9.368	7.0361	1555.26	9.255	6.951	1593.48
6	110	219192	460	∞	∞	300	9.3206	7.0005	1604.78	9.321	7	1604.78
7	120	223791	460	∞	∞	300	9.4999	7.1352	1577.17	9.385	7.049	1615.92

4. Fracture Analysis

4.1 INTRODUCTION

Fracture mechanics is broadly classified into two types: Linear Elastic Fracture Mechanic (LEFM) and elastic plastic fracture mechanic (EPFM). LEFM assumes small deformation and minimal yielding at the crack tip, while EPFM can account large deformation and plastic effects.

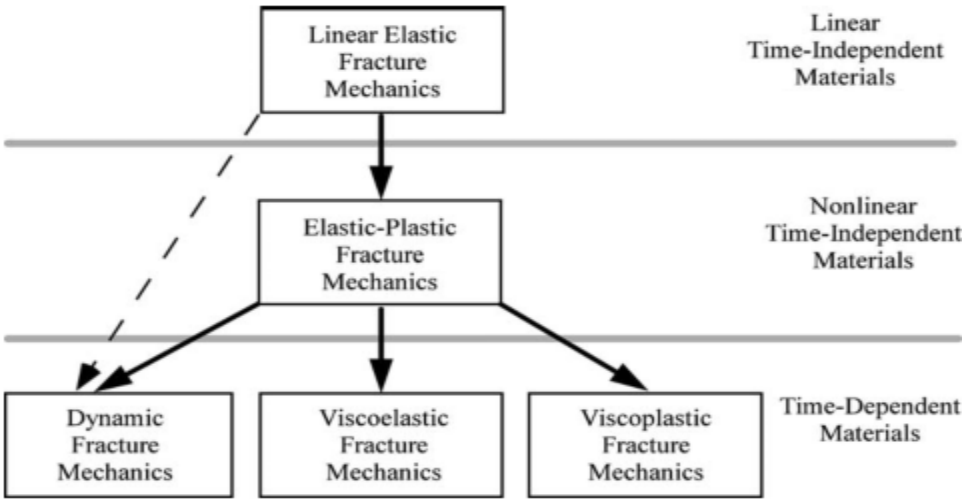

Fig 4.1 Simplified family tree of Fracture Mechanics. [42]

Table 4.1 Fracture behavior of selected materials [42]

Material	Typical Fracture Behavior
High strength steel	Linear elastic
Low- and medium-strength steel	Elastic-plastic/fully plastic
Austenitic stainless steel	Fully plastic
Precipitation-hardened aluminum	Linear elastic
Metals at high temperatures	Viscoplastic
Metals at high strain rates	Dynamic/viscoplastic
Polymers (below T_g)[b]	Linear elastic/viscoelastic
Polymers (above T_g)[b]	Viscoelastic
Monolithic ceramics	Linear elastic
Ceramic composites	Linear elastic
Ceramics at high temperatures	Viscoplastic

[a] Temperature is ambient unless otherwise specified.
[b] T_g — Glass transition temperature.

Thus, the rail with its weld is in the first category of high strength steel. And the Linear Elastic Fracture Mechanics is employed in fatigue crack growth analysis.

4.2 FLAW DETERMINATION

For flaw determination ultrasonic test is used and the flaw is determined using a crack tip diffraction technique.

4.2.1 Crack Tip Diffraction

When the geometry of the part is relatively uncomplicated and the orientation of a flaw is well known, the length of a crack can be determined by a technique known as ***crack tip diffraction.***

One common application of the crack tip diffraction technique is to determine the length of a crack originating from the backside of a flat plate as shown in figure 4.2. In this case, when an angle beam transducer is scanned over the area of the flaw, an echo appears on the scope display because of the reflection of the sound beam from the base of the crack (top image). As the transducer moves, a second, but much weaker, echo appears due to the diffraction of the sound waves at the tip of the crack (bottom image). However, since the distance traveled by the diffracted sound wave is less, the second signal appears earlier in time on the scope.

Crack height (a) is a function of the ultrasound shear velocity in the material (V_T), the incident angle (θ_R) and the difference in arrival times between the two signals (d_t).

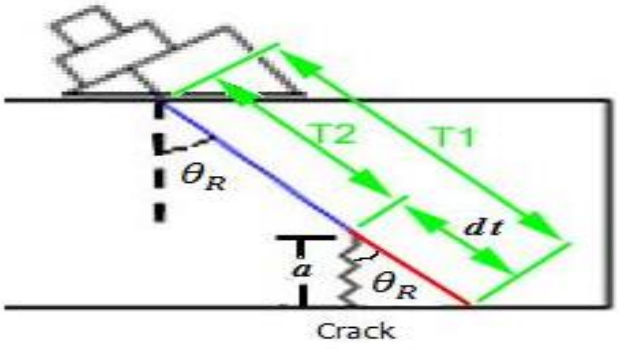

Figure 4.2 Angle beam Transduce

Since the beam angle and thickness of the material are the same in both measurements, two similar right triangles are formed such that one can be overlayed on the other. A third similar right triangle is made, which is comprised on the crack, the length and the angle. The variable d_t is the difference in time but can easily to a distance by dividing the time in half (to get the one- way travel time).

Multiplying the value, d_t by the velocity of the sound in the material. Using trigonometry, it can be written as:

$$a = (\text{Distance } d_t) * \text{Cos}\boldsymbol{\theta_R} \quad \textbf{[4.1]}$$

Therefore, the crack height is found to be:

$$\mathbf{a} = \frac{\boldsymbol{dtVT}}{\mathbf{2}} \text{Cos}\theta_R \quad \textbf{[4.2]}$$

If the material is relatively thick or the crack is relatively short, the crack base echo and the crack tip diffraction echo could appear on the scope display simultaneously (as seen in figure 4.3). This can be attributed to the divergence of the sound beam where it becomes wide enough to cover the entire crack length. In such cases, the angle of the beam striking the base of the crack is slightly different to the angle of the beam striking the tip of the crack.

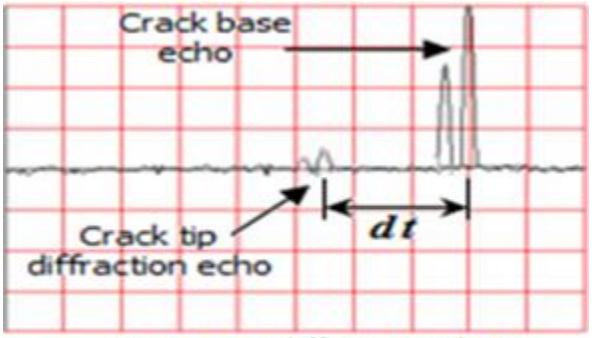

Fig 4.3 Base diffraction Echo [28]

For the flaw detection on the rail weld at the rail base a "crack tip diffraction" technique using an angled transducer is used so that this diffraction is captured at the middle of the base of the rail-weld so that, it could be used as a tip for discontinuity/flaw, and the length of the crack can be estimated.

Table 4.2 Shear Velocity in different media. **[28]**

Metal	Compressional Velocity	Shear Velocity
Aluminum	6320	3130
Steel	5890	3240
Cast Iron	4800	2400
Copper	4660	2330
Titanium	6070	3310

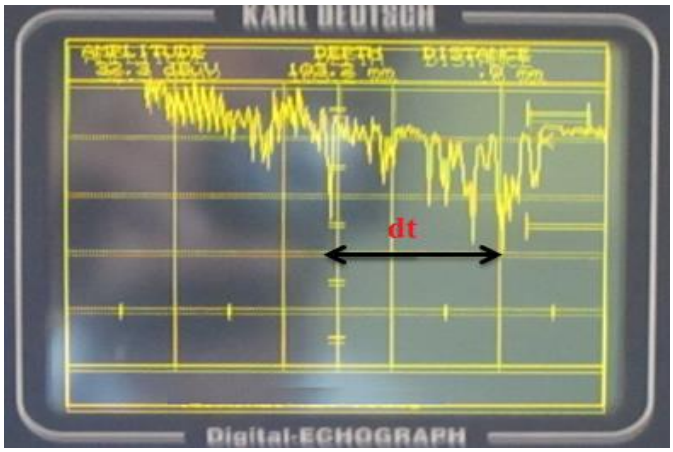

$\mathbf{a=\frac{dtV}{2}}\text{Cos}\theta_R=\frac{1}{2}(100\mu\text{sec})*(3130\text{mm/s})*\text{Cos}\,(60°)\cong$ **0. 07825mm**

Fig 4.4 UT for rail-weld at base using 60° transducer.

4.3 FATIGUE CRACK GROWTH

Mechanical components often contain discontinuities which can be considered as cracks. These initial cracks usually don't cause instant catastrophic failure of the component but subcritical crack growth can be present due to fatigue [34].

Fatigue crack propagation in dynamically loaded mechanical parts is generally presented in a double logarithmic diagram (log(da/dN) - log(ΔK)) consisting of three regions, Fig. 4.5:

→ Region I: slow crack growth region, no fatigue crack growth below the threshold value of the stress intensity factor ΔK_{th}, non-continuum crack growth mechanism;
→ Region II: uniform crack growth, "power law";
→ Region III: crack growth rapidly increases with ΔK asymptotically approaching the critical stress intensity range ΔK_c (instant full fracture).

The fatigue crack growth rate da/dN is defined as a crack extension during one loading cycle and the stress-intensity factor range ΔK is:

$$\mathbf{\Delta K = K_{max} - K_{min}} \qquad \mathbf{[4.3]}$$

…Where K_{max} and K_{min} stands for the maximal and minimal stress intensity factors, respectively.

As it can be seen in Fig. 4.5 the relationship between the logarithmic values of the stress-intensity factor range ΔK and fatigue crack growth rate da/dN is linear in region II. For this region Paris and Erdogan proposed the so called Paris Law [1]:

$$\frac{da}{dN} = \boldsymbol{C}(\Delta \boldsymbol{K}(\boldsymbol{a}))^{\boldsymbol{m}} \qquad [\mathbf{4.4}]$$

…Where C and m are material parameters.

***Table 4.3 Numerical Parameters in the Paris Regime* [38].**

Alloy	***m***	***C***
Steel	3	$1*10^{-11}$
Aluminum	3	$1*10^{-12}$
Nickel	3.3	$4*10^{-12}$
Titanium	5	$1*10^{-11}$

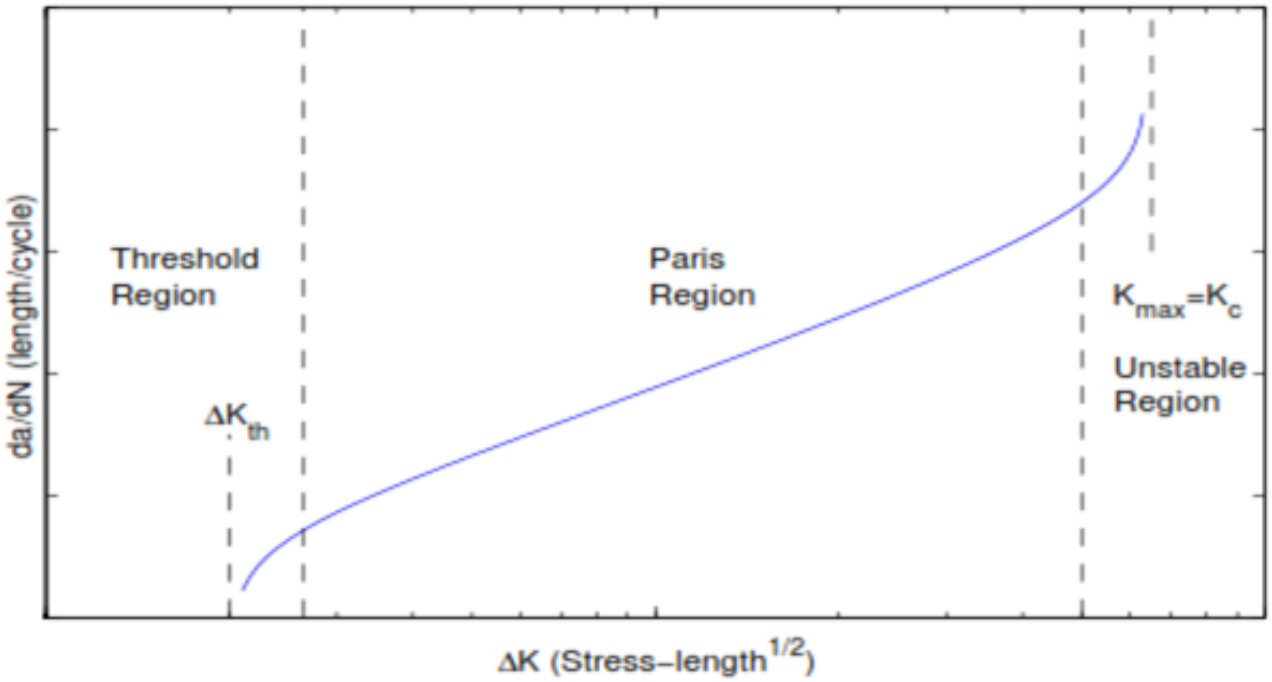

Figure 4.5: Fatigue crack growth vs. stress intensity factor [23]

By integrating (Eq. 4.4) the number of load cycles N_p required for the crack to propagate from an initial crack length a_0 to final crack length a_c can be obtained in the region of uniform fatigue crack growth [1]:

Imagine two bodies of the same material, each containing a crack under an opening load. The two bodies may have different sizes and different shapes, and lengths of the cracks in the two bodies and the loads on the two bodies may also be different. Regardless of all these differences, the field in the K-annulus depends on the boundary conditions through the stress intensity factor. That is, K is the only messenger between the external boundary conditions and the fracture process.

If K is the same for the two bodies, the fracture processes at the tips of the two cracks must be identical. The doctrine of the linear elastic fracture mechanics has been so summarized:

"The same K, the same fracture process," [39]

Fracture criterion phrased in terms of K. Within the fracture mechanics, the simplest way to account for the fracture process is to stipulate that the crack extends when the stress intensity factor K reaches a critical value, K_c . This critical value K_c is known as the toughness.

The stress intensity factor is a loading parameter. The toughness is a material parameter. For a given material, K_c is determined by a fracture test.

Representative values of toughness [39]:

→ Glass: K_c = lMPa$\sqrt{m}$.

→ Steel: K_c = lOOMPa $\sqrt{m}$.

→ Epoxy: K_c = lMPa $\sqrt{m}$.

The stress intensity factor K_I, K_{II}, and K_{III} are used in linear elastic fracture mechanics to characterize the local crack-tip/ crack-line stress and displacement field.

4.4 FRACTURE ANALYSIS OF WELDMENTS

4.4.1 Damage Tolerance of the Rail-Weld at Base

Based on fracture mechanic theory, fatigue crack growth models have been developed to evaluate damage tolerance in structures. This process can also be understood from the fatigue crack growth rate curve (Fig 4.5), also referred to as a da/dN versus ΔK curve, which is defined by Regions I, II and III. Region I includes the early stage of a fatigue crack and the crack growth rate. Also, defines the stress intensity factor threshold, ΔK_{th}, below which fatigue cracks should not propagate. Region II includes the intermediate crack propagation stage where the use of linear elastic fracture mechanics (LEFM) concepts is acceptable. Region III includes the fatigue crack growth at very high rates generated by the fast and unstable crack growth prior to final failure. The curve approaches to the fracture toughness, Kc.

For this study fatigue crack growth in the Region II is the concern, since it is where LEFM and Paris's Law can be applied. The steps of fatigue crack growth may be stated in this form: Determine the number of cycles N_f required for a crack grow from a certain initial crack size ai to the final crack size af, the crack length a corresponds to N loading cycles.

Power law described by Paris and Erdogan (1963) is a simple method for predicting fatigue crack propagation. It describes the fatigue crack propagation behavior in Region II. The equation represents the first application of fracture mechanics to fatigue which is given in equation 4.4:

$$\frac{da}{dN} = C\left(\Delta K(a)\right)^m$$

Where $\Delta K = K_{max} - K_{min}$, with K_{max} and K_{min} referring to the maximum and minimum values of stress intensity in the load cycles. The constants c and m are determined empirically from a log(ΔK) x log(da/dN) plot. But for this study the presumptive values for steel material are used as seen in Table 4.3.

The stress intensity factor is given by:

$$K=\sigma\sqrt{\pi a} \qquad [4.5]$$

…Where… σ-the stress at the crack tip. And the stress range is $\Delta\sigma$

$$\Delta K=\Delta\sigma\sqrt{\pi a} \qquad [4.6]$$

The number of cycles to failure, Nf, can be obtained by integrating (Eqn. 4.6) with respect to a from the initial crack size, ai , to the final crack size, af.

$$\mathbf{N_f}=\int_{ai}^{af}\frac{da}{c[\Delta\sigma\sqrt{\pi a}]^m} \qquad [\mathbf{4.7}]$$

The final crack size is determined from:

$$\mathbf{a_f}=\frac{1}{\pi}\left[\frac{KIc}{c[\Delta\sigma\sqrt{\pi a}]^m}\right]^2 \qquad [\mathbf{4.8}]$$

…Where K_{IC} is the fracture toughness. By integrating and substituting final crack size (Eqn. 4.8) into (Eqn. 4.7), the number of cycles to failure is obtained as:

$$\mathbf{a_f}=\frac{1}{\pi}\left[\frac{100}{1E-11[dk]^3}\right]^2=3.184\mathrm{E}+25/\mathrm{dk}$$

But, determination of dk is a complicated task for the rail; thus the code FRANC3D will be used and final crack size will be computed.

$$\mathbf{N_f}=\frac{af^{1-m/2}-ai^{1-m/2}}{c[\Delta\sigma\sqrt{\pi a}]^m\pi^{m/2}[-\frac{m}{2}]} \qquad [\mathbf{4.9}]$$

$$\mathbf{N_f}=\frac{\frac{af^{1-m/2}-ai^{1-m/2}}{c[\Delta\sigma\sqrt{\pi a}]^m\pi^{m/2}[-\frac{m}{2}]}=(3.184\mathrm{E}+25/\mathrm{dk})^{(1-\frac{3}{2})}-0.07825^{(1-\frac{3}{2})}}{1e-11*dk^m\pi^{(1-\frac{3}{2})}(-3/2)}=\frac{1.77\mathrm{E}-13(\mathrm{dk})^2-3.575}{-8.47E-12dk}$$

Thus, Extracting SIF from FRANC3D it can be possible to determine a_f and N_f , which are both a function of change in SIF.

5. ANALYSIS USING A FINITE ELEMENT MODEL

5.1 INTRODUCTION

The finite element method is a common tool within various fields of engineering. It is used for advanced numerical calculations and is developed from the theories of continuum mechanics, which studies equilibrium, motion and deformation of physical solids. FEM prerequisites that the mathematical models which describe the motions of the media has to be based on continuous functions.

In FEM the continuous functions are approximated by a discrete model where the body to be studied is divided into several smaller parts, so-called elements. The discretized model is composed by a number of element functions that are continuous over each separate element. These elements are connected in nodes, which is primarily where the calculations are made. Numerical values for the nodes are compiled to make the element functions an accurate approximation of the global function. Accuracy improves when the number of nodes increases [21].

5.2 ANALYSIS USING ABAQUS/CAE

Abaqus is a powerful FEM tool to analyze 3D problems in various fields. It is also capable of running Complex-harmonic analyses.

The element functions are gathered in the global equation system containing material and geometrical data. The forces applied on the element geometry are represented by load vectors that act in the nodes. The matrixes quickly increase in size and demand high computer performance to be solved. The nodal deflections are the solution to the equation system. The values between the nodes are received by interpolation with either linearly approximations or polynomials of n degrees.

In linear elasticity problems, the stiffness matrix is constant which brings linear element equations. Steel is modeled as a linear material.

Generally, analysis using Abaqus involves two major procedures, viz, preprocessing and postprocessing.

5.2.1 Preprocessing

ABAQUS has no built-in system of units. Thus, in this model SI (mm) is used as shown in Table 5–1

Table 5–1: Consistent units used in the model input and outputs

Quantity	Length	Force	Mass	Time	Stress	Density
SI(mm)	mm	N	Tone(10^3Kg)	S	MPa	10^3kg/mm^3

Parts define the geometry of the individual components of a model and, therefore, are the building blocks of an ABAQUS/CAE model. Parts can be created as native to ABAQUS/CAE, or can be imported created by other applications either as a geometric representation or as a finite element

meshes. Thus, for this thesis a model native to ABAQUS/CAE using the sketcher, by a deformed 3D extrusion option is created.

The first step in creating the model is to define its geometry. Thus, a three-dimensional, deformable body with a solid, extruded base feature is created.

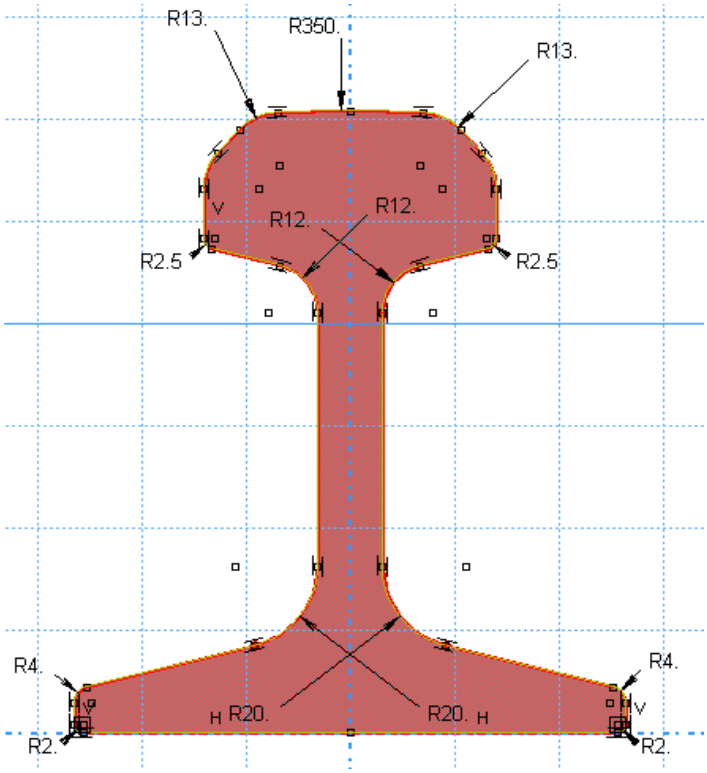

Figure 5.1: ***Modeling in ABAQUS sketcher***

The next step in creating the model involves defining and assigning material and section properties to the part. Each region of a deformable body must refer to a section property, which includes the material definition. In this model the rail is made of steel and assumed to be linear elastic with young's module of 210,000Mpa and a poisons ratio of 0.3, thus a single linear elastic material is created with properties tabulated in table 5.2

Table 5.2: Material property defined in the model

Material	P (10^3Kg/mm^3)	υ	E (N/mm^2)*1000
Base Rail	7.72E-06	0.3	210
Weld	~7.72E-6	0.25-0.34	190-225
Sleeper	2.30E-06	0.3	36

Each part created is oriented in its own coordinate system and is independent of the other parts in the model. Although a model may contain many parts, it contains only one assembly. The geometry of the assembly is defined by creating instances of a part and then positioning the instances relative to each other in a global coordinate system. Thus, the rails are assembled together to the weld lying on the sleeper supporting the wheel. The sleepers are assumed to be fixed on the layer underneath of it and connected to the rails by a representative dashpot coefficient and the rail is coupled to the wheel.

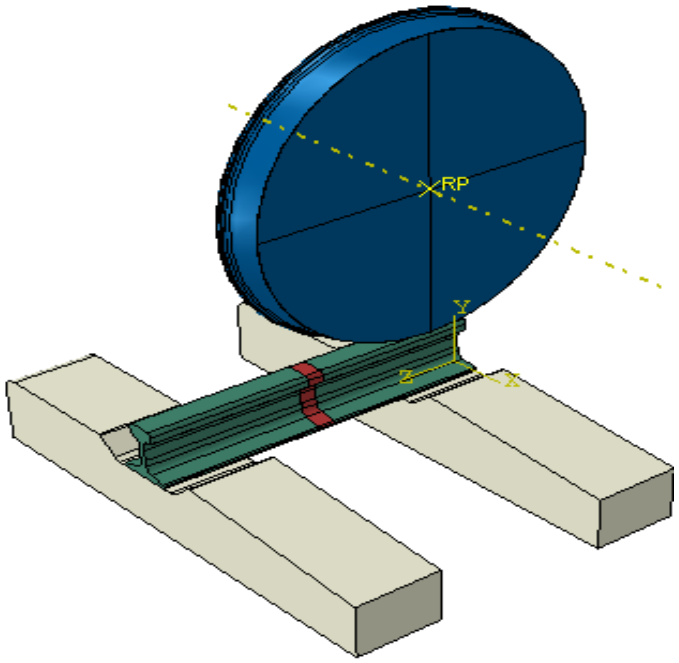

Figure 5.2: Assembly of parts in the model

Analysis steps used in this model can be broadly categorized as an initial step and analysis steps. They are dealt subsequently.

Abaqus/CAE creates a special initial step at the beginning of the model's step sequence and names it `Initial`. Thereby defining boundary conditions, predefined fields, and interactions are applicable at the very beginning of the analysis.

The initial step is followed by one or more analysis steps. Each analysis step is associated with a specific procedure that defines the type of analysis to be performed during the step.

In this thesis, a static linear perturbation step is used. Where in the first analysis step the wheel load is applied and in the second analysis step the wheel will move over the rail head.

The interaction between contacting surfaces consists of two components: one normal to the surfaces and one tangential to the surfaces. The tangential component consists of the relative motion (sliding) of the surfaces.

The contact constraint is applied in Abaqus when the clearance between two surfaces becomes zero. The surfaces separate when the contact pressure between them becomes zero or negative. But, in this thesis a partition is created on the rail and at the mid span, the weld, is separated from the parent rail with a different material property and a mesh. And interaction is created between the wheel and the rail, and the rail and the sleepers with their interaction properties.

Prescribed conditions, such as loads and boundary conditions, are step dependent, which means that the step or steps in which they become active is specified accordingly.

Boundary conditions are applied to those regions of the model where the displacements and/or rotations are known. Such regions may be constrained to remain fixed (have zero displacement and/or rotation) during the simulation or may have specified, nonzero displacements and/or rotations. Thus, a fixed boundary is set at the interaction of the sleeper to the underlying layer. The load on the rail is the load of the wheel, which is half the axle load, the load is applied at a reference point (RP) on the wheel so that the load will be transferred to the rail.

Finally before running the Job mesh has to be created. The mesh module contains tools that allow generating meshes on parts and assemblies created within Abaqus/CAE. In the model, a structure meshing is used. Structure meshing is a technique that gives the most control over the mesh because it applies pre-established mesh patterns to particular model topologies. Considerable care is taken to optimize the mesh size so as to get reliable results. Fig 5.3 shows the mesh of the assembly.

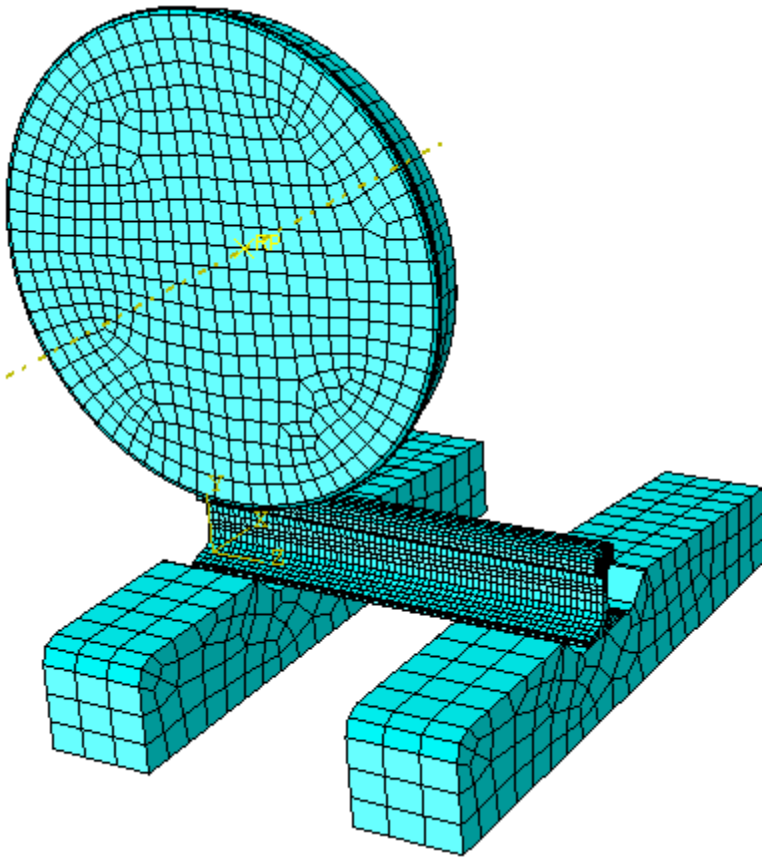

Figure 5.3: meshing of the assembly

Once defining a model is finished, the model is analyzed using the Job module. The Job module allows interactively submitting a job for analysis and monitoring its progress.

5.2.2 Post Processing

The Visualization module provides graphical display of finite element models and results. It obtains model and result information from the output database; it is controlled what information is written to the output database by modifying output requests in the Step module.

The result of the Hertzian contact pressure is applied to the rail as shown in the next figure and after applying the pressure the von-misses stress is determined.

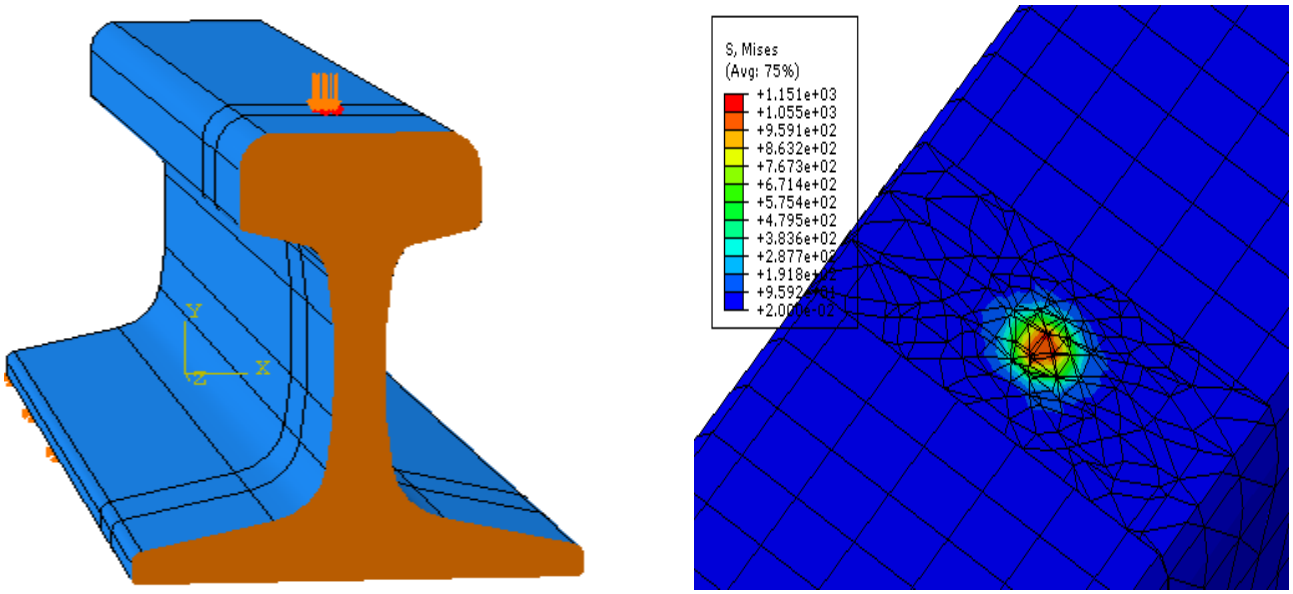

***Figure 5.4: Assigning Contact Pressure* [Left]; *Von-Misses-Stress* [Right]**

Finally the job file (.odb) is exported to FRANCE3D

5.3 FRACTURE ANALYSIS USING FRANC3D

5.3.1 Introduction

FRANC3D development started at Cornell University in the late 1980's, evolving in to a program has been used worldwide in academic and industry for analyzing crack growth in a complex 3D structures. [18].

Franc3D is a program that inserts and extends a crack and/or voids in a pre-existing finite element meshes to see a fracture response of material.

The general flow of usage of FRANC3D can be summarized in Fig. 5.4

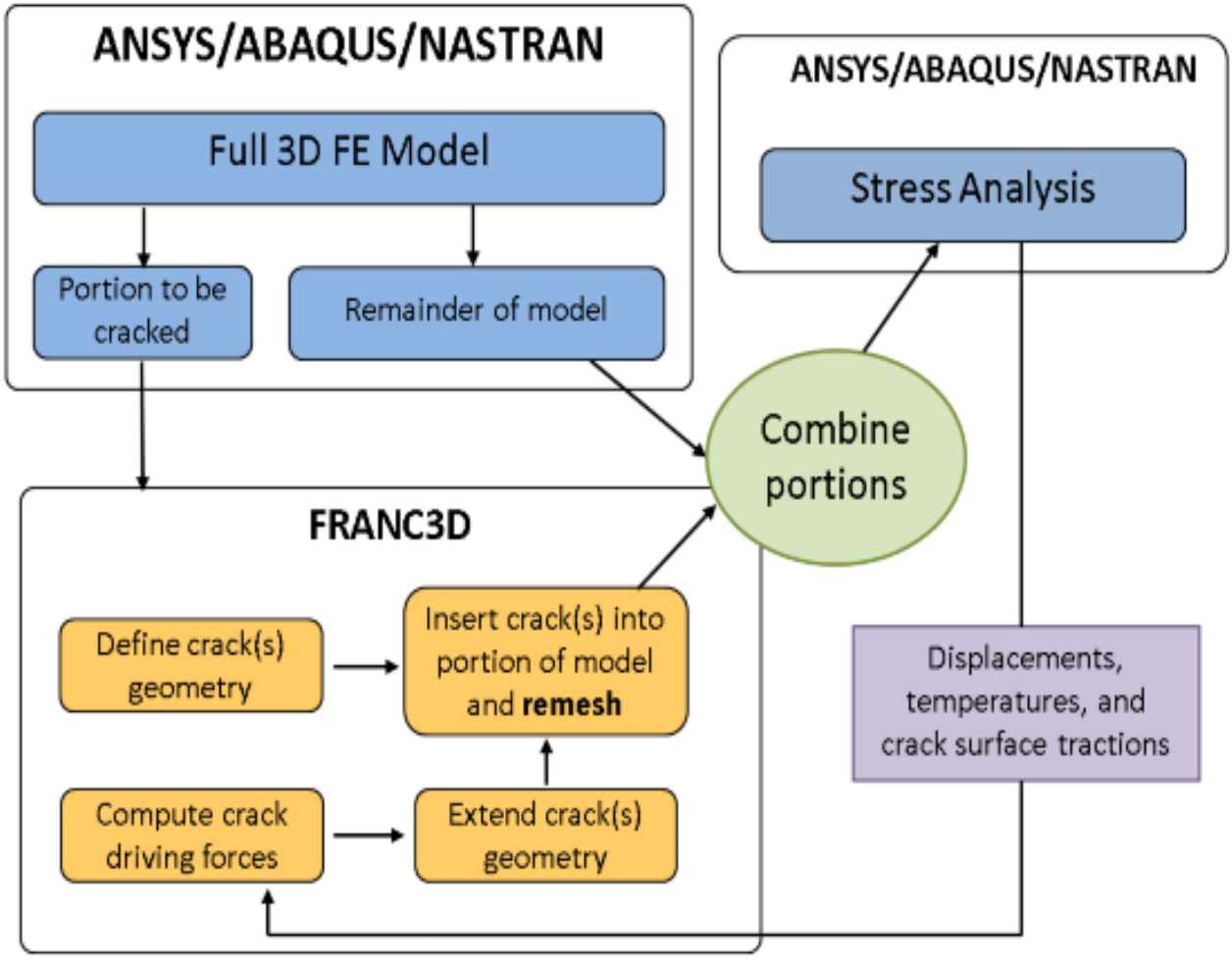

Figure 5.5: Basic flow of Steps in using FRANC3D [18]

Crack geometry, in this thesis, is assumed to be a kidney shaped (elliptical) as per the assumption of Linear Fracture Mechanics.

5.3.2 Crack Insertion

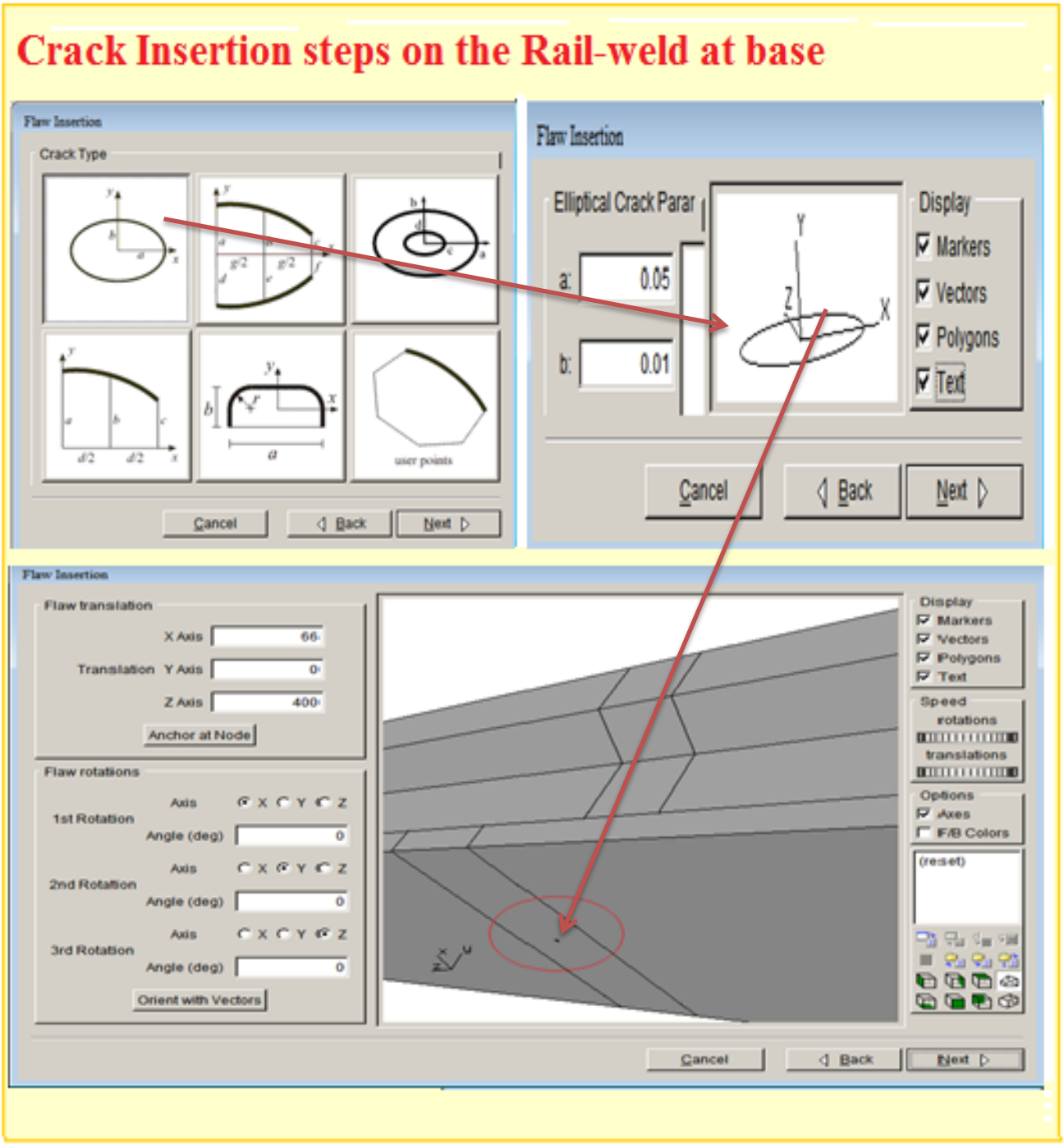

Figure 5.6: Crack insertion steps in FRANC3

5.3.3 Model remeshing with the Crack.

After completion of the crack insertion it is required to remesh the model with the inserted crack

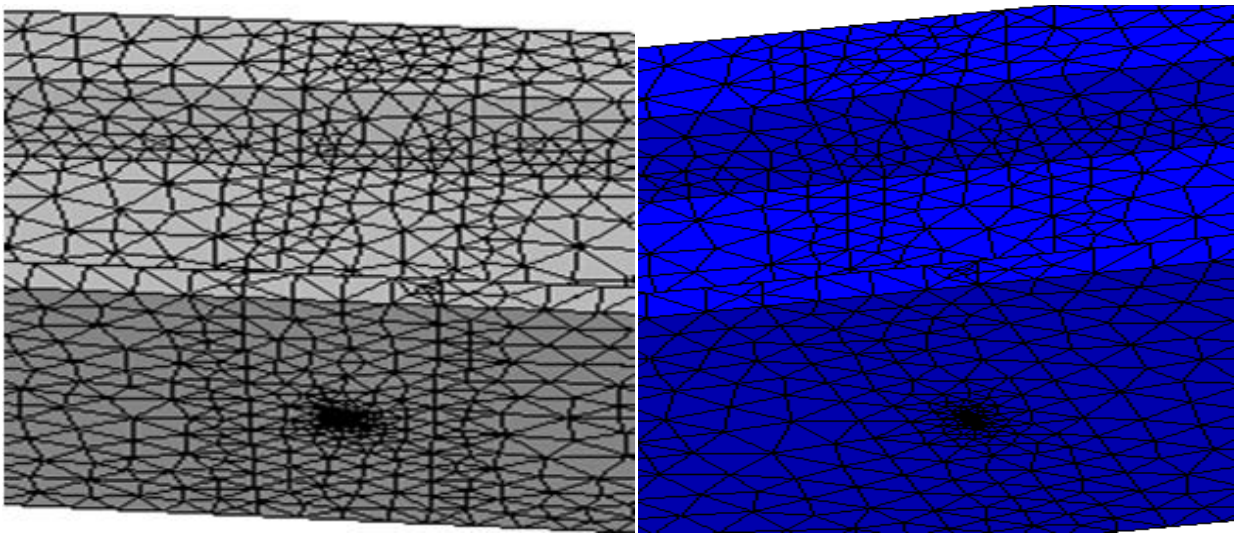

Figure 5.7: The remeshed model in FRANC3D [Left]; The remeshed model in ABAQUS/CAE [Right]

5.3.4 Computation of Fatigue life

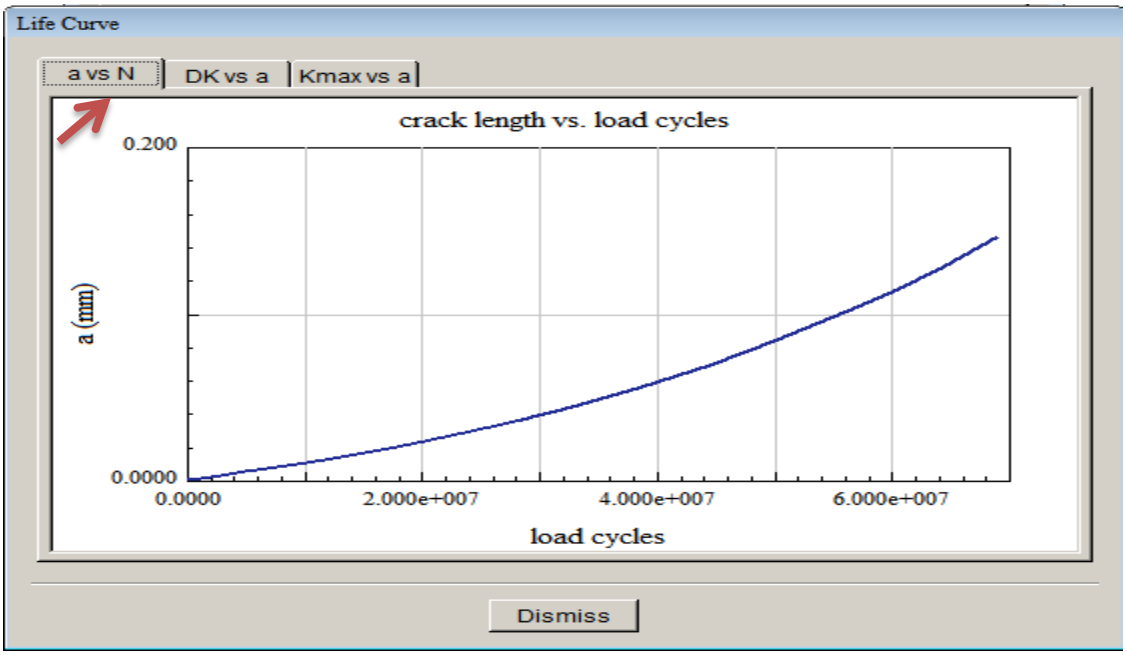

Figure 5.8: crack growth vs. number of cycles

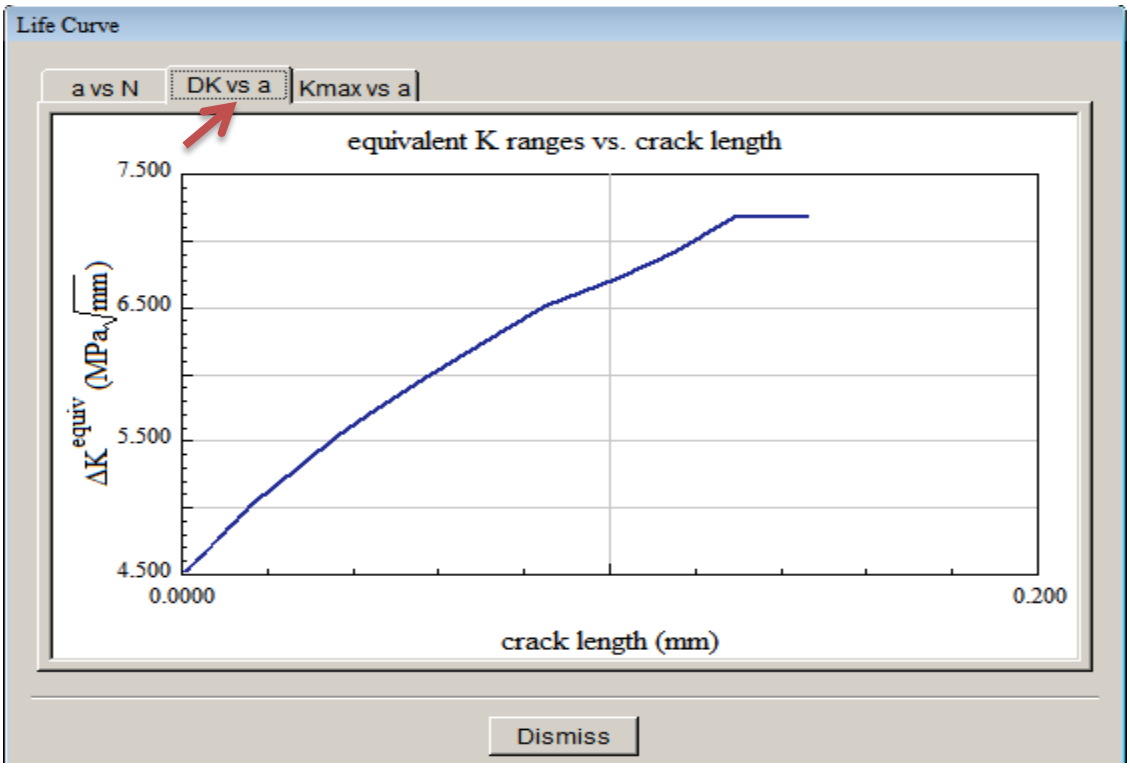

Figure 5.9: crack growth vs. ΔK

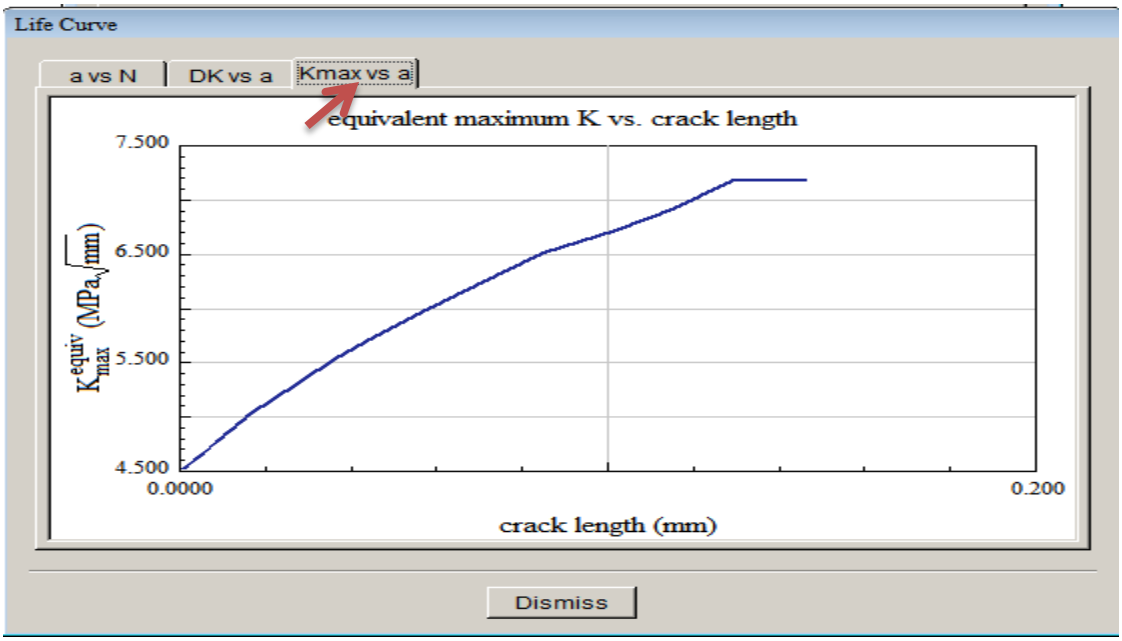

Figure 5.10: crack growth vs. K_{max}

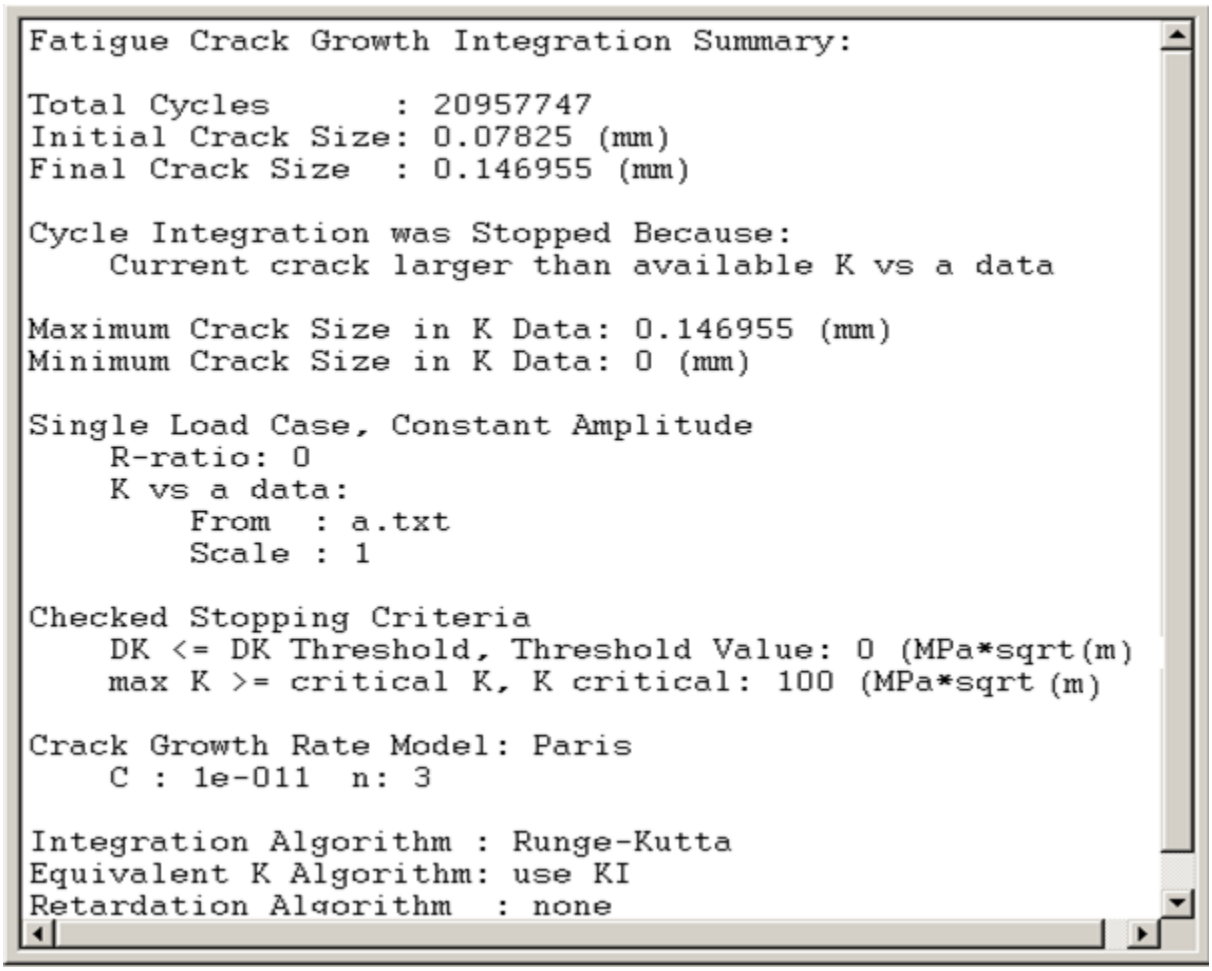

Figure 5.11: Fatigue life output

So, as per the FRANC3D's computation the growth of crack size from [a_o=0. 07815] to critical crack size [a_c=0.146955] requires a repeated wheel loading of 20,957,747.

Or it can be possible to express in gross tonnage, i.e. 20,957,747cycles of 12.5T wheel load

MGT=20,957,747*12.5Ton/1,000, 000≈**261.97MGT**

Table 5.3: initial crack vs. fatigue cycles

	a_i	N	MGT

0	69,730,408	871.63
0.00001	69,730,326	871.62
0.0001	69,633,686	870.42
0.001	68,623,550	857.8
0.01	59,748,477	746.86
0.055	30,888,459	386.11
0.07825	***20,957,747***	***261.97***
0.1	13,324,663	166.56
0.14	2,004,927	25.06
0.1469	20,849	0.26

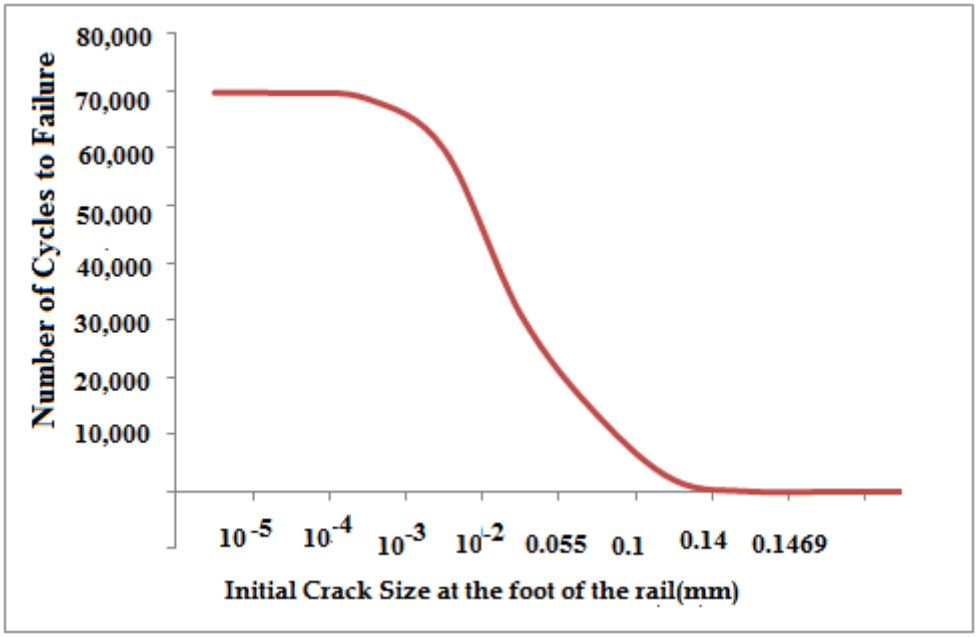

Figure 5.12: Fatigue life vs. initial crack size

6. RELIABILITY ANALYSIS USING PROBABILISTIC APPROACH

6.1 INTRODUCTION

Structural reliability analysis, in general, can be simplified into calculating the following integral i.e. calculating the failure probability of the structure

$$P_f = \iint_{G(x)\leq 0} f_x(X)dx \quad \textbf{[6.1]}$$

$$= \int \ldots \int_{g(x)\leq 0} fx(X)dx = \int \ldots \int_W I(g(x))fx(x)dx \quad \textbf{[6.2]}$$

…Where X- the random variable associated with the assessed structure

g(x) - is the limit state function such that:

$$g(x)\begin{cases} > 0, for\ X\ in\ the\ safe\ set\ of\ structures \\ = 0, for\ X\ in\ the\ Limit\ State\ Surface \\ < 0, for\ X\ in\ the\ faiure\ set \end{cases}$$

$f_x(x)$ is the probability function of X.

I(g(x)) is the indicator function

The compliant 1-P_f is the reliability of the structure.

$$\mathbf{P_r = 1 - P_f} \quad \textbf{[6.3]}$$

The corresponding reliability index β is defined as

$$\boldsymbol{\beta = -\Phi^{-1}(P_f)} \quad \textbf{[6.4]}$$

…Where: Φ is the standard normal cumulative distribution function

6.2 RELIABILITY OF RAIL-WELDS BY THE LEFM APPROACH

Rail defects are directly related to the serviceability of tracks. So that, the limit state of serviceability exists on a state of crack growth. When the critical crack size, a_c is specified, limit state functions for rails subjected to N stress cycles can be defined as:

$$\mathbf{Z = g(x) = a_c - a_{(N)}} \quad \textbf{[6.5]}$$

Where, $a_{(N)}$ is a crack size after a rail is subjected to N stress cycles. A crack size corresponding to the number of cycles can be obtained by the Paris and Erdogan's kinetic crack growth law as seen before once $a_{(N)}$ exceeds the critical crack size failure will happen.

After transformation by Rosenblatt transformation, the reliability index is directly related to the probability of failure (as D increases the limit state moves away from the origin and the probability of failure decreases): as described as;

$$\mathbf{P_f = \Phi(\beta)} \quad \textbf{[6.6]}$$

…Where, ϕ(.) is the cumulative function of the standard normal variant.

6.3 FATIGUE DAMAGE ACCUMULATION FUNCTION

Integrating equation (4.4) from a_1 to a_2 corresponding to the number of stress cycles N_1 and N_2;

$$\int_{a1}^{a2} \frac{1}{y\sqrt{\pi a}} da = \int_{N1}^{N2} CS^m dN \quad \textbf{[6.7]}$$

According to Madsen (1985), a function reflecting the damage accumulation from crack size a_1 to a_2 can be defined as:

$$\Psi(a1, a2) = \int_{a1}^{a2} \frac{1}{y\sqrt{\pi a}} da \quad \textbf{[6.8]}$$

The damage accumulation function is related to the load accumulation by:

$$\Psi(a1, a2) = CS^m(N_2 - N_1) \quad \textbf{[6.9]}$$

…Where S^m is the mean stress range effect, which is an m order moment of the probability density function of a stress amplitude parameter.

An actual rail is usually subjected to a variable amplitude load process as alluded to before. Two possibilities are the cycle-cycle counting and the mean-stress range effect method to consider the fatigue under a variable amplitude stress. The method to count step-by-step each stress occurred in a rail is not practical. The mean stress-range effect method might be appropriate to the study for the fatigue damage accumulation in rails.

The mean stress range can be evaluated as:

$$S^m = \int_0^\infty s^m fs(s) ds \quad \textbf{[6.10]}$$

Where, fs(s) is the probabilistic density function of the stress range parameter, S is assumed to follow the stationary Gaussian random process. For rails, the Rayleigh distribution would be the most appropriate for the estimation of S since the train load stress can comprise of two components: one is static and the other is dynamic stress .If the stress range parameter follows a reyleight distribution the mean stress effect can be shown as follows:

$$S^m = (So\sqrt{2})^m \Gamma\left(\frac{m}{2} + 1\right) \quad \textbf{[6.11]}$$

..Where

$$\Gamma\left(\frac{m}{2} + 1\right) = \frac{m}{2}^{\left(\frac{m}{2}+1\right)} e^{\frac{m}{2}} \sqrt{2\pi} \quad \textbf{[6.12]}$$

So is a statistical parameter which is expressed as

$$S_0=S\sqrt{\frac{2}{\pi}} \quad \textbf{[6.13]}$$

$$S_0=1151\sqrt{\frac{2}{\pi}}=918.6\text{N/mm}^2$$

6.4 LIMIT STATE FUNCTION FOR THE RAIL-WELD BY THE LEFM APPROACH

Rail defects are directly related to the serviceability of tracks so that the limit state of serviceability exists on a state of crack growth. When the critical crack size, ac is specified, limit state functions for rails subjected to N stress cycles can be defined as

$$Z=g(x)=\Delta a \quad \textbf{[6.14]}$$

…Where, Δa is the range of crack size between the initial and the final crack size subjected to N stress cycles. A crack size corresponding to the number of cycles can be obtained by the Paris and Erdogan's kinetic crack growth law as seen before. Once $a_{(N)}$ exceeds the critical crack size failure will happen.

Since the function $\Psi(a1, a2)$ defined earlier can be expressed as

$$\Psi(ac, ao) = \Psi(aN, ao) = 0 \quad \textbf{[6.15]}$$

$$\Psi(ac, ao) = CS^m(N\text{-}N_o)= 0 \quad \textbf{[6.16]}$$

$$\Psi(ac, ao) = \int_{ao}^{ac} \frac{1}{(y\sqrt{(\pi a)^n}} da \quad \textbf{[6.17]}$$

Where, a_o is the initial crack size, and No is the crack initiation period. The initial crack size is the crack size from which the fatigue crack will propagate. It is a lower limit for the crack size which can be a defect in the weldment.

$$\mathbf{g(x)=}\int_{ao}^{ac} \frac{1}{(y\sqrt{\pi a})^m} da - CS^m(N - No) \quad \textbf{[6.18]}$$

$$\mathbf{g(x)=}\frac{ac^{(1-\frac{m}{2})}-ao^{(1-\frac{m}{2})}}{(1-\frac{m}{2})(1.12\sqrt{1.12\pi^m}} - \frac{\sqrt{2\pi}CN(So)^m * \frac{m}{2}^{(\frac{m}{2}+\frac{1}{2})}}{e^{\frac{m}{2}}} \quad \textbf{[6.19]}$$

6.5 AFORM ALGORITHM [44]

In this method, point in design space is chosen to initiate the algorithm. While not necessarily the best place to start, the most common point is the vector of nominal or mean values y * = {μ1, μ2…μN} (David Robinson, 1998).The following procedure is used for the determination of β (reliability index) in this thesis:

1. using the Rosenblatt transformation find standardized, independent random Variables evaluated at the current design point: u*=uy
2. Calculate the Jacobian transformation matrix evaluated at the current design

$$\mathbf{J}=\left[\begin{array}{cccc}\frac{\partial u_1}{\partial y_1} & \frac{\partial u_1}{\partial y_2} & \cdots & \frac{\partial u_1}{\partial y_n}\\ \frac{\partial u_2}{\partial y_1} & \frac{\partial u_2}{\partial y_2} & & \vdots\\ \vdots & & \ddots & \\ \frac{\partial u_n}{\partial y_1} & \cdots & & \frac{\partial u_n}{\partial y_n}\end{array}\right]_{\mathbf{y}^*} \quad \textbf{[6.20]}$$

3. Evaluate the performance function and the associated gradient at the current design point:

$$g(y^*)=g(u^*) \quad \textbf{[6.21]}$$

$$\Delta^*=\Delta g(u^*)=(J^{-1})^T\Delta g(y^*) \quad \textbf{[6.22]}$$

Where the gradient is defined

$$\Delta g(U^*)=\left\{\frac{dg}{du1},\frac{dg}{du2},\ldots,\frac{dg}{dun}\right\} \quad \textbf{[6.23]}$$

4. Move to a new design point and calculate a new safety index:

$$U^*_{New}=[(\nabla^*)^TU^*-g(U^*)]\nabla^*/(\nabla^*)^T\nabla^* \quad \text{(Reduced Space)}$$

$$Y^*_{new}=y^*+J^{-1}(U^*_{new}-U^*) \quad \text{(Design Space)} \quad \textbf{[6.24]}$$

5. Calculate the safety index

$$\beta=(U^{*T}U^*)^{\frac{1}{2}} \quad \textbf{[6.25]}$$

6. Finally determine probability of failure using Table 6.1 Or from the chart Fig 6.1

Table 6.1 Hasofer-Lind Reliability index versus probability of failure

$\mathbf{P_f}$	0.1	0.01	0.001	0.0001	0.00001	1E-06	1E-07	1E-08	1E-09
β	0.128	2.33	3.09	3.71	4.26	4.75	5.19	5.62	5.99

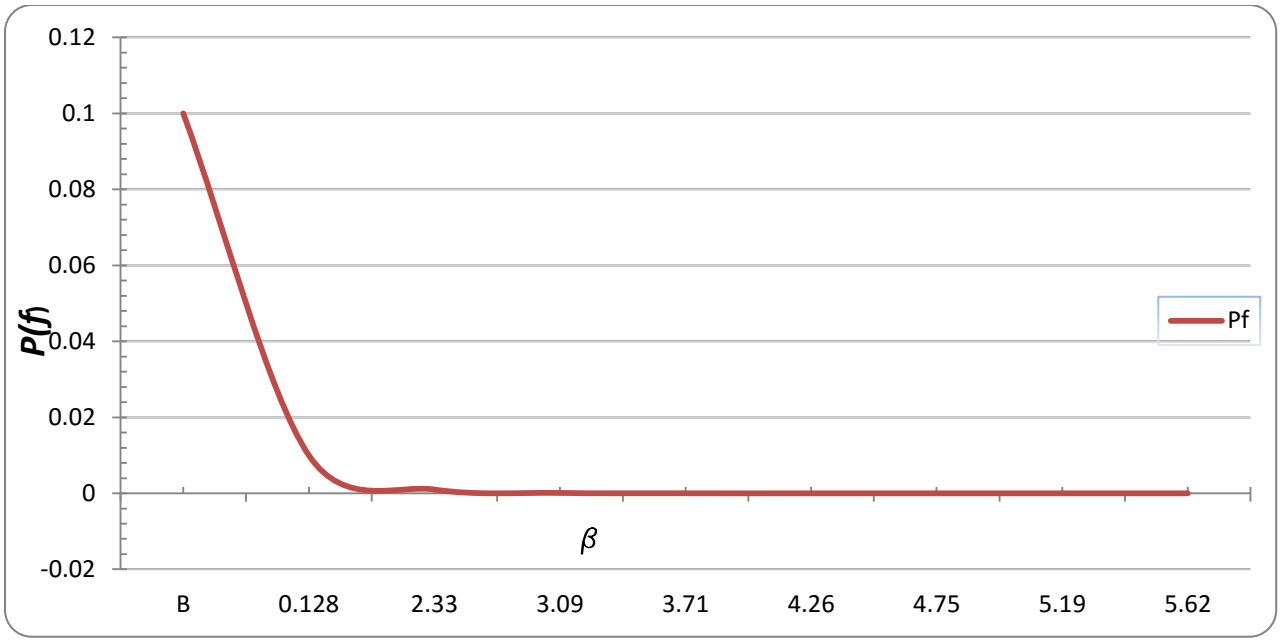

Figure 6.1: Hasofer-Lind Reliability index versus probability of failure

6.5.1 Reliability of Rail-Weld

Using the initial and the final crack size as random variable as shown in table 7.2

Table 6.2: random variables

	crack size	Distribution	COV
a_i	0.07825	Lognormal	0.2
a_c	0.146955	Lognormal	0.2

Applying Rosenblatt transformation, normal variables for log normal distribution:

For the First Variable, Y_1

$$U_1=\Phi^{-1}[H(y_1)]=\frac{lnY1-\lambda 1}{\varepsilon 1} \quad \textbf{[6.26]}$$

$$U_2=\frac{lnY2-\lambda-h\left(\frac{\varepsilon 2}{\varepsilon 1}\right)lny1-\lambda 1)}{\varepsilon 1\sqrt{1-h^2}} \quad \textbf{[6.27]}$$

y1 is for initial crack size; and y_2 for final crack size

The probability density function is given by

$\lambda=\ln(y)=\ln(\mu)-0.5\ln(1+k^2)$

λ_1=ln(0.07825)-0.5*ln(1+0.2^2)=-2.5675

$\varepsilon_1=\sqrt{1+0.2^2}$=1.0198

$\sigma_1=\mu_1*k_1$=0.07825*0.2=0.01565

Assuming a positive correlation of 0.4 for the two random variables

$\eta_1=(\rho/\varepsilon 1)*(\sigma 1/\mu 1)=\frac{0.4}{1.0198}*\frac{0.01565}{0.07825}=0.078$

$\mathbf{u}_1=\frac{lny1-\lambda 1}{\varepsilon 1}=$ 0.98ln(y1)+2.5609

Also for the second variable, Y_2

λ=ln(y)=ln(μ)-0.5ln(1+k^2)

λ_2=ln(0.146955)-0.5*ln(1+0.2^2=-1.9372

$\varepsilon_2=\sqrt{1+0.2^2}$=1.0198

$\sigma_2=\mu_2*k_2$=0.146955*0.2=0.029

Assuming a positive correlation of 0.4 for the two random variables

$\eta_2=(\rho/\varepsilon 2)*(\sigma 2/\mu 2)=\frac{0.4}{1.0198}*\frac{0.03}{0.147}=0.078$

$$U_2=\frac{lny2-\lambda 2-h2\left(\frac{\varepsilon 2}{\varepsilon 1}\right)(lny1-\lambda 1)}{\varepsilon 2\sqrt{1-h^2}}=\mathbf{0.98552lny_2\text{-}0.09855lny1+0.19092}$$

Then, at the current design point the Jacobian can be determined

$$\mathbf{J}=\begin{bmatrix}\frac{0.9806}{y1} & 0\\ \frac{-0.0772}{y1} & \frac{0.9836}{y2}\end{bmatrix}=\begin{bmatrix}12.531 & 0\\ -0.986 & 6.6917\end{bmatrix}$$

Using the performance function from Eq. 7.22

$$\mathbf{g(x)}=\frac{ac^{(1-\frac{m}{2})}-ao^{(1-\frac{m}{2})}}{(1-\frac{m}{2})(1.12\sqrt{1.12\pi^m}}-\frac{\sqrt{2\pi}CN(1577.31)^m*\frac{m}{2}^{(\frac{m}{2}+\frac{1}{2})}}{e^{\frac{m}{2}}}=\frac{1}{3.91}\left[\frac{1}{\sqrt{ao}}-\frac{1}{ac}\right]-\frac{\sqrt{2\pi}CN(1577.31)^m*\frac{m}{2}^{(\frac{m}{2}+\frac{1}{2})}}{e^{\frac{m}{2}}}$$

g(0.07825,0.146955)=-1.854

Then calculating the gradient,

$\nabla g(y^*)$=-5.8451, 2.2711

$$\nabla^* = (J^{-1})^T * \nabla g(y^*) = \begin{vmatrix} 0.0798 & 0.0118 \\ 0 & 0.1494 \end{vmatrix}^T \begin{Bmatrix} -5.8451 \\ 2.2711 \end{Bmatrix} = \{-0.4399, 0.3393\}^T$$

The new design point (in reduced space and the associated safety index are therefore,

From Eqn. [7.24]

$$\mathbf{U^*_{New}} = \frac{[\{-0.4399, 0.3393\}(0,0)^T - (-1.854)]\{-0.4399, 0.3393\}}{\{-0.4399, 0.3393\}\{-0.4399, 0.3393\}^T} = \mathbf{(-1.6304, -1.2573)^T}$$

β from Eqn. 7.28, $\beta = [$(-1.6304,-1.2573)(-1.6304,-1.2573)$^T]^{0.5}$

and, in the original design space,

$$\tilde{y}^* \approx y^* + \mathbf{J}^{-1}(\tilde{\mathbf{u}}^* - \mathbf{u}^*)$$

$$= (0.0783, 0.147) + \begin{bmatrix} \mathbf{0.0798} & \mathbf{0} \\ \mathbf{0.0118} & \mathbf{0.1494} \end{bmatrix} [\begin{Bmatrix} \mathbf{-1.6304} \\ \mathbf{-1.2573} \end{Bmatrix} - \begin{Bmatrix} \mathbf{0} \\ \mathbf{0} \end{Bmatrix}]$$

$$= \{-0.832, -0.147\}$$

These results are then used as an input for the next iteration. As summarized in Table 6.3

Table 6.3: Results of the Iterations

Iteration	Input	Output
	y*	β
1	[0.07825, 0.147]	6.114
2	[0.0832, 0.147]	5.9987
3	[0.0633, 0.1148]	5.6991
4	[0.044, 0.095]	5.528
5	[0.0224,0.0707]	4.6868
6	[0.0055, 0.043]	2.06

[And β=2.06], interpolating the result between 2.33 and 1.28

P(f)=0.0331

R=1-P(f)=**96.69%**

Thus, at this point it's possible to determine the reliability of the weld at the base because of fatigue crack, to a **96.69%**

7. ESTIMATION OF INSPECTION INTERVAL

7.1 INTRODUCTION

The majority of system failures do not occur without any warning signs. This is especially true for failures caused by degradation. By examining the failure-critical indexes during scheduled inspections, actions can be taken to address degraded components and prevent big losses due to failures.

In this paper, it is assumed that an imminent failure can be noticed when an inspection is conducted during a long time period right before the failure. Clearly, by conducting frequent inspections, failures can always be detected and prevented. However, the total inspection cost will be very high if the inspection interval is too short. On the other hand, if the inspection interval is too long, a coming failure may not be effectively detected and the total cost due to failures will be high. Therefore, an inspection interval balancing these two costs needs to be identified.

A model for determining inspection interval to minimize the maintenance cost is proposed in this paper. By conducting inspections for components with degradation characteristics, failures will be prevented, maintenance cost will be reduced and the process throughout can be improved.

Therefore, a failure detection criterion for a unit needs to be established based on engineering knowledge. It could be a fixed time period such as an inspection that is conducted within y months before the occurrence of failure. It also can be a fixed percentage of life consumption such as an inspection that is conducted after p% of the failure times. In this paper, fixed time period is used. The value of the interval can be determined based on engineering knowledge, past failure information and warning signs such as degraded performance of a component.

To better understand the failure detection criterion based on fixed time period of life, it is better to define the failure detection interval as time as t for the unit under consideration, and k as the fixed integral multiplier. If an inspection is conducted in interval t, 2t,… kt,…, then the failure will be noticed before it occurs. Therefore the intervals [kt, (k+1)t] is called failure detection zones.

If an inspection is conducted within a failure detection zone, then the coming failure will be noticed. Otherwise, a failure will not be noticed during inspection and it will occur later.

7.2 INSPECTIONS FOR DETECTING COMING FAILURES

Two objectives are usually considered when determining an inspection interval. They are: 1) improving the system availability, and 2) minimizing the overall cost. This paper is aimed at minimizing the overall cost.

The following assumptions are used:

→ Inspection intervals are based on calendar time, not system (or component) age (such as mileages, hours of operation), etc.
→ Failure time is a random variable following a cumulative distribution function f(t).
→ The time required for inspection is negligible.
→ If an inspection is within a certain percentage p: $(0 < p < 1)$ of a coming failure time, then the system will be replaced and the failure is prevented.
→ System is replaced either at failure or at inspection if the failure time of the system meets the failure detection criteria.
→ A new cycle starts (the system is renewed) when the system is replaced.
→ Inspections do not introduce failures for NDT's are used for inspection.

For a given inspection interval t, the first question arising is the probability of noticing a coming failure. If the probability is very low, then it's required to select a smaller t to increase the chance of detecting coming failures.

7.3 INSPECTION INTERVAL CRITERIA

There are two commonly used criteria for determining an inspection interval. One is for minimizing the average cost within one inspection cycle, and the other is for minimizing the long term average cost. To explain the differences between these two it is good to assume a failure of a component which can be detected any time after 90% of its life has been consumed. Inspections are scheduled every 20hrs of operation. A failure will cost ETB50. An inspection will cost ETB5 and a preventive replacement will cost ETB20. Now assume a new component failed after 18 Inspections hours of operation. Since the failure occurs before the first inspection which is at 20 hours, the failure cannot be prevented. Therefore, the length of this replacement cycle is 18 hours, and the cost is ETB50. The failed component is replaced with a new one and a new cycle started. Assume this newly installed component will fail at 21 hours. 90% of its life is 18.9 hours. Since the scheduled inspection is at 20 hours of operating, which is between 18.9 and 21, the failure will be noticed before it occurs. The component is replaced at 20 hours. The cost of this inspection is ETB25 (inspection cost + preventive replacement cost) and the length of this cycle is 20 hours.
The average cost per unit time in one cycle is calculated as follows. The cost per time for the first replacement cycle is ETB50/18 = ETB2.7778/hour; the cost per time for the second replacement cycle is ETB25/20 = ETB1.25/hour. The average cost per unit time in one cycle is the average of these two. It is (ETB2.7778+ ETB1.25)/2 = ETB2.0139/hour. The long term average cost is the total cost divided by the total operation time. This is (ETB50+ ETB25)/(18+20) = ETB1.974/hour. This is the same as the average cost per cycle divided by the average length of one cycle, if both the numerator and denominator are divided by 2. The formulas for the two cost rates are given next. For a given renewal (replacement) cycle, the expected average cost rate in one cycle is:

$$C_s(x) = \text{Expected}\left[\frac{\text{Short Term Cost in One Cycle}}{\text{Time of one ccle}}\right] \qquad [7.1]$$

Equation 7.1 is the expected one cycle cost rate, or the *short term cost rate*. It is used when different components are expected to be used over an operation period and its purpose is to minimize the cost

per unit time in one replacement cycle only.
The expected long term cost rate with an inspection time interval of x can be calculated based on the renewal reward process theory, and it is

$$C_L(x) = \left[\frac{\text{Long term Expected Cost in One Cycle}}{\text{Expected Time of one ccle}}\right] \quad [7.2]$$

The long term cost rate in (Equation 7.2) used when the same inspection interval and the same type of components are planned to be used for a long time. The objective is to find an inspection interval to minimize the long term cost rate. The following three cost types are considered in the calculation:

→ $\mathbf{C_P}$ is the cost if a coming failure is noticed before it occurs. This is the cost of a preventive replacement.
→ $\mathbf{C_f}$ is the cost if a failure occurs without being noticed during previous inspections. This is the cost of a failure replacement.
→ $\mathbf{C_{insp}}$ is the cost of conducting one inspection.

Clearly, the cost of preventing replacement should be less than the cost in case of a failure, so C_P should be less than C_F. The cost of conducting an inspection should also be less than the cost of a failure replacement, so C_{insp} should be less than C_F.

7.4 INSPECTION INTERVAL FOR MINIMIZING LONG TERM COST RATE

If a failure occurs before the first inspection, it will never be noticed through inspection, so the cost rate for this failure is:

$$\mathbf{C(x) = \frac{Cf}{t}} \quad \mathbf{[7.3]}$$

If a failure occurs in the first detection zone, it can be noticed by the first inspection, so the cost rate for this failure is:

$$\mathbf{C(x) = \frac{Cp+Cinsp}{t}} \quad \mathbf{[7.4]}$$

If a failure occurs between the first and the second detection zone, then it cannot be noticed by inspection, so the cost rate for this failure is:

$$\mathbf{C(x) = \frac{Cf+Cinsp}{t}} \quad \mathbf{[7.5]}$$

The total costs related to rail defect inspection include:
→ Costs for operating inspection vehicles

→ Costs for repairing detected rail defects & train delay
→ Costs for repairing broken rails & train delay
→ Costs of broken-rail-caused derailment damage & train delay

7.5 RAIL DEFECT INSPECTION COST MODEL

The model developed by the Association of American Railroad is used to predict costs of defect inspection, repairing a detected rail defect or broken rail and Train delay cost due to repairing a detected defect or broken rail. In this thesis this model is used for a determination of an inspection interval with updated cost data in the model

7.5.1 Cost of repairing a detected rail defect or broken rail

The Association of American Railroads (AAR) developed the following models to estimate the cost for repairing detected defects and broken rails (Wells and Gudiness 1981). In this thesis the AAR's models with updated rail cost information is used.

The costs for repairing detected rail defects and corresponding train delay is a multiplication of the number of detected rail defects and repair & train delay cost per defect. Based on the model developed by (Orringer et al. 1988; Orringer 1990), the annual number of detected rail defects is:

$$\mathbf{DDC}= \left[\frac{\mathbf{Wreplace}*\mathbf{Lreplace}(\mathbf{Pnew}-\mathbf{0.95Pold})}{\mathbf{2000}} + \mathbf{Cd,repair}\right](\mathbf{1}-\boldsymbol{t}) \qquad \textbf{[7.6]}$$

DDC = cost for repairing a detected rail defect ($)
$W_{replace}$ = weight of replacement rail, in pounds per yard (141)
$L_{replace}$ = length of replacement rail, in yards (3)
P_{new} = price of new rail, in dollars per ton ($1470)
P_{old} = price of scrap rail per net ton ($588)
$C_{d,\ repair}$ = direct cost (labor, materials, equipment) for repairing a detected rail defect ($10,070)
t = federal and state marginal income tax rate (0.35)

Based on the information above, an average of $6,671 to repair a rail defect is estimated. The actual cost will vary depending on infrastructure and operational circumstances. Some undetected rail defects could grow into rail breaks, a large number of which may be identified by either track circuits or by visual inspections (Dick 2001; Schaffer 2008).

The AAR model for repairing broken rails is similar to the one for detected defects and is shown as follows (Wells and Gudiness 1981):

$$\mathbf{SDC}= \left[\frac{\mathbf{Wreplace}*\mathbf{Lreplace}(\mathbf{Pnew}-\mathbf{0.95Pold})}{\mathbf{2000}} + \mathbf{Cs,repair}\right](\mathbf{1}-\boldsymbol{t}) \qquad \textbf{[7.7]}$$

SDC = cost for repairing a broken rail ($)

C_S, repair = direct cost (labor, materials, equipment) for repairing a broken rail ($10,640)

Other variables are as defined above. Based on the model, an average of $7041 for repairing a broken rail is estimated.

7.5.2 Train delay cost due to repairing a detected defect or broken rail

The time required to repair a rail defect is dependent on the size, type and location of defect, and various other factors. Schlake et al. (2011) estimated train delay time by traffic density and the time to repair a rolling stock service failure using simulation tools. Delay functions for repairing a detected rail defect or broken rail is adopted in this thesis.

7.5.2.1 Train delay cost due to repairing a detected rail defects

$$C_{DDT} = C_0 A_D \exp(B_D X) \quad [7.8]$$

Where:

C_{DDT} = train delay cost due to fixing a detected rail defect ($)
C_0 = train delay cost per hour, $232
A_D = 1.503 (Schlake et al. 2011)
B_D = 0.0811 (Schlake et al. 2011)
x = number of trains per day (T/0.006312/365) (T: annual traffic density in MGT) ≈ 11

Based on the information above, an average of $851 loss from train delay for an average of 25MGT is estimated and this loss is from the delay of an average of ≈ 11trains due to repairing a detected defect in the rail.

7.5.2.2 Train delay cost due to repairing broken rail

$$C_{SDT} = C_0 A_S \exp(B_S X) \quad [7.9]$$

Where:

C_{SDT} = train delay cost due to fixing a broken rail ($)
A_S = 3.559 (Schlake et al. 2011)
B_S = 0.0805 (Schlake et al. 2011).Other variables are as defined above.

Based on the information above, an average of $2002 loss from train delay is estimated assuming an average of 25MGT and this loss is from the delay of an average of ≈ 11 trains due to repairing broken rail

7.6 Optimization of Ultrasonic Rail-weld Inspection Frequency

To arrive at an economical annual inspection frequency four cost models are to be dealt.

7.6.1 Cost of Inspection

For a track segment, the costs for operating inspection vehicles are:

$$C_{insp} = \frac{L}{V} C_{hr} \qquad [7.10]$$

C_{insp} = rail inspection cost ($)
L = track length (miles)
V = average inspection vehicle speed (mph)
C_{hr} = inspection cost per hour per vehicle ($/hour)

Senior track engineers from a major railroad indicated that the speed of inspection (V) is generally between 15 to 20 mph and the average inspection cost per hour per vehicle (Chr) is approximately $300.[10]

Table 7.1: Cost of inspection for varying inspection frequency

Annual Inspection Interval	Cost of Inspection($)
1	15
2	30
3	45
4	60
5	75
6	90
7	105
8	120
9	135
10	150

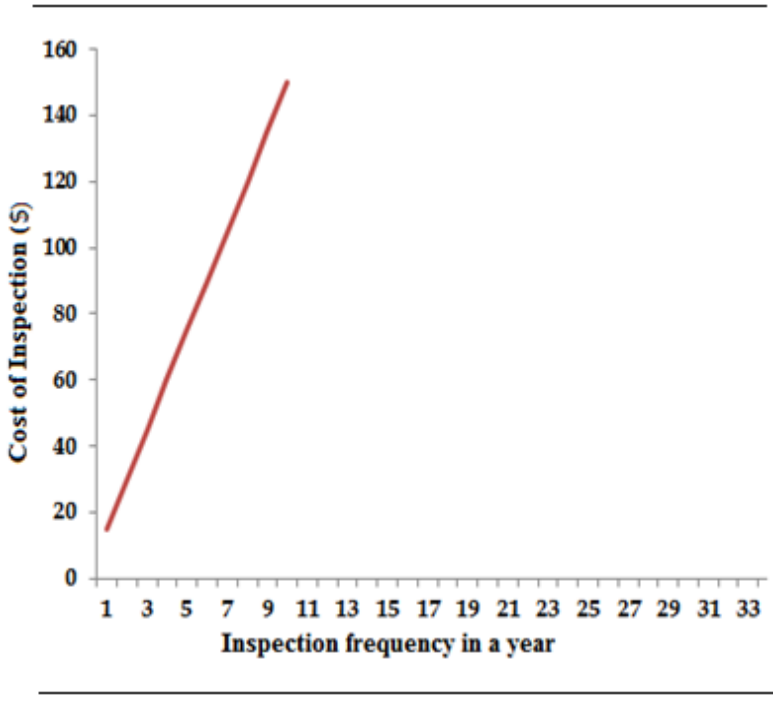

Figure 7.1: Cost of inspection for varying inspection frequency

7.6.2 Rail Defect Repair Cost

$$\mathbf{N_{def}} = \frac{\mathbf{S(K)L}}{\mathbf{h}(\frac{\mathbf{T}}{\mathbf{K}} - \mathbf{q})} \quad \textbf{[7.11]}$$

Where…

N_{def} is the number of detected rail defects (note: current regulations require either immediate removal of rail defects or a prescribed remedial action until they are removed);

S(K) is the annual number of broken rails per mile by rail defect inspection frequency (=0.00097*2/k);

L is segment length;

T is annual traffic density in million gross tons, and

K is annual rail defect inspection frequency;

h and θ are parameters related to inspection efficiency, are 0.0108, and 1, respectively, (Orringer 1990).

The total rail defect repair & train delay cost (C_{def}) is:

$$\mathbf{C_{def}} = \frac{\mathbf{S(K)L}}{\mathbf{h}(\frac{\mathbf{T}}{\mathbf{K}} - \mathbf{q})}(\mathrm{DDC} + \mathbf{C_{DDT}}) \quad \textbf{[7.12]}$$

Where,

DDC is cost for repairing a detected rail and

C_{DDT} is the corresponding train delay cost.

Based on the above model, for instance for an inspection to be undertaken twice a year the rail defect repair cost is estimated to be $66 and the average cost for varying annual inspection frequencies is estimated as shown in the next table.

Table 7.2: Rail defect Inspection cost for varying inspection frequency

Annual Inspection Interval	Rail defect repair cost($)
1	56.30
2	65.37
3	68.69
4	72.37
5	76.47
6	81.05
7	86.22
8	92.10
9	98.84
10	106.64

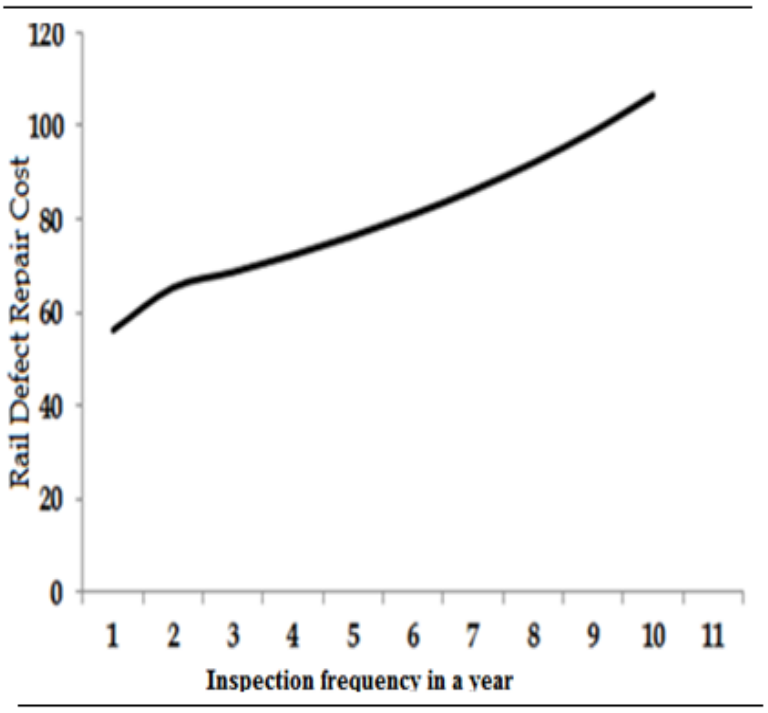

Figure 7.2: Rail defect Inspection cost for varying inspection frequency

7.6.3 Broken Rail Repair Cost

Similarly, total broken rail repair & train delay cost (C_{bre}) is:

$$\mathbf{C_{bre} = S(K)\,L(SDC + C_{SDT})} \qquad \mathbf{[7.13]}$$

Where,

SDC is cost for repairing a broken rail and

C_{SDT} is the corresponding train delay cost.

The number of broken-rail-caused freight-train derailment is estimated as a multiplication of the number of broken rails (S(K)xL) and the proportion of rail breaks causing derailments (w). For each train derailment, the total consequence cost includes property damage cost (pDA) and train delay cost (CDA). So train- derailment-related cost is:

$$\mathbf{C_{bre} = S(K)\,L\,(pDA + C_{DA})} \qquad \mathbf{[7.14]}$$

Based on the above model, for instance for an inspection to be undertaken twice a year broken rail repair cost is estimated to be $66 and the average cost for varying annual inspection frequencies is estimated as shown in the next table.

Table 7.3: Rail break repair cost for varying inspection frequency

Annual Inspection Interval	Rail break repair cost($)
1	17.54
2	8.77
3	5.85
4	4.39
5	3.51
6	2.92
7	2.51
8	2.19
9	1.95
10	1.75

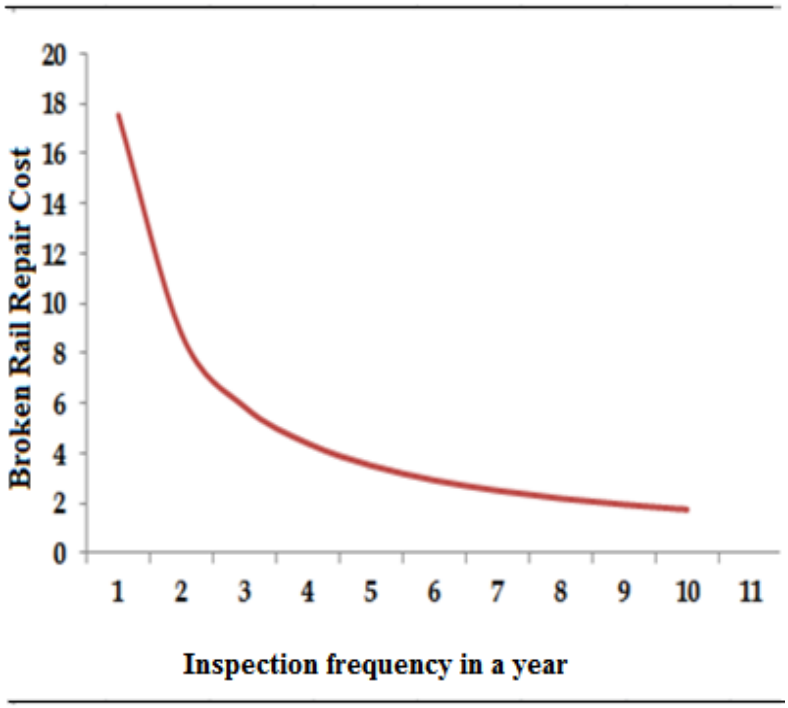

Figure 7.3: Rail break repair cost for varying inspection frequency

7.6.4 Derailment Damage Cost

$$C_{derail}=S(K)\,L\Phi(\mu DA+C_{DA}) \qquad [7.15]$$

Where,

μDA is damage cost

Φ **is the proportion of rail causing derailment**

Based on the above model, for instance for an inspection to be undertaken twice a year derailment damage cost is estimated to be $40.83 and the average cost for varying annual inspection frequencies is estimated as shown in the next table.

Table 7.4: derailment damage cost for varying inspection frequency

Annual Inspection Interval	Derailment Damage Cost($)
1	81.65
2	40.83
3	27.22
4	20.41
5	16.33
6	13.61
7	11.66
8	10.21
9	9.07
10	8.17

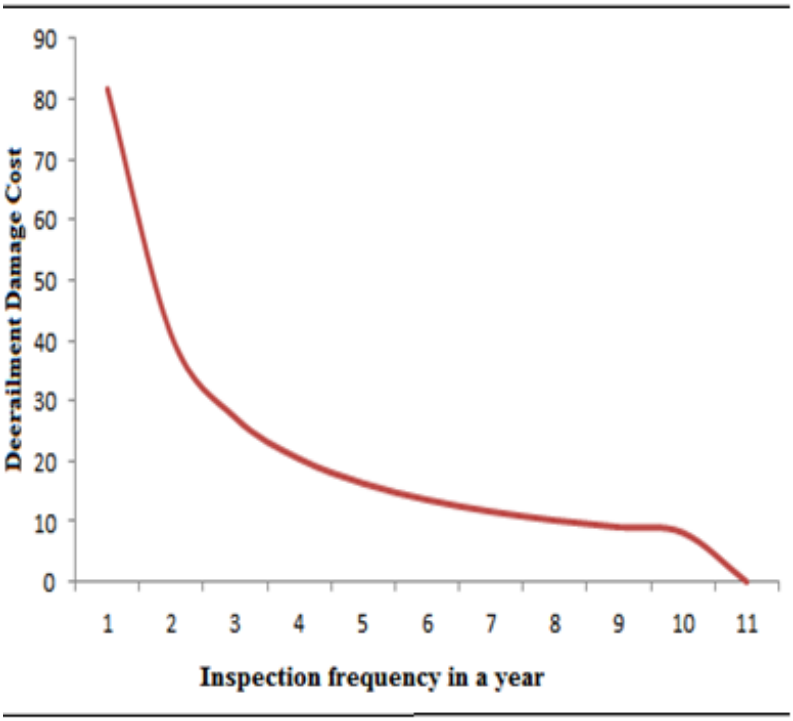

Figure 7.4: derailment damage cost for varying inspection frequency

Given the total number of rail inspections per year (K), the total cost is: From (eq. 5) to (eq. 14)

$$K\frac{L}{V}C_{hr}+\frac{S(K)L}{h(\frac{T}{K}-q)}(DDC+C_{DDT})+S(K)\,L(SDC+C_{SDT})+S(K)\,Lw(pDA+C_{DA}) \quad \textbf{[7.16]}$$

Table 7.5: Total cost for varying annual inspection frequency

Annual Inspection frequency	TOTAL cost($)
1	170.49
2	144.97
3	146.76
4	157.17
5	171.31
6	187.58
7	205.39
8	224.50
9	244.86
10	266.56

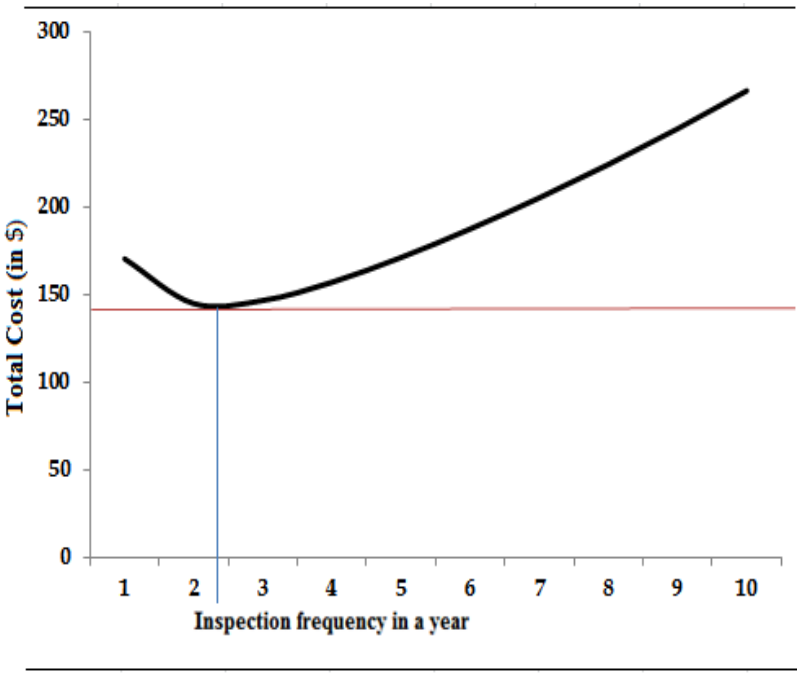

Figure 7.5: Total cost for varying annual inspection frequency

Therefore, the inspection interval from the point of minimizing total cost is determined to be between 2 to 3. Approximated to 2.35 times a year (inspection in every five month interval)

8. CONCLUSION, RECOMMENDATION AND FUTURE WORKS

8.1 CONCLUSION

In this thesis the response of a rail-weld to fatigue load is determined under static and dynamic loads, the results of the mathematical model is compared with results of a FEM and are nearly equal. Using the concept of Linear Fracture Mechanics the response of a number of cycles to failure is determined to be highly sensitive to fatigue crack growth rate and using an ultrasonic flaw detecting machine the initial crack size is estimated to be 0.1469mm and by increasing the initial crack size it is tried to show the sensitivity of the remaining life of the weld until the final crack size of 0.146955mm reaches and any increment beyond this critical crack size results failure. Hence, the number of cycles of loading that results attainment of the critical crack size is determine to b 20,957,747cycles of wheel passage over the weld. Finally, the defect detecting inspection interval to minimize the overall cost from the crack growth is determined. The following key points are worth mentioning as a concluding remark:

i) Initial crack size

With a very small initial crack size increment, the remaining service life to failure highly decreases. Thus, It can be concluded that decreasing the initial crack size has a lot to do with increment of serviceability of the rail-welds.

ii) Contact stress at Weldments

The contact stress increases with decrement in material property (E and υ); it can be concluded that the contact stress at the weldment is greater than the contact stress at the base rail regarding wheel-rail contact stress.

iii. Fracture toughness

With the SIF less than the fracture toughness of the material, the crack is stable but, as the fracture toughness is exceeded, the crack propagation to fracture will be very fast; Thus, It can be concluded that the fracture toughness of material is a guarantee for a longer service life.

iv. Estimated Inspection Interval

The reliability of rail-welds to fatigue load taking the initial and final crack size as random variables is determined to be 96.69% and an inspection interval for defect detection is estimated to be 5months

8.2 RECOMMENDATION

The result of this paper can be a starting point to develop a methodology for further detail repair and replacement of the rail, Maintenance strategy.

8.3 FUTURE WORKS

As an extension of this study, the following are recommended:

1. Development of Risk assessment and maintenance strategy models.
2. Crack propagation analysis in multiple mode of failure and/or multiple flaws at different positions.

3. Modeling welds using specially made plug-in softwares, which are all commercial, can accurately represent the weld especially the temperature dependent variables in the rail-weld interaction.
4. Analysis in different load cases, in different load combinations.
5. Development of models compatible to Ethiopia for Economic Inspection Interval than adopting models done by other researchers.
6. Fracture testing (laboratory testing) on the weldment to determine the exact value of material parameters.
7. Dynamic amplification of contact stress for weld irregularity.

REFERENCES

[1]. Paul C. Paris, Mario P. Gomez, and William E Anderson, "The Trend in Engineering 13", 1961

[2]. D. Sarah, A Lambic, "Mechanical Testing and Calibration of ultrasonic Testing" Laboratory Of Material Engineering Tallin University Of Technology, 2014.

[3]. Indian Railway Institute of Civil Engineering, PUNE 411011," Welding Technique", March 2006.

[4]. Fortune Magazine. (2014, June 15). City Mega Project Off Track with Replacement Rail Required. Volume 15, No. 737.

[5]. National Standards of the People's Republic of China," Hot-rolled steel rails for railway", General Administration of Quality Supervision, Inspection and Quarantine of the People's Republic of China, 2007.

[6]. Y Chen , F V Lawrence, C P L Barkan, And J A Dantzig "Weld Defect Formation In Rail Thermite Weld" Energy Technology Division, Argonne National Laboratory, Argonne, Illinois, USA, 2006.

[7]. J.W. Ringsberg*, B.L. Josefson And A. Skyttebol, "Fatigue Crack Growth In Welded Rails" Department Of Applied Mechanics, Chalmers University of Technology, SE-412 96 Göteborg, Sweden,

[8]. Saurabh Kumar, "Study of Rail Breaks: Associated defects and maintenance strategies" Lulea university of Technology, Department of Civil and Environmental Engineering.

[9]. Transport research board of the national academy, Final report for high speed rail IDEA Project 41, "Reliability of Improved Thermite Welds", Sep, 2014

[10]. X. Liu, C.T. Dick, and M.R. Saat, "Optimizing Ultrasonic Rail Defect Inspection to Improve Transportation Safety and Efficiency", The Second T&DI Congress, in Orlando, Rail Transportation and Engineering Center (RailTEC), Department of Civil and Environmental Engineering at the University of Illinois FL, June 8-11, 2014.

[11]."Addis Ababa Light Rail Transit Project Preliminary Design," Design Report, China Railway Group, 2010.

[12]. C. P. Lonsdale, "Thermite Rail Welding: History, Process Developments, Current Practices and Outlook for The 21st Century", Conrail Technical Services Laboratory Altoona, PA 16601

[13]. Melisa E Bona, "The effect of straightening and grinding of welds on track roughness", Thesis submitted for the degree of Master school of Civil Engineering, Queen's land university of technology, July 06.

[14]. Australian Rail Track Corporation LTD, "Alumino-Thermic Welding Manual" Engineering Practices Manual, Civil Engineering, June 7, 2013.

[15]. Government of India Ministry of Railways, "Indian Railway Standard Specification for fusion welding of rails by Alumino-Thermic Process," Issued by Research design and Standards organization.

[16]. X Lei* and Q Feng, "Analysis of stability of continuously welded rail track with finite elements", Department of Civil Engineering, East China Jiaotong University, Jiangxi, People's Republic of China. PP 225-235,

[17]. Zerbist. U.; Lauden R.; Eden L.; Smith R.; "Introduction to the Damage Tolerance Behavior of Railway Rails," Philadelphia, PA., 1978.

[18]. Fracture Analysis Consultant, Inc. "FRANC3D Reference Manual," 2011

[19]. John D. "Structural Reliability Theory and Risk Analysis", Chicago, IL, December, 2004.

[20]. "Levels of Reliability Method" lding Society, Miami, FL, 1991.

[21]. Dassault System center of simulation Excellence, "Abaqus 6.12 Theory Manual," January, 1998.

[22]. "Railway Applications-Track Alumino-Thermic Welding of Rails," Napoleon, OH, February, 1997.

[23]. Joshua H.; "Fatigue Crack Growth Analysis with Finite Element Method and A Monte Carlo Simulations," MSc thesis, Faculty of Virginia Polytechnic Institute and state University, Blacksburg, VA, 2014

[24]. "Wheel and Track profile in Use and Maintenance," Building sustainable and efficient tram depot for cities in the 21st century, Tramstore, 2012

[25]. Huairui G.; Ferense, S.; Athenasios, G.; Pengying N., "On Determining Optimal Inspection Interval for Minimizing Maintenance Cost", Tramstore, 2015

[26]. "Welding Simulation with Abaqus,"Abaqus Technology Brief, 2007

[27]. John E.; Per M.; "Welding Simulations with Finite Element Analysis,", Degree Project, 2004

[28]. "Introduction to Non Destructive Testing Techniques," Ultrasonic Testing, 2004

[29].C.P Londale, "Thermite Rail Welding: History, Process Development, Current Practices, Current Practices, and Outlook for the 21st century," Conrail Technical Service Laboratory Altoona, PA, 2007

[30]. Hassen F.; Seyed M., "Horizontal Split Web Fracture of Flash butt Welded Rail," Facuty of Engineering University of Tehran, Iran, 2007.

[31]. "Indian Railway Standard Specifications for Fusion Welding of Rails by Alumino-Thermic Processes," Ministry of Railways, Research, Design and Standard Organization, 2012.

[32]. Dijs S.; Serjejs, M., "Analysis of Factors affecting Fracture of Rails welded by Alumino-Thermic Welding," 2007.

[33]. M. Saarna; A. Laansoo., "Rail and Rail-weld Testing," 4th International DAAM Conference, Taalin Estonia, 2004

[34].Peter J.; Thomas T.,"Fatigue Behavior of Steel Highway Bridge Detail," Virginia Transportation Research Council, Charlottesvile, Virginia, 2011

[35]. Marcela R.; Jose, M., "Reliability Analysis for Probabilistic fatigue crack growth," 21st Brazilian Congress of Mechanical Engineering, Talis, 1994.

[36]. Zhigang Suo, "Fracture Mechanics," http://imechanica .org /node/7448.

[37]. Gonez, P.; Gubeljak, N.; Potocnic R, and Glodez, S, "Fracture Mechanics Parameter of 42CrMo4 Steel," Advanced Engineering, 2010.

[38]. David R., "Fatigue," Department of Material Science and Engineering, Massachusetts Institute of Technology, Cambridge MA, 2001

[39]. Zhigang Suo, "Linear Elastic Fracture Mechanics," http://imechanica.org/ node/7448.

[40]. Kalker J. J. (1991): Wheel-rail rolling contact theory. Wear, 144, 243-261.

[41]. Sajjad Zeynali. "Checking the Role of Slope in Generated Von Mises Stress of Railroad," Department of Mechanical Engineering, University of Tabriz, Tabriz, Iran, Adv- Environ. Biol., 8(6), 1745- 1751, 2014

[42]. T.L Anderson, "Fracture Mechanics Fundamentals and Applications," Indianapolis, IN, October 21, 1997.

[43]. "Requirements Concerning Materials and Welding, "International Association of Classification Societies.

[44]. David G Robinson, "A Survey of Probabilistic Methods used in the Reliability and Uncertainty Analysis Analytical Techniques," Sandia report, 1998.

[45]. Tianquiao Tang, "Failure Finding Interval Optimization For Periodically Inspected Repairable Systems," A thesis submitted in conformity with the requirement for the degree of Doctor of philosophy, Graduate Department of Mechanical and Industrial Engineering, University of Toronto, 2012

APPENDICES

A-1: Rail and Wheel Profile

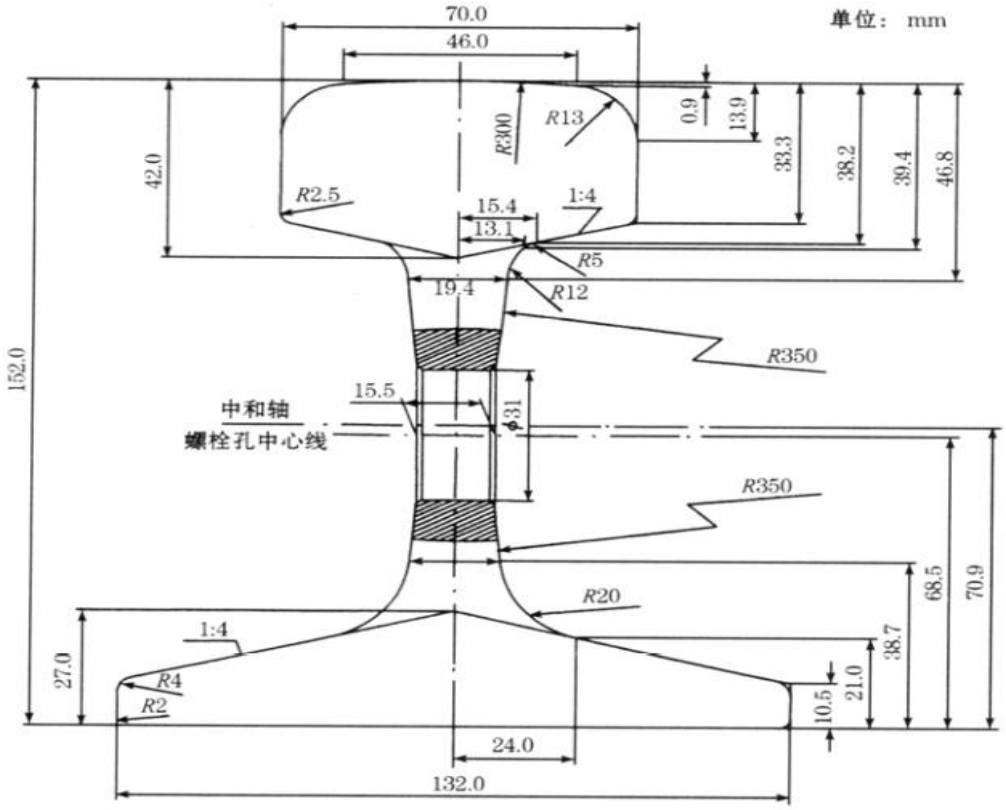

Figure A.1-1: Rail Section 50Kg/m [5]

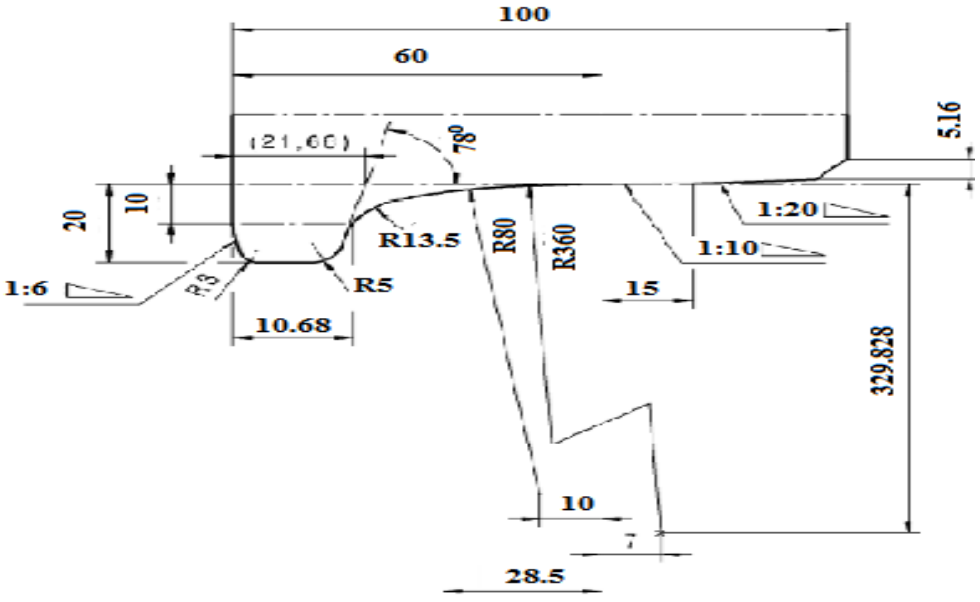

Figure A.1-2: Wheel profile [24]

A-2: Abaqus/CAE Output

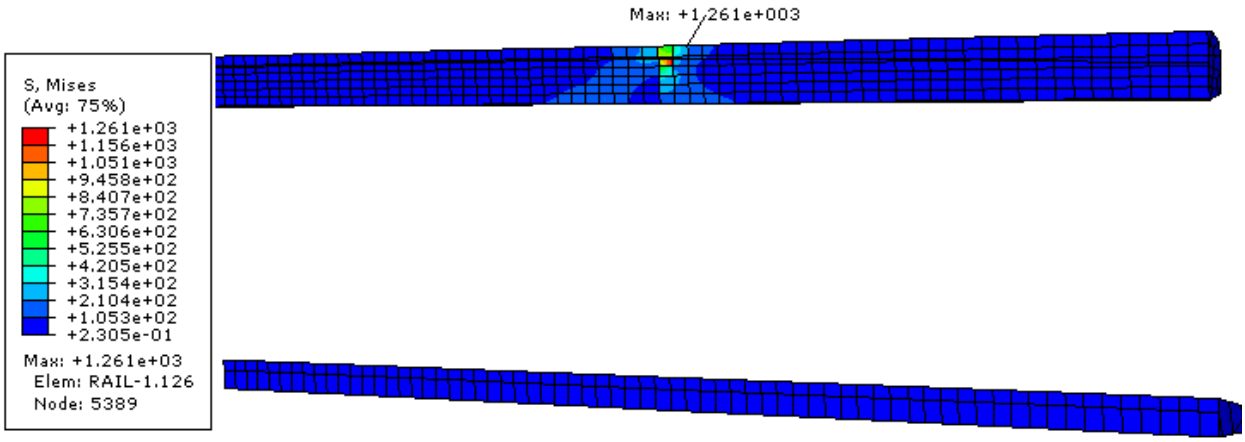

Figure A-2-1: Maximum Misses stress on the rail-weld at the head. Sectioned in the x@(x=66mm from one end)

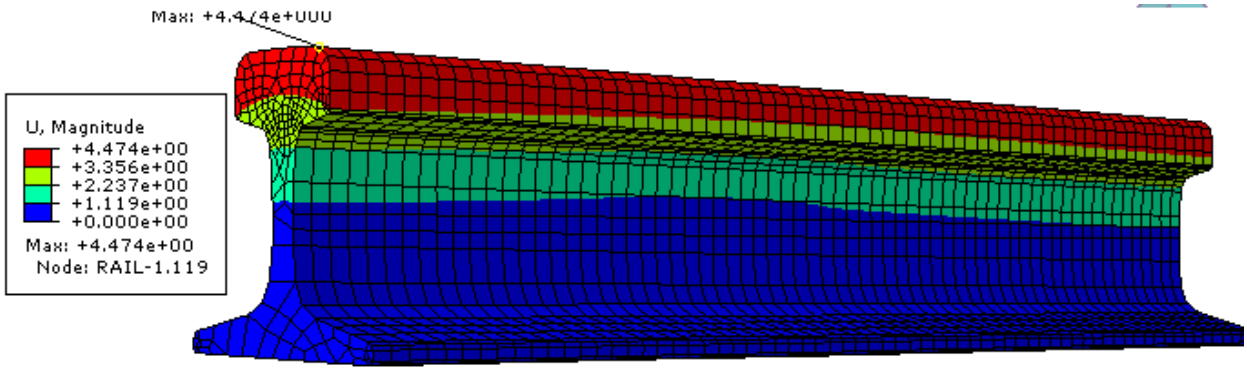

Figure A-2-2: Deformation of the rail in a discrete contour.

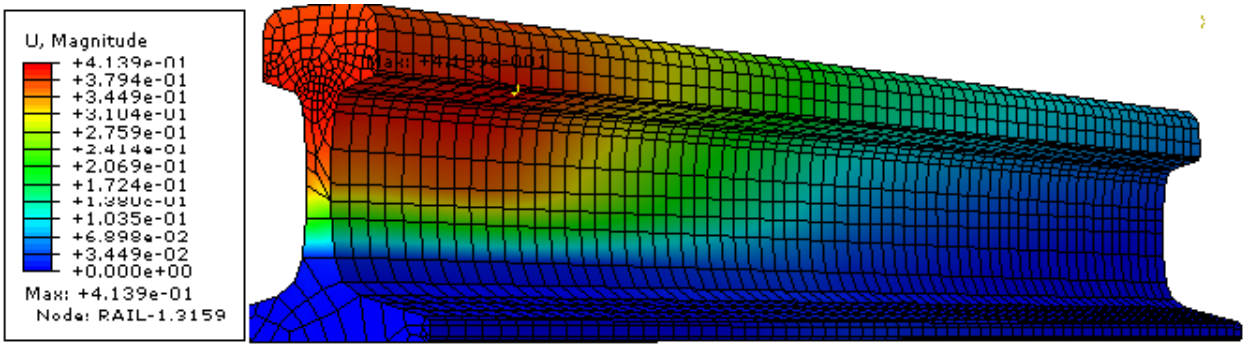

Figure A-2-3: Deformation of the rail in a continuous contour loaded at the left end.

A-3: FRANC3D Output

```
Fatigue Crack Growth Integration Summary:

Total Cycles       : 69730408
Initial Crack Size: 0 (mm)
Final Crack Size   : 0.146955 (mm)

Cycle Integration was Stopped Because:
    Current crack larger than available K vs a data

Maximum Crack Size in K Data: 0.146955 (mm)
Minimum Crack Size in K Data: 0 (mm)

Single Load Case, Constant Amplitude
    R-ratio: 0
    K vs a data:
        From   : a.txt
        Scale  : 1

Checked Stopping Criteria
    DK <= DK Threshold, Threshold Value:0(MPa*sqrt(m)
    max K >= critical K, K critical: 100 (MPa*sqrt(m)

Crack Growth Rate Model: Paris
    C : 1e-011   n: 3

Integration Algorithm : Runge-Kutta
Equivalent K Algorithm: use KI
Retardation Algorithm   : none
```

Figure A-3.1: Fatigue life summary for a zero initial crack size

```
Fatigue Crack Growth Integration Summary:

Total Cycles       : 69730326
Initial Crack Size: 1e-005 (mm)
Final Crack Size   : 0.146955 (mm)

Cycle Integration was Stopped Because:
    Current crack larger than available K vs a data

Maximum Crack Size in K Data: 0.146955 (mm)
Minimum Crack Size in K Data: 0 (mm)

Single Load Case, Constant Amplitude
    R-ratio: 0
    K vs a data:
        From   : a.txt
        Scale  : 1

Checked Stopping Criteria
    DK <= DK Threshold, Threshold Value: 0(MPa*sqrt(m)
    max K >= critical K, K critical: 100 (MPa*sqrt(m)

Crack Growth Rate Model: Paris
    C : 1e-011   n: 3

Integration Algorithm : Runge-Kutta
Equivalent K Algorithm: use KI
Retardation Algorithm   : none
```

Figure A-3.2: Fatigue life summary for a [0.00001mm] initial crack size

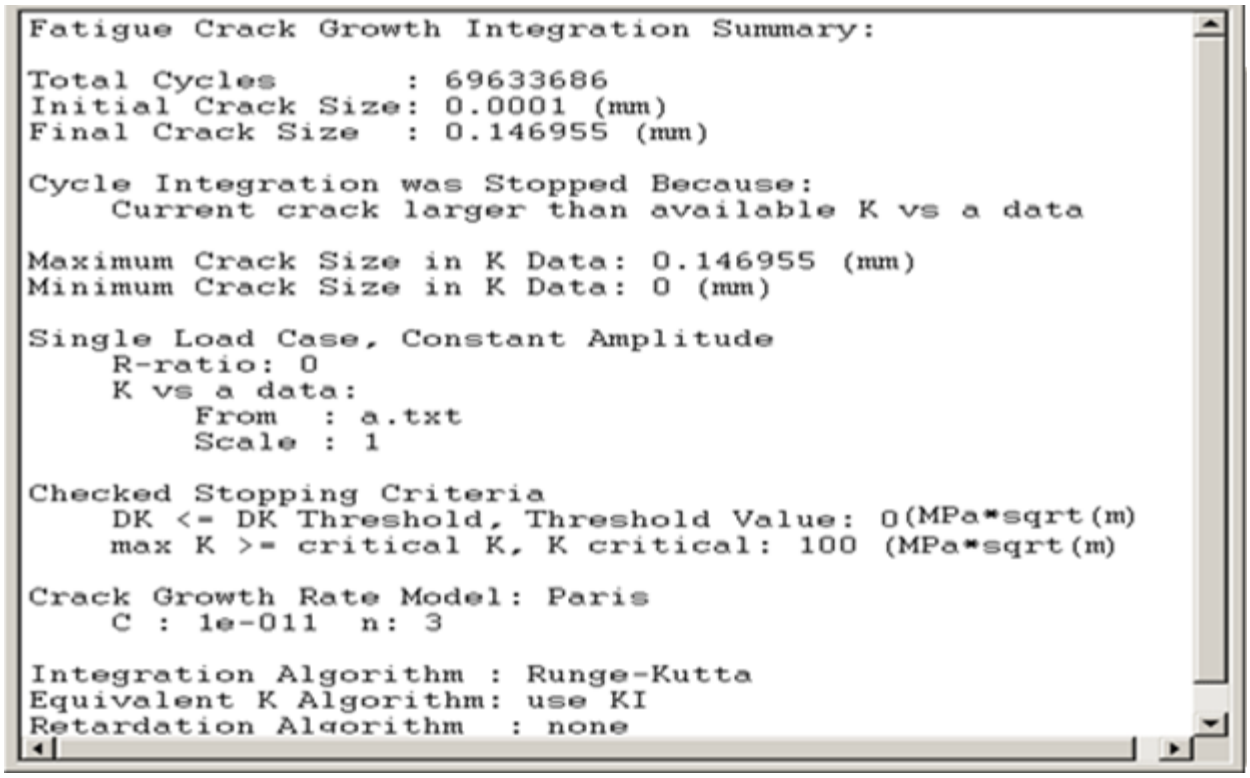

Figure A-3.3: Fatigue life summary for a [0.0001mm] initial crack size

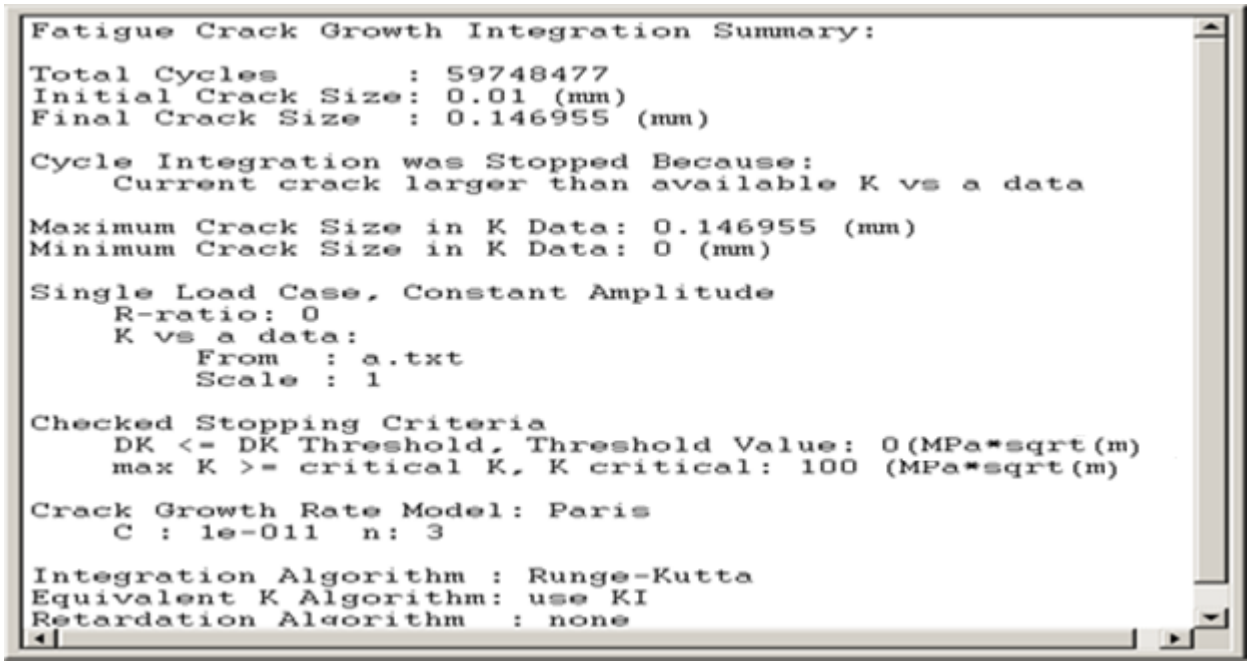

Figure A-3.4: Fatigue life summary for a [0.01 mm] initial crack size

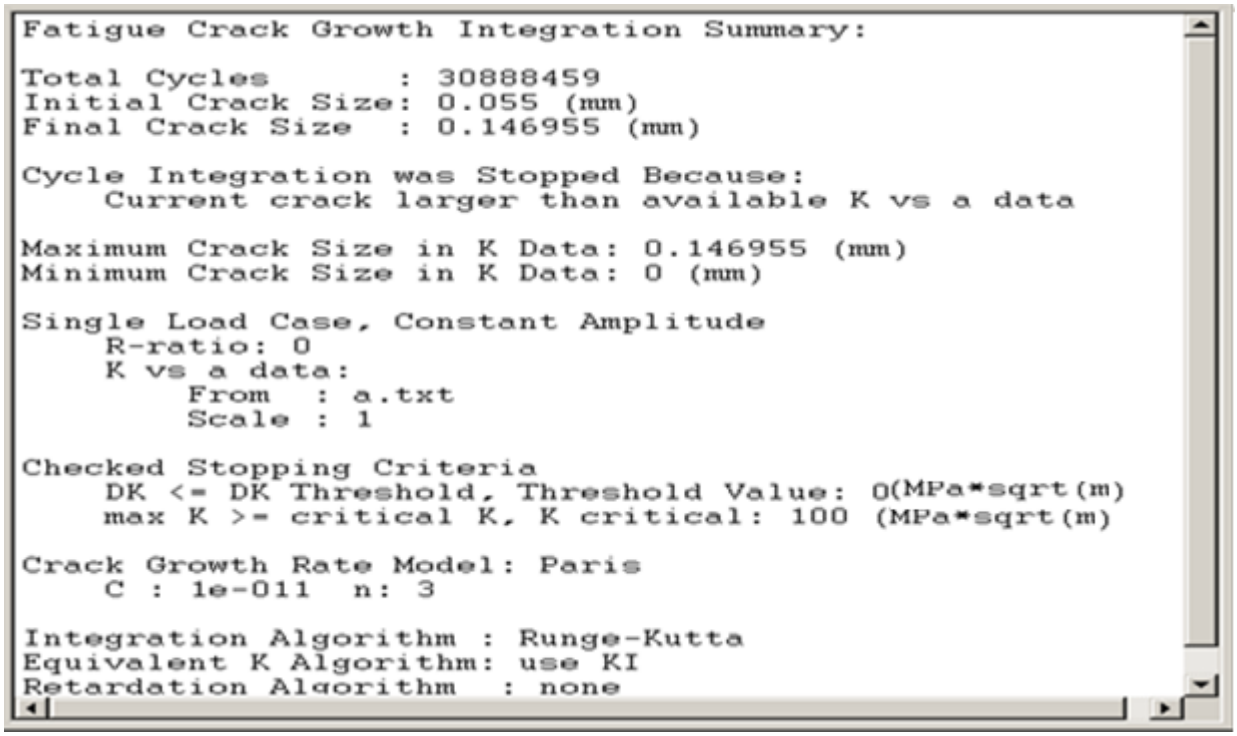

Figure A-3.5: Fatigue life summary for a [0.055mm] initial crack size

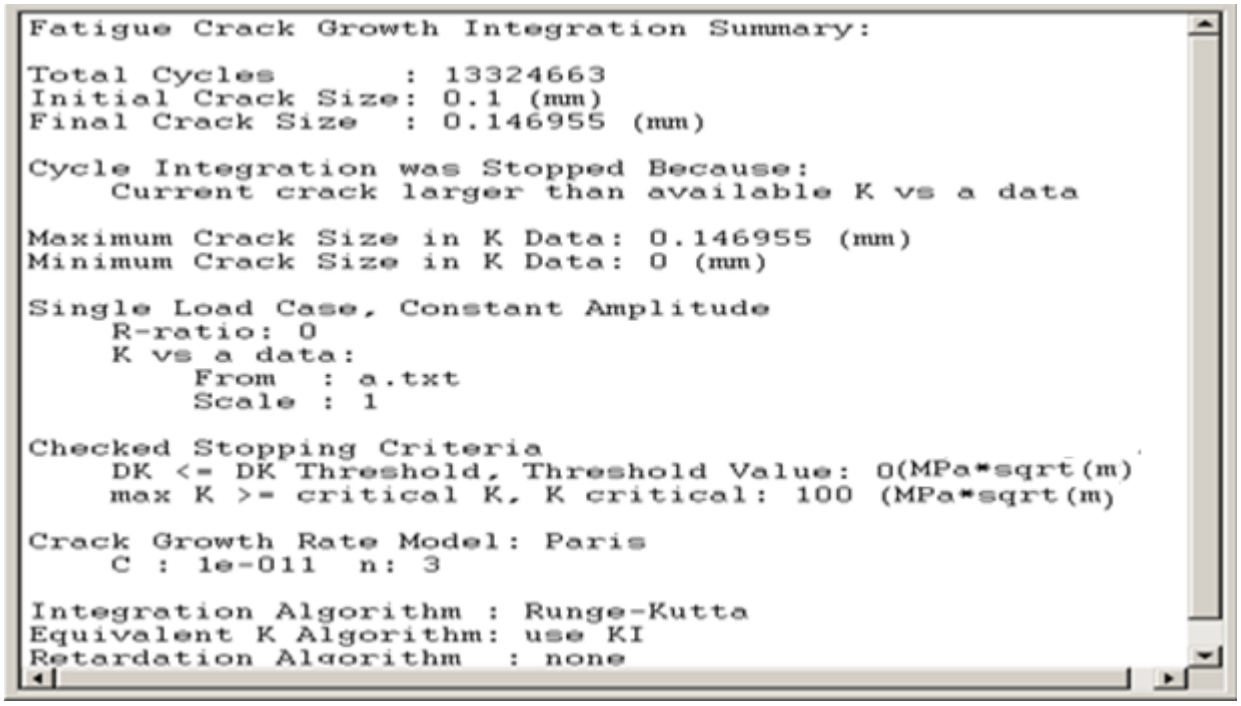

Figure A-3.6: Fatigue life summary for a [0.1mm] initial crack size

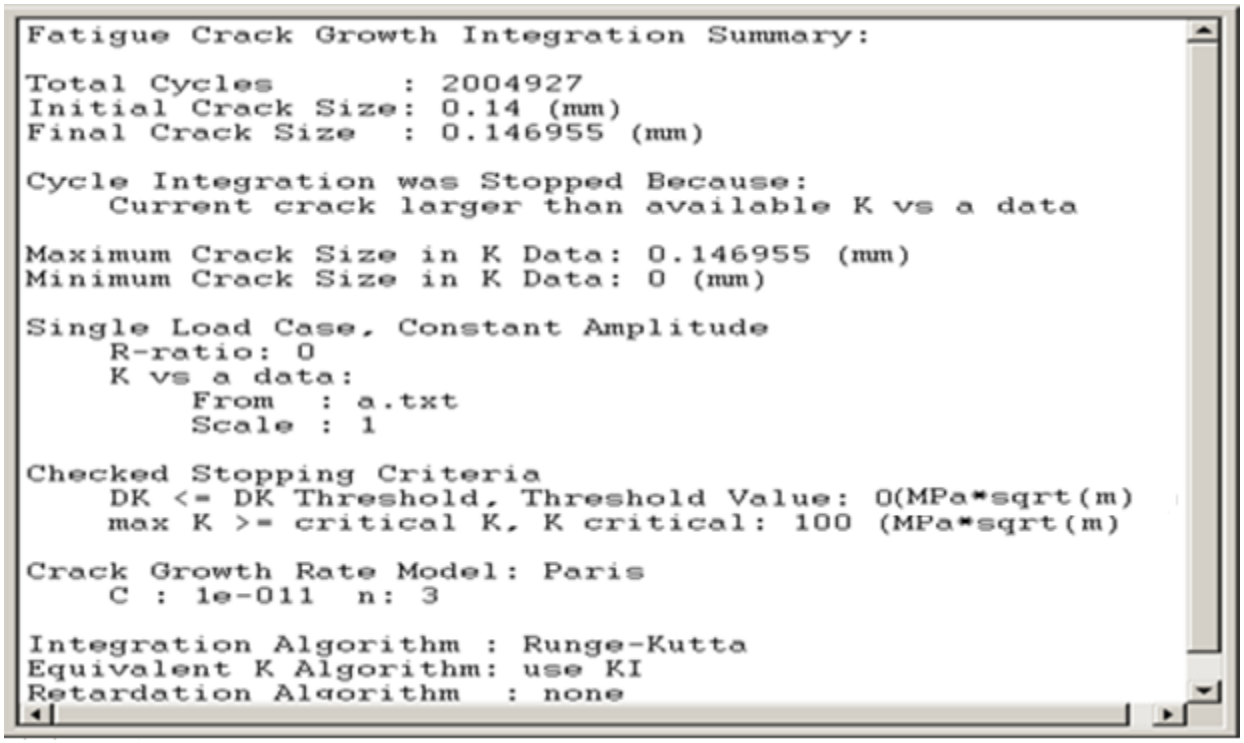

Figure A-3.7: Fatigue life summary for a [0.14 mm] initial crack size

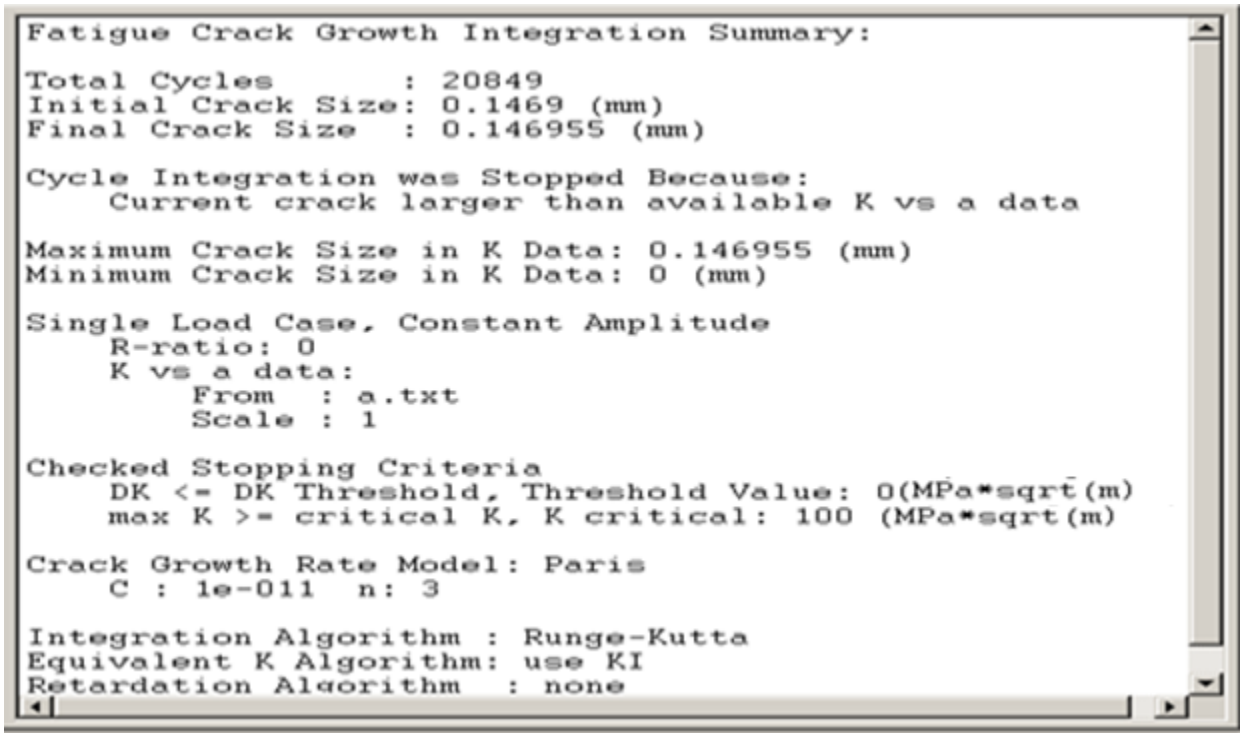

Figure A-3.8: Fatigue life summary for a [0.1469mm] initial crack size

A-4 OTHER WELD-TESTS

A-4-1 RAIL WELD HARDNESS TESTS

Hardness tests are to show the distribution of hardness in rail base material, weld and HAZ. The hardness test is the easiest way to estimate the quality of the rail weld in the first approximation. By its own it cannot be used to determine the quality of a weld and usually it is complementary to other test methods discussed later. The hardness numbers (BHN) are to illustrate the type microstructure of the weld and HAZ.

A-4-2 RAIL WELD BEND TESTS

Rail bend test is carried out to determine the quality of the rail weld by the means of examining results of the static bending test. Rail is either bent to some qualifying criterion load or to break. After the rail fracture the fracture surfaces are examined for macrostructure e.g. visual defects such as inclusions, lack of weld.

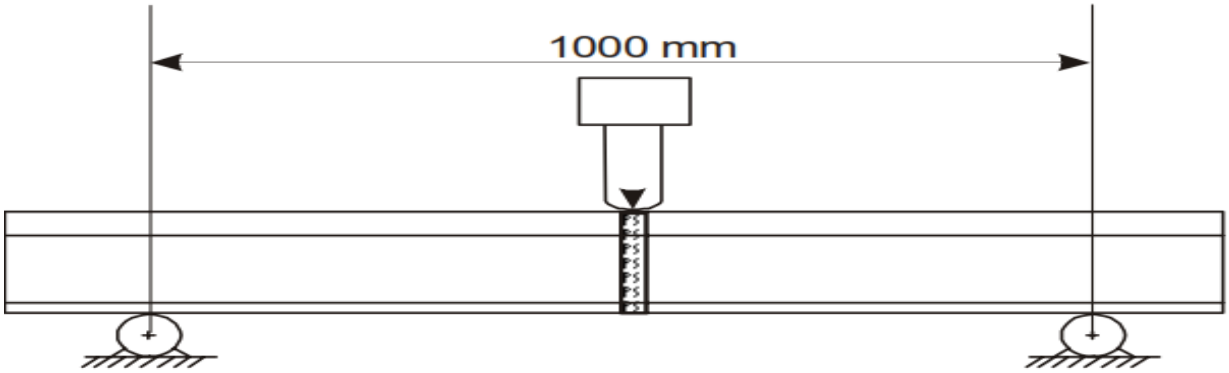

Figure A-4-1: Three Point Bend Testing Scheme [33].

The maximum loading speed is 1 mm/s. The parameters measured are load at break and maximum deflection. The load is applied at two loading points 300 mm apart. Load is applied until the rail fractures or deflects 100 mm, whichever comes first.

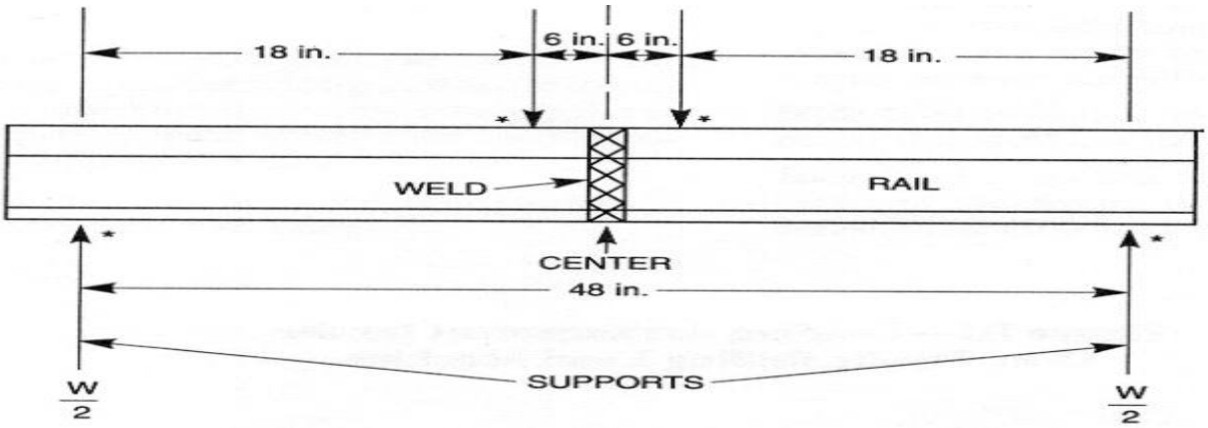

Figure A-4-2: four-point bend test scheme suggested by the ANSI/AWS D15.2-94[33]

A-4-3 RAIL WELD FATIGUE TESTS

Rail fatigue testing is carried out, accordingly to pr EN 14730-1 in the case of TW and pr EN 14587-1 in case of FBW, on a rail weld with a 4-point type of bend test scheme. The qualifying criterion for cyclic load is, with ratio

min/max load ratio of 0.1 and frequency of 10 Hz, a minimum of $5x10^6$ cycles. According to ANSI/AWS D15.2-94 the rail weld fatigue testing is suggested to be carried out by rolling load test scheme. Test speed is 60 cycles per minute (1Hz) for total of 2 million cycles or to the failure whichever comes first

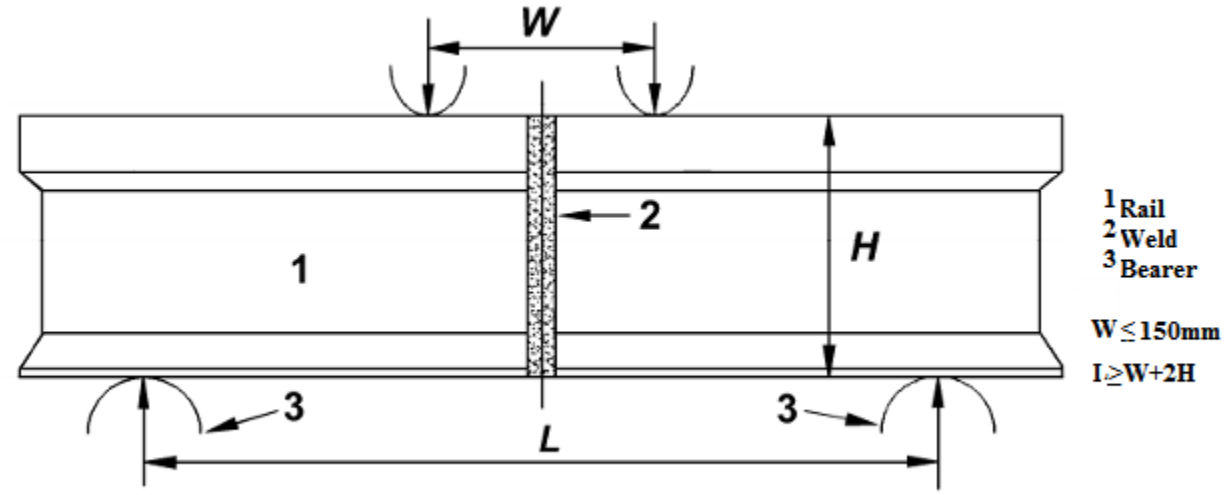

Figure A-4-3: Rolling load test scheme. [22]

3

A-5: EXCELL TEMPATES

A-5.1 HERTZIAN CONTACT PRESSURE COMPUTING EXCELL TEMPATE

Static Vertical Load (Ton)	12.5		
Vertical Force, F_v(N)	122,625.00		
Do you need Dynamic Amplification? (Y/N)	Y		
	Passenger	Freight	
Train Speed(Km/hr)	120	120	
Coefficient, φ	1.16	1.38	
Coefficient, n	0.2	0.2	
Amplification Factor, K^{dyn}	1.69	1.83	
Vertical Dynamic Load, Fv(N)	207,817.11	223,790.63	
Interaction Parameters			
R_1(mm)	460	460	
R_2 (mm)	∞	∞	
R_1'(mm)	300	300	
R_2'(mm)	∞	∞	
A+B	0.002753623	0.002753623	
B-A	9.343E-06	9.34319E-06	
From the Value of θ m	1.161	1.162	
n	0.872	0.872	
K_1	1.38004E-12	1.38004E-12	
K_2	1.38E-12	1.38E-12	
a(mm)	9.385321011	9.385321011	
b(mm)	7.04909554	7.04909554	
P_o(N/mm²)	1,500.58	1,615.92	

Material Property INDEX

	Over Stiffness	Under Stiffness
E_1	2.1E+11	2.1E+11
E_2	2.1E+11	1.90E+11
ν_1	0.3	0.3
ν_2	0.3	0.34

*1 is for the wheel and 2; for the rail.

A-5.2 DETERMINATION OF HASOFER-LNDEX RELIABILITY INDEX

Template for detrmination of reliability Index, β

Mean crack	σ	ζ	λ	η	Y^*_{NEW}	`	U'_{New}	g(x)	β	J		J^{-1}		$(J^{-1})^T$	
0.07825	0.01565	1.0198	-2.5675	0.078	0.08312	0.4	-4.841	-1.854	6.1137	12.531	0	0.0798	0	0.0798	0.01176
0.14695	0.02939	1.0198	-1.9373	0.078	0.12722		3.7339			-0.9861	6.6935	0.0118	0.1494	0	0.1494

$g(u_1,u_2)$		C	m	X*	$\nabla g(u_1,u_2)$		∇^*
-1.854		1E-11	3	-4.78	-5.85	2.27	-0.4399
				-1.65			0.3393